METHYL MERCAPTAN ADSORPTION/OXIDATION ON ACTIVATED CARBONS

by

SVETLANA BASHKOVA

A dissertation submitted to the Graduate Faculty of Chemistry in partial fulfillment of the requirements for the degree of Doctor of Philosophy at The Graduate School and University Center of the City University of New York

2005 (Year Degree Awarded)

UMI Number: 3187436

ProQuest Information and Learning Company
300 North Zeeb Road
P.O. Box 1346
Ann Arbor, MI 48106-1346

This manuscript has been read and accepted for the
Graduate Faculty in Chemistry in satisfaction of the
dissertation requirement for the degree of Doctor of Philosophy.

Professor Teresa J. Bandosz

_____ _____

Date Chair of Examining Committee

Professor Jerald W. Koeppl

_____ _____

Date Executive Officer

Professor Teresa J. Bandosz

_____

Professor Urs Jans

_____

Professor David Locke

_____

Supervision Committee

THE CITY UNIVERSITY OF NEW YORK

Abstract

METHYL MERCAPTAN ADSORPTION/OXIDATION ON ACTIVATED CARBONS

by

Svetlana Bashkova

Adviser: Professor Teresa J. Bandosz

Activated carbons of different origins were used as adsorbents for methyl mercaptan (MM). The samples were further oxidized and urea-treated to study the effect of oxidation and introduction of nitrogen on their MM adsorption capacities. The surface of the carbons was characterized by Boehm titration, potentiometric titration, thermal analysis (TA) and X-ray Fluorescence Analysis (XRF).

The content of carbon, hydrogen, and nitrogen was determined by elemental analysis. The porous structure of the carbons was studied using nitrogen adsorption isotherms at –196°C. The adsorption capacities of the carbons towards MM were found from the dynamic tests. The results showed that MM capacities of the carbons studied were higher in wet conditions than in dry conditions, indicating the lack of chemisorbed oxygen in a latter case. It was found that the ability of carbon to adsorb MM depends strongly on its surface chemistry, particularly on the surface pH, the presence of basic oxygen-containing groups and ash content. Both nitrogen and iron were noticed to catalytically enhance the adsorption of MM through an electron transfer mechanism.

From a structural point of view, the adsorption process was enhanced by the presence of small micropores, where the reaction products are stored. These reaction products were analyzed by TA and Gas Chromatography – Mass Spectrometry (GC/MS).

The results revealed that the main product of MM adsorption/oxidation is dimethyl disulfide (DMDS), which is adsorbed in pores smaller than 50 Å. In some cases oxidation proceeded further leading to the formation of methyl methanethiosulfonate (MMTS).

The competition for adsorption sites between water (moist conditions) and DMDS was noticed. The latter molecule, due to its strong adsorption, won the competition in the carbon pore system. On the other hand, water facilitated dissociation of MM, considering that the surface pH of the carbon is above the required threshold of about 7.6, and thus ensured the efficient removal process.

From the inverse gas chromatography (IGC) experiments the heats of adsorption were calculated at different temperatures. It was found that in dry and anaerobic conditions the heat of MM adsorption depends on surface chemistry and particularly on the presence of basic oxygen-containing groups.

Acknowledgment

I would like to express my gratitude to everybody who helped me through the process of working and completing this dissertation.

First of all I want deeply to thank my mentor Professor Teresa Bandosz for giving me an opportunity to work on such an interesting topic and for introducing me to the exciting chemistry of activated carbons. I also highly appreciate her methods of work, that is to be demanding and understanding at the same time. I want to thank her for taking me to the conferences and giving me the opportunity to get to know other researchers.

I am in great appreciation to Dr. Andrey Bagreev, who helped me through the whole process. He introduced me to the basics of carbon chemistry and adsorption and I kept learning the new information from him through the whole way of working on my dissertation. He guided me by means of a good advice and scientific discussions, and participated in preparation of all my papers along with Professor Bandosz.

I express my endless gratitude to my husband Misha, who supported me in all the ways and always remained loving and patient.

I would like to thank my colleagues, Anna Kleyman, Yehya Elsayed and Danh Nguyen-Thanh for creating a wonderful atmosphere inside the lab and for always being supportive and friendly. Many thanks are to Anna Kleyman for her kindness and ability to help when it was needed. I am also very grateful to Habibur Rahman for telling me about Prof. Bandosz's lab and research.

Finally, I wish to thank Professor Urs Jans and Professor David Locke for serving as my supervision committee members, for their constructive comments during committee meetings and the revision of this dissertation.

Table of Contents

List of Tables

List of Figures

1. INTRODUCTION

Adsorption is the process in which molecules of a liquid or gas contact and adhere to a solid surface. Adsorption processes are classified as either physical or chemical. Physical adsorption occurs when London dispersion forces bind the adsorbing molecule to the solid substrate. Chemical adsorption takes place when covalent or ionic bonds are formed between the adsorbing molecule and the solid substrate. For the adsorption process to be effective, the surface of a solid should contain all accessible areas, including inner network of pores with diameters down to molecular dimensions. Such solids are known as adsorbents and the most commonly used ones among them are activated carbons.

Activated carbon is the generic term used to describe a family of amorphous carbonaceous adsorbents with an extensively developed internal pore structure. Activated carbon consists of layers that are less regularly organized than graphene layers and are also curved with the pronounced cross-linking. Schematic representation of an activated carbon is presented on Figure 1 [1]. Due to the activation process, carbon layers are separated by pores, most of which are assumed to be slit-shaped [2]. IUPAC has designated a classification based upon a division of pores into micro- (< 20 Å), meso- (20-500 Å), and macropores (>500 Å) [3]. This classification is mostly based on the differences in the adsorption mechanisms occurring in those pores: (i) enhanced adsorption in micropores, (ii) capillary condensation in mesopores, and (iii) bulk liquid condensation of vapors in macropores. The adsorption in macropores becomes

significant only at very high pressures. At low and medium pressures, adsorption is significant only in micro- and mesopores.

Figure 1. Schematic structure of an activated carbon [1].

A wide variety of activated carbon products are available on the market. They exhibit different characteristics depending upon the raw material and activation technique used in their production [4]. Some of the most common raw sources of carbon are bituminous coal, wood, coconut shell, peat, petroleum residues and polymers. Coal is by far the most widely used raw material in the industrialized countries. Most activated carbons are produced from coal, mostly bituminous coal but also lignite and anthracite. Such companies as Norit America, Calgon Carbon, Chemviron and Atochem North America are involved in the production of coal-based activated carbons. Examples of other raw materials used to produce activated carbon are sawdust and wood. Wood is used by Westvaco in the United States and is a waste product from the company's own paperboard operations. Norit obtains wood raw materials as waste products from the sawdust milling industry in the United Kingdom.

In developing countries coconut shells are by far the most widely used raw materials. Coconut shells have a high volatile content and give a lower yield of activated carbon than coal, but their abundant supply as a waste product from a coconut oil production proves to be relatively competitive to coal-based activated carbon.

The activation techniques most commonly used by commercial production operations are based on physical and chemical processes. In the process of physical activation the carbon porous structure is developed as a result of heating at high temperatures in the absence of oxygen to dehydrate and carbonize, followed by activation with steam, carbon dioxide or other agents to introduce porosity. The air is added to the process so as to burn the gases without burning the carbon. Steam activation is used throughout for the activation of carbon made from peat, coal, coconut shells, lignite, or wood. Hard materials, like coconut shell, coal and petroleum pitch produce almost nothing but micropores, while a soft material like peat always gives many mesopores as well.

Chemical activation is principally used for the activation of wood-based carbons, which are mostly mesoporous with low mechanical stability and low density [5]. Chemical activation differs from physical activation in that carbonization and activation occur simultaneously. The raw material, for instance wood chips, is mixed with an activating and a dehydrating substance such as phosphoric acid or zinc chloride [6-10]. The activation takes place at a low temperature: 500°C is the norm, but sometimes it can go up to 800°C. The phosphoric acid causes the wood to swell and open its cellulose structure [6, 8, 9]. During the activation, the phosphoric acid acts as a stabilizer and ensures that the carbon does not collapse again. The result is a very porous activated

carbon full of phosphoric acid. This is later washed out and re-used in the next production. Other chemical reagents commonly used as activation agents are zinc chloride [5, 7, 10, 15], potassium and sodium hydroxides [11-14], potassium carbonate [16, 17] and others.

In selecting an activated carbon, it is important to have a clear understanding of both the structural and surface characteristics of the material in order to optimize the performance capabilities. Carbon surface chemistry is the combination of surface complexes formed by combining carbon atoms with other elements such as oxygen, nitrogen, hydrogen, phosphorus and sulfur [18, 26]. The major chemical forms in which heteroatoms are present are functional groups and heterocyclic compounds analogous to those in organic compounds. Carbon surface oxides have been extensively investigated, since oxygen is the next most frequent element present on the surface of carbon materials. It was found that basal planes of graphite are attacked by molecular oxygen only at their periphery or at defect sites such as vacancies [19-21]. Most of the oxygen-containing functional groups are introduced into the carbon surface by oxidation with gases like oxygen, ozone, nitrous oxide, nitric oxide, etc., and solutions of nitric acid, alkaline permanganate, hydrogen peroxide, acidic permanganate, and acidic dichromate. The most common oxygen-containing functionalities are carboxylic acids, phenols, ketones and esters [22-25]. These functional groups have been traditionally split into two groups according to their acidic or basic character in aqueous solution (Figure 2).

Surface acidic groups are well studied [18, 22, 25-27]. The main functionalities found at the edges of basal planes are carboxyls, lactones, phenols and lactols, which behave as acidic centers in Brönsted-type acid-base reactions [18, 22, 25, 27]. Some

oxygen can also be substituted for edge carbon atoms such as xanthene- or ether-type oxygen, which is very difficult to detect because of its chemical inactivity.

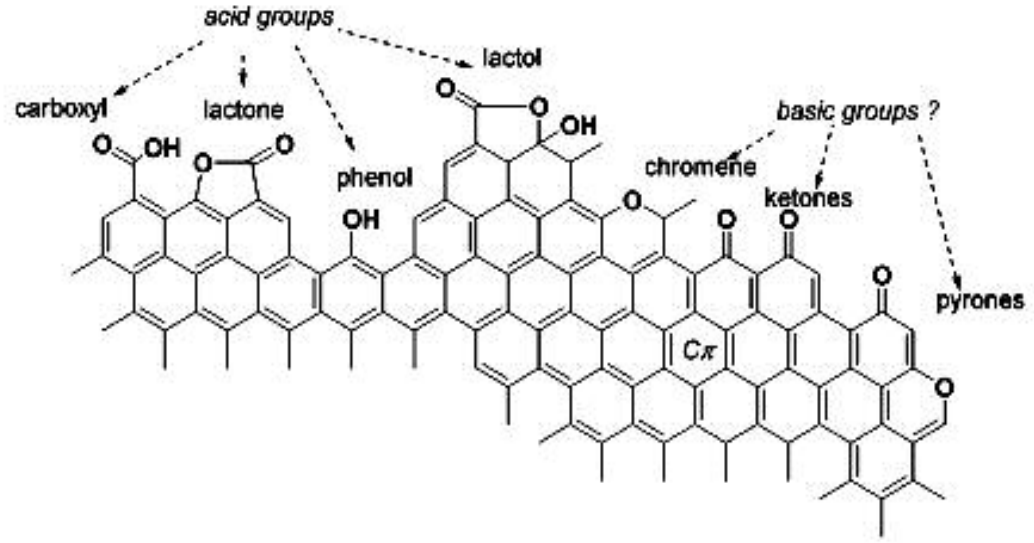

Figure 2. Some of the oxygen-containing groups present on the activated carbon surface [34].

The nature of surface basic groups is not that clear and is still the subject for debate. The proposed surface models that account for carbon basicity are either oxygen-containing surface groups of diketone, quinone [25, 28], pyrone-like [23, 29] and chromene type [32, 33] or delocalized π electrons of aromatic rings and unsaturated valences [25, 28, 30-34]. The formation of basic surface oxides occurs at the active sites (free valence C atoms) generated by heat treatment due to decomposition of carboxyl, lactone, and phenol groups. Based on a few chemical reactions it was concluded by Voll and Boehm [29] that γpyrone-like is the most favorable one. Some computational results [33, 34] also showed that pyrone sites are strong bases according to the Brönsted definition and if present in a sufficient amount on the carbon surface are responsible for the overall carbon basicity. Pyrone-like structures are formed by air re-exposure of heat-

treated carbons [33-35] and are the combination of a non-neighboring carbonyl group and ether oxygen atom. Such structures in addition to their acid-base chemistry may appear as redox centers as well [34].

Besides oxygen, nitrogen presence in carbonaceous materials is of a great importance as well. It was found to enhance the catalytic activity of carbons [36-47]. Nitrogen-containing carbons can be prepared by heat treatment with such compounds as ammonia [36, 37, 41], HCN gas [37], urea [42-45], uracil, aniline, melamine and 3-hydroxypyridine [45, 46]. Another way to prepare carbons with nitrogen is to use nitrogen- containing precursor materials like acridine, carbazole, polyacrylonitrile [47, 48] or porous vinyl pyridine resin [49]. The geometrical shape of the latter one allows the insertion of the required heteroatoms and controls the composition and content of impurities.

The functionality of nitrogen in carbon materials has been studied widely [37, 46-53] with X-ray photoelectron spectroscopy (XPS) being one of the most successful methods of analysis. The possible forms of nitrogen are presented in Figure 3. Among those, pyrrolic, pyridinic and quaternary (N-Q) nitrogen groups were found to be predominant forms of nitrogen functionalities in coals. Other possible nitrogen-containing groups present on the surface of activated carbons are amines, ammonium, nitro-, nitroso-, and ciano groups.

Moreover, the relationship was established between the positions of a nitrogen atom in a graphene plane and its semiconductor characteristics, especially the band gap. In the classical work of Mrozowski [52] such an approach made it possible to explain many electrophysical properties of carbon adsorbents. Furthermore, Strelko et al.

evaluated the effect of nitrogen functionalities in catalytic activity of carbons in electron transfer reactions [53]. This study showed that the insertion of nitrogen atoms into the graphite lattice lowers the band gap, thus producing higher electron mobility and lowering the electron work function at the carbon/gas interface compared with pure carbons.

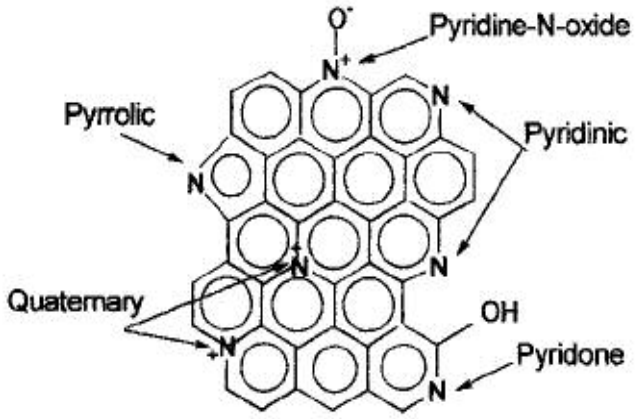

Figure 3. Some of the nitrogen-containing groups present on the activated carbon surface [42].

Following the above-mentioned facts, it is clear that the presence of heteroatoms in the form of functional groups and heterocycles in the carbon network significantly increases the adsorption of polar molecules [3, 54-68]. Besides, the higher the polarity of the molecule the more important is the nature and amount of surface groups. The process of adsorption of polar gases is rather complex and depends not only on interactions due to dispersion forces but also on polar interactions between adsorptive molecules in the gas phase and between adsorptive molecules and the surface of the carbon. On the other hand, unmodified activated carbon with a mainly non-polar surface, would be useful for the adsorption of molecules of low polarity such as hydrocarbons. For such molecules

adsorption depends mainly on dispersion forces and is influenced by the porous structure [61, 69].

Another important feature that may influence the performance of the activated carbon as an adsorbent is its amount of ash. Ash is defined as the inorganic, inert, and amorphous part of the carbon precursor. The chemical nature of ash varies with the type of base material and fluctuates even within the same type of carbon. This ash consists mostly of inorganic salts and/or metal oxides, commonly of iron and calcium. It comes initially from the precursor and can be removed from the carbon by rinsing or soaking in water or acid.

Carbons high in ash content (up to 15 %) often have alkaline pH and are usually made from lignite, peat or coal. Even though the higher the ash content the less the amount of actual activated carbon present for the adsorption of impurities, certain metals present in the ash may have a catalytic effect on the adsorption process. Thus, for the adsorption/oxidation of hydrogen sulfide, iron, calcium and zinc oxides were found to be effective [70-75]. On the other hand, composite adsorbent CuO/ZnO prepared by the precipitation route and synthesized feroxyhyte (α-FeOOH) were able to adsorb/oxidize H_2S and some organosulfides (CS_2, COS) at low temperature conditions [72, 76-78]. For the adsorption of another sulfur-containing compound, SO_2, the oxides of copper, silica, aluminum, iron, and calcium are effectively employed [72, 79]. More so, for all the above adsorption/oxidation reactions to occur, the presence of oxygen and some moisture in the feed stream are required.

To study the complexity of the carbon surface and structure several methods of analysis have been employed. The geometrical structure of activated carbons is usually

characterized by its pore size distribution (PSD) most commonly obtained form adsorption of nitrogen [80-84]. However, several other experimental methods are available for particular kinds of materials or for specific ranges of pore sizes. Thus He, Ar and CO_2 adsorption [85-88] has been used to measure ultramicropores ($\leq$ 7 Å), while mercury porosimetry [3] and NMR spin-lattice relaxation [89] provide the accessibility to measure macropores. Such methods as X-ray diffraction (XRD) and small angle neutron scattering have been widely used to determine pore sizes in well-ordered materials, such as zeolites [90] and partially ordered porous materials, such as pillared clays [91], silica gels [92], and sol-gel systems [93].

The surface chemistry of activated carbons has been studied for many years by various chemical and physicochemical methods. The best-known and relatively simple one was proposed by Boehm [26] to determine chemical functionalities on the carbon surface. In this method, the acidic group content is determined by neutralization with some bases of increasing strength, while the number of basic groups is estimated by neutralization with hydrochloric acid. To study the evolution of acidic groups during oxidation or reduction of activated carbons in terms of their *pK* values, potentiometric titration could be applied [94, 95]. Although, both methods are quite successful in characterization of the carbon surface, they are limited to the identification of carboxylic, phenolic and lactonic groups, leaving behind other forms of functional groups. Therefore, such methods as diffuse reflectance infrared Fourier transform (DRIFT) spectroscopy [96-98], X-ray photoelectron spectroscopy (XPS) [99, 100], and X-ray absorption near edge structure (XANES) spectroscopy may provide a larger view [101-104]. As described in a paper by Biniak and coworkers [105], the spectroscopic data revealed the

presence of carbonyls, alcohols (or ethers) and some nitrogen functional groups (pyrrole-, pyridone-, and pyridine-like species) on the non-modified carbon surface as the most abundant species. Consequently, the oxidation of the non-modified carbon with nitric acid showed an increased concentration of surface oxides, such as carboxylic anhydrides, alcohols, keto-ester and keto-enol structures, and pyridine-N-oxide species in the case of nitrogen functional groups. In addition to this, temperature programmed desorption (TPD) is often used for the characterization of surface complexes [106, 107]. TPD makes it possible to determine the concentration and the thermal stability of the complexes but does not allow the exact identification of the chemical form of the complexes. Therefore Zhuang and coworkers [108] found an alternative way to combine DRIFT spectroscopy with transient kinetic (TK) and TPD techniques. These combined techniques allowed the successful identification of the surface complexes, which are responsible for the CO_2 and CO evolution in TPD. Thus, CO_2 desorption with a peak temperature of 900 K was assigned to the decomposition of lactone and/or acid anhydride, whereas CO desorption with a peak temperature of 973 K resulted mainly from carbonyl and/or ether type complexes.

However, when we need to link rapidly the surface properties of activated carbons to their adsorption properties, inverse gas chromatography (IGC) at infinite dilution is the best technique to be used. It was applied to study the effect of oxidation of activated carbons on their dispersive and specific interaction with hydrocarbons to show the correlation between the acidity of carbons and the energy of the specific interactions [109]. Furthermore, it was demonstrated by using the IGC method that it is possible to

identify separately the effects of microstructure and surface chemical functionality on adsorbate interactions with carbonaceous materials [110, 111].

For their highly developed porous structure and large surface area, as well as for the diversity of functional groups and presence of metals in their surface chemistry, activated carbons are widely used as adsorbents for the removal of gases and organic pollutants from air and water streams [24, 59, 69, 112-116]. Besides the adsorbent properties, the adsorption process is also dependent on the nature of adsorbate and adsorption conditions. Thus, the characteristics of adsorbate may include polarity, hydrophobicity, size of the molecule, and the nature of functional groups and adsorption process itself could be temperature- and time- dependent.

The removal of sulfur-containing compounds has been of a great scientific and practical importance. With the growing popularity of fuel cells, which are expected to play a major role in the world's energy future, the removal of such compounds as hydrogen sulfide, thiols, and thiophenes has become a problem of today. These compounds are part of hydrocarbon fuels, including natural gas, biogas, petroleum-based liquids (e.g. gasoline, diesel fuels) and coal. Such fuels could be used for the production of hydrogen in fuel cells but one of the hurdles is the presence of sulfur compounds, which quickly poison both the reforming catalyst and the electrocatalysts within the fuel cell itself. Because of the concern that high-sulfur gasoline could decrease the effectiveness of advanced catalytic converters, EPA mandates that by 2005 the nation's largest oil refiners must reduce the sulfur content of gasoline by 90%, from an average of 300 parts per million (ppm) to 30 ppm [117]. EPA also calls for an equally large reduction in diesel fuel's sulfur levels (to 15 ppm) by mid-2006 [118].

Natural gas, which is the feedstock of choice for stationary fuel cells for power generation has the highest hydrogen-to-carbon ratio to enable the production of a gas richer in hydrogen. However, pipeline natural gas typically contains up to 15 ppm of sulfur compounds, including naturally occurring species such as COS and H_2S, as well as odorant compounds mercaptans, disulfides and/or thiophenes. All these sulfur compounds must be removed to low ppb levels prior to the reforming step.

The removal of sulfur containing compounds may be divided into three major categories, including passive adsorption, selective catalytic oxidation (SCO), and hydrodesulfurization (HDS). HDS that is the catalytic reaction between organic sulfur compounds and hydrogen is widely applied for the removal of toxic sulfur materials from petroleum products. Hydrogen sulfide and hydrocarbons are formed in this process and H_2S is subsequently reacted with O_2 in the Claus process to produce H_2O and elemental sulfur. In SCO different catalysts are used for selective conversion of various organosulfur compounds (CH_3SH, CH_3SCH_3, CH_3SSCH_3, COS, CS_2, thietane, thiophene, 2,5-dimenthyl thiophene, dibenzothiophene) typically found in industrial streams [petroleum, pulp & paper and so on] into valuable chemical intermediates (H_2CO, CO, H_2, maleic anhydride and concentrated SO_2 that can be used for producing H_2SO_4).

Different materials have been effectively tested for desulfurization purposes, from commonly used adsorbents such as activated carbons [119-121], clays [122-125], and zeolites [126-129] to catalysts of zinc, copper, cobalt, molybdenum, and nickel supported on previously mentioned adsorbents [130-137] or other types of porous supports (alumina, silica, molecular sieves) [138-146].

The research described here is concentrated on the removal of methyl mercaptan (MM) from air on activated carbons. Furthermore, if this removal process is successful it could be potentially applied to desulfurization of natural gas for fuel cell operations.

Methyl mercaptan (CH_3SH) is a colorless gas, which is the simplest and the most volatile thiol. It is usually added as an odorant to the processed natural gas due to its strong odor of a rotten cabbage. It exhibits high toxicity at very low concentrations and has a very low odor threshold (one part in $5x10^{10}$ part of air) [147]. Its occupational exposure limit is 0.5 ppm or 0.9 mg/m^3 [148]. It is also found in the blood, brain, and other tissues of humans and animals and occurs naturally in certain foods. Methyl mercaptan is emitted to the atmosphere from various industries. The main industrial sources are petroleum, paper, viscose, and food industries.

The small size of the CH_3SH molecule (4.19 Å [149]) indicates its possible adsorption in ultramicropores (<10Å), where adsorption forces are stronger due to the overlapping potentials of the pore walls. Adsorption is also likely to take place via dispersive interactions with the carbon surface and is expected to be stronger than in the case of H_2S (3.82 Å) due to the presence of hydrocarbon moiety in the MM molecule. Thiols are also known to be stronger acids than corresponding alcohols. The pK_a of CH_3SH is 10.3 and that of CH_3OH is 15.2 [149, 150]. In addition, the bond strength of S-H is 80 kcal/mol, which makes it easier to break than the O-H bond (102 kcal/mol) in CH_3OH [151]. Thus, the adsorption of MM may go through dissociation of the CH_3SH molecule to CH_3S^- and H^+ ions on a basic carbon surface, where the pH of the surface is expected to be higher than pK_a of a MM molecule. Another important factor required for this reaction to occur is the presence of water on the surface, which should facilitate the

dissociation of MM. In case of the pH of carbon surface being smaller than the pK_a, the adsorption of CH_3SH can happen without a dissociation step but due to weak acid-base interactions with the basic oxygen groups on the carbon surface. Moreover, the adsorption process can be affected by the presence of metal ions as constituents of ash [152].

Because the adsorption process occurs in the presence of oxygen, whether it is oxygen from air or oxygen as a part of oxygen-containing functional groups on the carbon surface, MM is expected to be oxidized to dimethyl disulfide (DMDS) as its most probable oxidation product. For further oxidation to occur, a stronger oxidant might be needed.

2. OBJECTIVES

The main objective of the following research is to describe the process of adsorption/oxidation of methyl mercaptan from wet air streams on commercial activated carbons. This is achieved by using the following approaches:

1. Qualitative and quantitative characterization of the activated carbon surface in terms of:
    a. Functional groups of different types (Boehm and potentiometric titrations).
    b. pH of the carbon surface.
    c. Ash and inorganic metals as its constituents (DTA/TG, XRF analyses).
2. Characterization of the activated carbon structure in terms of:
    a. Surface area (N_2 adsorption at –196ºC).
    b. Porosity (N_2 adsorption at –196ºC).
    c. Pore Size Distributions (PSDs) (DFT approach).
3. Study of the methyl mercaptan adsorption capacity on the activated carbon surface (breakthrough capacity test) and its dependence on the surface and structural characteristics of carbons.
4. Modification of the activated carbon surface (H_2O_2, urea) to increase the performance of the activated carbon as methyl mercaptan adsorbent.
5. Identification of the products of methyl mercaptan adsorption/oxidation on activated carbons (DTA/TG, GC/MS, IGC).
6. Evaluation of the role of water and ash in the oxidation process.
7. Proposal of the mechanism of methyl mercaptan adsorption/oxidation on activated carbons.

3. BACKGROUND

3.1. CH_3SH Adsorption on Mineral Adsorbents.

3.1.1. Metals.

Over the last decade, organosulfur chemistry on transition metal surfaces has received special attention by the surface science community due to its importance in the catalysis and fuel industries. Different metals have been tested for desulfurization purposes. Thus, the decomposition of CH_3SH has been studied on Ni (111) [153], Ni (110) [154], Ni (100) [155], Fe (100) [156], Fe (110) [157], Cu (100) [158], W (001) [159], W (211) [160], Pt (111) [161], Ru (001) [162], Mo (110) [163], Si (100) [164] and Al [165]. On the surface of these metals CH_3SH decomposes by S-H bond cleavage to form methyl thiolate intermediate (CH_3S^-). The C-S bond cleavage of the methyl thiolate has been reported on Ni (100), Ni (111), Mo (110), Fe (100), Cu (100), Si (100) and W (211), yielding methane and H_2 as gaseous products along with surface carbon and sulfur. The temperature required for C-S bond cleavage seems to be insensitive to the nature of the metal surface, occurring around 300 K in most cases.

The information regarding S-H and C-S bond-breaking in thiols is obtained from vibrational and X-ray photoelectron studies and offers a clear illustration of the use of surface spectroscopy to identify intermediates such as methyl thiolate. Vibrational spectroscopy also provides information regarding the nature of intermediates present on the surface. For example, in the case of methanethiol reaction, the absence of the ν (S-H) mode near 2570 cm^{-1} in the electron energy loss spectrum indicates that the S-H bond has been broken [155, 156, 161, 163]. All of the other losses can be assigned to vibrational modes of the methyl thiolate intermediate.

Several different mechanisms for methyl thiolate reactions have been proposed, resulting in a similar product distributions and reaction temperatures on many transition metal surfaces. Thus, the model proposed for Mo (110) [163] involves C-S bond cleavage to the corresponding radical species, which rapidly react with hydrogen to produce gaseous methane or further decompose to produce irreversibly bound hydrocarbon fragments and H_2 (Figure 4).

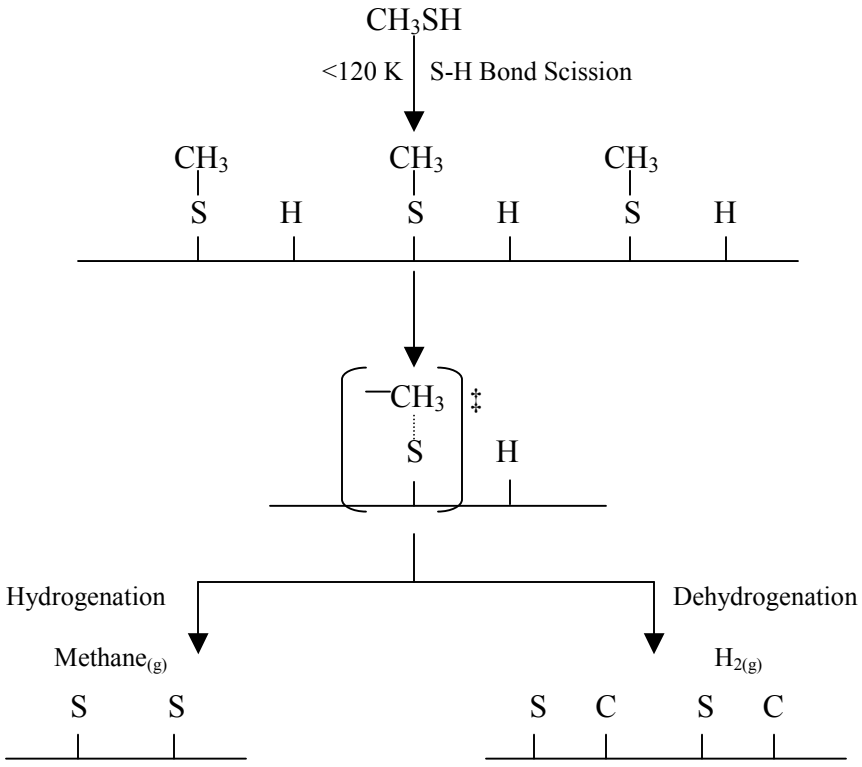

Figure 4. Scheme for methanethiol reaction on Mo (110) [163].

A similar scheme was proposed on Ni (111) [153], although ethane was a minor reaction product, presumably from CH_3 recombination. A slightly different mechanism was suggested for reaction on Fe (100) [156]: methyl radicals were formed below the methane evolution temperature trapped on the surface and produced methane after combining with surface hydrogen. A similar mechanism took place on Si (100) [164], where the scission of the C-S bond occurred at 670 K. Si (100) sample was also annealed at 870 K, which led to the removal of surface S in a form of Si-S and dehydrogenation of the proportion of CH_3 moiety to produce surface carbon.

On Pt (111) and Ni (100) surfaces, the major reaction products were hydrogen, methane, and ethylene, and both methyl thiolate and thioformaldehyde species (CH_2S^-) were reported as intermediates [155, 161]. The only other intermediate found on Pt (111) were σ–bonded SCH species [168].

It was also noticed that reactivity of the thiolates is dependent on surface coverage and therefore on intermolecular interactions. Moreover, thiol reactivity on Mo and Ni surfaces suggested that there might be slight mechanistic variations on transition metal surfaces that could be reflecting differences in hydrogenation activity [166].

The above-mentioned studies examined methanethiol decomposition on metal single crystals and provided better understanding of the desulfurization processes. However, it has been established that the most significant catalytically active component in industrial desulfurization catalysts is a metal sulfide [166, 167, 169]. It was found that sulfur inhibits C-S and C-H bond breaking on Mo (110) [169], thereby leading to a lower reactivity but higher selectivity in most cases. Related studies on other sulfided metal

surfaces, such as Fe (100) [156], Ni (110) [154], Ni (111) [153] and W (001) [159], indicate that surface sulfur indeed generally inhibits thiol reaction.

Peterson and Schulz [169] have studied ethanethiol decomposition on MoS_2 (0001) and found that ethanethiol decomposes to ethylene and hydrogen sulfide. The proposed mechanism included dissociative adsorption of ethane thiolate surface species, which underwent hydride elimination to give ethylene. Hydrogen sulfide formation was proposed to happen via hydrogen combination with lattice or adsorbed sulfur.

The proposed reaction mechanism is shown on Figure 5.

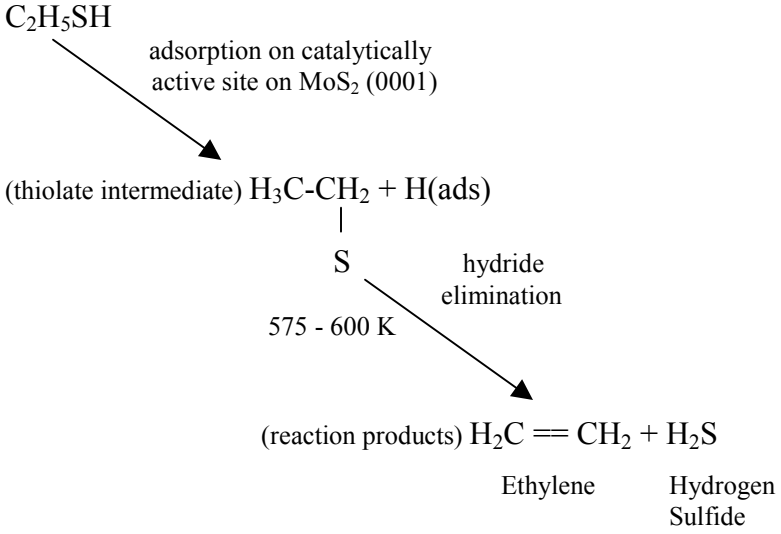

Figure 5. Proposed ethanethiol reaction pathway on a defective MoS_2 (0001) surface [169].

The ideal MoS_2 (0001) surface is terminated by large fully coordinated sulfur anions, and thus, as it was reported, lacks the reactivity. However, the surface of MoS_2 (0001) studied by Peterson and Schulz contained a sufficient amount of surface defects to cause the decomposition of ethanethiol. They suggested that most likely defects occurring on the sulfur-terminated basal plane would be sulfur vacancies, leaving coordinately unsaturated Mo^{+VI} sites. Such sites are very reactive and have been suggested as the actual sites where desulfurization occurs on industrial catalysts [170].

However, when desulfurization studies were performed on sulfided Mo (110) [169, 171], a decrease in desulfurization activity occurred (20 % that of methanethiol reacted on the clean surface), which was assigned to the blocking of the Mo surface by sulfur. A similar effect was noticed for methanethiol reaction on Fe (100), where almost all the methanethiol desorbs without decomposition, only trace amounts of methane are detected and hydrogen is not observed [156]. On Ni (110), sulfur also stabilized methyl thiolate with respect to decomposition such that the methane yield increased while the hydrogen yield decreased [154].

Furthermore, exploring the ways to increase the catalytic activity of a metal surface, oxidized metals were introduced as a new possibility of thiols' reaction with oxygen instead of sulfur [166]. The reactivity of oxidized metals is of interest because metal oxides are often used as starting catalyst materials, which subsequently react with the sulfur-containing species to generate working catalysts.

One of the metal oxides proposed for desulfurization is ZnO. It is a major component of industrial catalysts for methanol synthesis and it is also used industrially to remove sulfur from petroleum feedstock. Thus, Dvorak and coworkers have studied the

reaction of methanethiol on zinc oxide and Cs-modified zinc oxide surfaces [172]. They found that at low temperatures, methanethiol reacts via acid-base interaction with the surface, in which the thiol hydrogen is removed leading to a thiolate species coordinated to a surface zinc cation. These species are stable on the surface up to 500 K. Between 500 and 700 K, the C-S bond in the thiolate is cleaved, leaving surface-bound sulfur and carbon-containing species. The methyl groups are removed from the surface by recombination with hydrogen to yield methane and recombination with another methyl to yield ethane. The methyl groups can also undergo dehydrogenation to yield ethylene and acetylene, or partial oxidation via reaction with lattice oxygen to yield CO and formaldehyde (CH_2O). Carbon is removed from the surface as gaseous products above 500 K, and atomic sulfur remains bound to the zinc sites of the surface.

The addition of submonolayer amounts of Cs did not significantly alter the kinetics of C-S bond cleavage, whereas Cs multilayers were found to significantly lower the activation barrier for C-S bond cleavage.

The adsorption of methanethiol was also studied on SiO_2, Al_2O_3, TiO_2, and ZrO_2 [173]. It was determined that CH_3SH H-bonds with surface OH groups on all these adsorbents. For silica it is the only way for adsorption, while coordination as well as dissociative adsorption leading to formation of OH groups and molecular water occurs on the three other oxides. Two types of Brönsted acidity were established. In the presence of an excess of adsorbed sulfur-containing molecules, a reversible increase in the OH groups' acid strengths occurs for all four oxides. It was shown that molecular CH_3SH H-bonded to the oxygen atom of surface OH groups induced this effect. For silica this interaction resulted in an increase of the ν (OH) frequency shift with increasing coverage

of CH_3SH. In the case of alumina, titania, and zirconia, dissociative adsorption of CH_3SH resulted in the appearance of new OH groups that account for an increase of Brönsted acidity revealed by a high number of H-bonded CO molecules and a decreased number of Lewis acid sites that are occupied by the products of the reaction of CH_3SH with the surface (SH, OH, and H_2O). These new OH groups are the most acidic among those that normally exist on the surface of the considered metal oxides.

3.1.2. Zeolites.

Zeolites are found to be active catalysts for the decomposition of thiols and sulfides without the use of expensive hydrogen in the dehydrosulfurization process (DHS) [174]. Thus, Ziolek and coworkers used NaX, MNaY and MHNaY (M= Li, K, Rb, Cs) zeolites to study chemisorption and catalytic transformation of R_2S compounds [174]. Three kinds of the R_2S compounds have been found: (i) dissociatively-adsorbed molecules, (ii) R_2S coordinated with the extra lattice cations and (iii) hydrogen-bonded species. It was determined that transformation of R_2S compounds on zeolites depends on the nature of the adsorbed species and on the strength of C-S and S-H bonds in the adsorbed molecule. According to Mortier's electronegativity equalization principle [175], the difference in the values of the zeolite electronegativity and an electronegativity of the adsorbed molecule predicts the possibility and rate of proton transfer. Therefore, if the zeolite has a higher electronegativity than the adsorbed molecule, a proton transfer from the zeolite to the molecule can promote electronegativity equalization for the entire compound. On the other hand, if the molecule has a higher electronegativity than the zeolite, the proton transfer to the zeolite lattice occurs. Since the electronegativity of

ethanethiol used by Ziolek [174] is lower than for the zeolites applied in this study, the possibility of S-H bond dissociation was excluded. This was confirmed by the results of FTIR study of C_2H_5SH adsorption on NaX and NaY zeolites. These results indicated that the cleavage of the S-H bond does not occur because a band at ~2550 cm^{-1} (ν (S-H)) is present in both IR spectra (on NaX and NaY) and no OH groups were generated as a result of a proton attack on the zeolite oxygen. Moreover, a broad band at ~3400 cm^{-1} was observed, showing the hydrogen bonding between C_2H_5SH molecules and the zeolite surface.

Garcia and Lercher [176], on the basis of the spectroscopic measurements, proposed the following models for the thiol-adsorbed structures on the hydrogen forms of the zeolites:

(a)

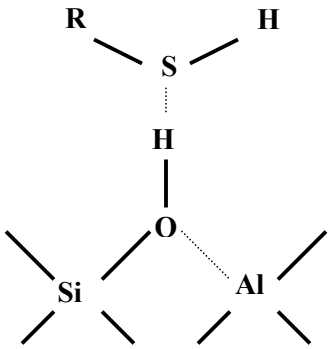

(b)

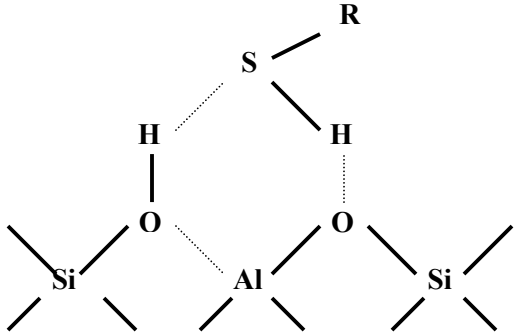

They also concluded that thiol interaction with the acidic OH groups of the zeolites depends on both the strength of the zeolite acidity and the nature of thiol.

The situation became different when various alkali-metal-exchanged Y zeolites [174] were applied. Such zeolites are more active in the transformation of thiols than their

hydrogen forms. Thus, spectroscopic studies showed that the coordinative bonding between sulfur from thiol and alkali metal cation of the zeolite occurs and leads to the weakness of the C-S bond. More so, the conversion of ethanethiol decreased with the decrease of the cations Lewis acidity. However, not only Lewis acidic sites were found to be involved in the coordinative adsorption of C_2H_5SH in the thiol transformation but also Lewis basic centers.

The products of ethanethiol decomposition at 623 K included hydrocarbons, sulfides and thiophene as a side reaction product. Distribution of the products varied between alkali-metal-exchanged zeolites and their protonated forms. Thus, a high selectivity to thiophene was observed on MNaY, whereas MNaHY exhibited a high selectivity to diethyl sulfide [174].

3.2. CH_3SH Adsorption on Activated Carbons.

Unlike such sulfur-containing molecules as hydrogen sulfide and sulfur dioxide, not too many studies have been done on the adsorption of methanethiol (also called methyl mercaptan) (MM) on activated carbons. Those few papers that have been published give some insight on the studies of the oxidation mechanism of methyl mercaptan on activated carbons [152, 177] as well as on the effect of carbon surface impregnation on the adsorption ability of MM [178-180].

In the work of Katoh and coworkers [152] the oxidation mechanism of CH_3SH was studied on the wet activated carbon fiber (ACF). ACF was made from coal tar and had a surface area of 1300 m^2/g, micropore radius of 9Å, and micropore volume of 0.8 cm^3/g. It was also found to contain 98 ppm of iron.

As a result of MM adsorption/oxidation, DMDS was formed stoichiometrically from MM and was detected in the outlet of the ACF column. However, when MM was mixed with H_2S, complete oxidation to methane sulfonic acid has been reported [152].

Katoh and coworkers also studied the possible mechanism of MM removal by ACF. They explained the oxidation of MM based on the chemical activity of superoxide anion radical (O_2^- ·) formed in the reaction of a thiolate radical (CH_3S·) with oxygen. They also suggested that on the wet ACF surface O_2^- · could slowly be changed into hydrogen peroxide (H_2O_2) by reaction with H^+. It was also noted that iron present in ACF could catalytically participate in the oxidation process by the following reaction pathways:

$$Fe^{2+} + H_2O_2 \rightarrow Fe^{3+} + OH^- + OH\cdot \quad (3.1)$$

$$Fe^{3+} + O_2^{-}\cdot \rightarrow Fe^{2+} + O_2 \quad (3.2)$$

Furthermore, complete oxidation to methane sulfonic acid was accomplished in a mixed supply of MM with H_2S. Oxidation process was reported to go through the oxidation of DMDS (formed by partial oxidation of MM) with OH radical:

$$2\ CH_3SH \rightarrow CH_3SSCH_3 \quad (3.3)$$

$$CH_3SSCH_3 + 6\ OH\cdot \rightarrow 2\ CH_3SO_3H \quad (3.4)$$

In a different work, Dalai and coworkers [177] used Hydrodarco activated carbon catalyst (ICI America Inc. Wilmington, DE). The characteristics of this carbon included

surface area of 487 m^2/g, mean pore radius of 2.9 nm, and total pore volume of 1.0 cm^3/g. The feed gas contained 1000 ppm of MM in N_2 with the O_2/CH_3SH ratio varying from 1.1 to 1.33 times the stoichiometric ratio. Experiments were performed for 3-hour periods in a fixed bed reactor containing 0.25-5.0 g of Hydrodarco activated carbon. The temperature and pressure ranges were 323-448 K and 122-364 kPa respectively.

As a result of adsorption/oxidation process DMDS and water were formed. However, when the supply of air for oxidation was cut off, the only product to appear in the outlet stream was MM. This indicates that MM was oxidized with oxygen and mostly to DMDS with the trace amounts of CS_2 and $(CH_3)_2S$ produced at 473 K. Carbon dioxide was also produced in small quantities and increased with reaction temperature as well as with the supply of oxygen to the reaction. It was established that CO_2 production could be kept at minimum by using an O_2/CH_3SH ratio in the feed gas close to 1.1 times the stoichiometric ratio. As a result, a higher conversion of CH_3SH could be achieved.

According to Dalai et al. the following reaction mechanism is taking place:

Sorption

$$O_2 + 2\ X \rightarrow O\text{-}X + O\text{-}X \quad (3.5)$$

$$CH_3SH + X \rightarrow CH_3SH\text{-}X \quad (3.6)$$

where X represents an active site.

Surface reactions

$$2\ CH_3SH\text{-}X + O\text{-}X \rightarrow (CH_3)_2S_2\text{-}X + H_2O\text{-}X + X \quad (3.7)$$

$$(CH_3)_2S_2\text{-}X \rightarrow (CH_3)_2S_2 + X \quad (3.8)$$

$(CH_3)_2S_2\text{-}X + 7\ (O\text{-}X) \rightarrow 3\ (H_2O\text{-}X) + 2\ (CO_2\text{-}X) + 2\ (S\text{-}X) + X$ (3.9)

$S\text{-}X + 2\ (O\text{-}X) \rightarrow SO_2\text{-}X + 2\ X$ (3.10)

$H_2O\text{-}X \rightarrow H_2O + X$ (3.11)

$CO_2\text{-}X \rightarrow CO_2 + X$ (3.12)

$SO_2\text{-}X \rightarrow SO_2 + X$ (3.13)

Based on these reactions the following conclusions were made. The sorption of SO_2, CO_2, and H_2O is molecular, while that of oxygen (3.5) is dissociative. Surface reactions (3.8) and (3.9) are competitive with the latter one only taking place if the excess of O_2 is present in the feed stream. The surface reaction (3.7) is rate controlling due to assumed negligible external mass transfer and pore diffusional resistances.

Finally, authors have developed the rate equation and showed that the conversion of MM is largely influenced by its partial pressure and is almost independent from the partial pressure of O_2.

Furthermore, some authors have tried to modify the activated carbon surface in order to increase the removal of CH_3SH [178-180].

Thus, Shin and coworkers used KI, KIO_3, Na_2CO_3, and NaOH to impregnate activated carbon fibers of different origin [178, 179]. Among those was cellulose-based, polyacrylonitrile-based, phenol resin-based, and pitch-based.

The adsorption characteristics of MM and the adsorption equilibrium have been studied using Bench-scale apparatus and Cahn balance, respectively [179]. The concentration of MM was 100 ppm, inlet flow rate 0.5 L/min, and the mass of the sample 15 mg. Before impregnation, adsorption amounts of MM were 75 mg/g for PAN-based,

47.6 mg/g for cellulose-based, 31.3 mg/g for phenol resin-based, and 19.2 mg/g for pitch-based ACF respectively. Clearly, PAN-based and cellulose-based appeared to be the most effective for MM removal and were treated with impregnation chemicals mentioned above. As a result of impregnation, the capacity of carbon samples was increased to a different extent depending on an impregnation component. Thus, Na_2CO_3 and NaOH did not significantly affect the adsorption capacity of MM, while KI and KIO_3 increased it highly. More so, cellulose-based ACF was more effective for KI and KIO_3 impregnation than PAN-based ACF. The increase in capacity for cellulose-based ACF was about 200 times for both KI and KIO_3, resulting in capacity values of more than 8,000 mg/g.

The adsorption capacities for activated carbon were smaller than for ACF, which could be due to various factors. ACF, which comes in many forms of material, can have larger surface area than activated carbon, is highly microporous and exhibits a higher mass transfer rate for adsorption and desorption processes [181].

Even though no reaction mechanism was proposed, the authors indicated that catalytic decomposition of MM on KIO_3/ACF and KI/ACF is likely to take place.

Turk and coworkers proposed another activated carbon modification approach [180]. They used ammonia in conjunction with granular activated carbon (GAC) for the removal of H_2S and CH_3SH from air streams. Both virgin and caustic coal-based activated carbon samples were used in the experiments. For the tests with MM, the following experimental conditions were applied: gas mixture of 350 ml/min of 1% CH_3SH in nitrogen, 1090 ml/min of purified air saturated with moisture, and a 10 ml/min stream of ammonia, for a total flow of 1450 ml/min at a CH_3SH concentration of 2400

ppm by volume. Effluent CH_3SH was monitored by smell to a definite recognition threshold of 2×10^{-3} ppm [180].

The results showed an advantage of 8:1 for the NH_3/GAC process over virgin carbon and of 3:1 and 4:1 over activated carbon impregnated with KOH and NaOH, respectively.

Due to the presence of moist air, oxidation of MM took place and it was presumably converted to DMDS. Though no reaction mechanism was suggested for MM adsorption using NH_3/GAC process, it is likely to be similar to H_2S adsorption, which proceeds in the following way:

$$3\ NH_3 + 3\ H_2S \leftrightarrow 3\ NH_4HS \quad \text{(fast equilibrium)} \quad (3.14)$$

$$NH_4HS + 1.5\ O_2 \rightarrow NH_4HSO_3 \quad \text{(rate controlling)} \quad (3.15)$$

$$NH_4HSO_3 \leftrightarrow NH_3 + SO_2 + H_2O \quad \text{(fast equilibrium)} \quad (3.16)$$

$$2\ NH_4HS + SO_2 \rightarrow 3\ S + 2\ NH_3 + 2\ H_2O \quad \text{(fast redox)} \quad (3.17)$$

$$3\ H_2S + 1.5\ O_2 \rightarrow 3\ S + 3\ H_2O \quad (3.18)$$

In this process ammonia plays a role of a catalyst, thus facilitating the adsorption process and production of elemental sulfur in the case of H_2S or DMDS in the case of MM.

4.EXPERIMENTAL SECTION

4.1. Materials.

4.1.1. Choice of Carbons.

Adsorption of MM was performed on five activated carbon samples of various origins. The carbons studied were BAX-1500 (wood based carbon from Westvaco), S208 (coconut shell based carbon from Waterlink Barnabey and Sutcliffe), PCB (coconut shell based carbon from Calgon Carbon), Centaur® (bituminous coal based catalytic carbon from Calgon Carbon), and BPL (bituminous coal based carbon from Calgon Carbon).

All of the initial and modified carbon materials (see below) were subjected to CH_3SH adsorption in the dynamic breakthrough capacity test descried in the "Methods" section. After stopping the test and purging the carbon samples with air, they were considered exhausted and designated with an additional letter "E".

To evaluate the dual role of water (section 5.6) two more carbons were added to the study: Maxsorb carbon (mesophase pitch based from Kansai) and SCN polymer based synthetic carbon [49].

4.1.2. Washing of Carbons.

Initial samples were washed with water in a Soxhlet apparatus to a constant pH of the leachate. Those carbons that were not washed with water are referred to "as received".

4.1.3. Oxidation of Carbons with H_2O_2.

Four of the water-washed carbon samples (BAX, S208, PCB, and BPL) were oxidized with hydrogen peroxide. Briefly, 10 grams of carbon were treated with 100 mL of 35 % H_2O_2 and left on the stirrer for 22 hours. After this treatment, the samples were washed in a Soxhlet apparatus to remove excess oxidant and other water-soluble species. Final samples are referred to as BAX-O, S208-O, PCB-O, and BPL-O.

4.1.4. Treatment of Carbons with Urea/Introduction of Nitrogen Functionalities.

In order to introduce nitrogen groups, four of the water-washed carbons (BAX, S208, PCB, and BPL) were treated with a saturated solution of urea. Briefly, 10 grams of carbon were treated with 60 ml of saturated urea and left on the stirrer for 48 hours. The urea-treated samples were heated in nitrogen at the rate of 10ºC/min to 450 and 950ºC and maintained at these temperatures for 1 hour. After heat treatment the samples were water-washed to remove any excess of urea decomposition products. The modified carbons are referred to as for instance, BAXU-450, where U refers to urea modification and 450 represents the temperature of heat treatment.

These four urea-treated samples were compared to some nitrogen-containing carbons, which were polymer based (SCN-1, SCN-3, SCN-4 [45, 53, 54]) and bituminous coal based (Centaur®, mentioned earlier). SCN-1 was obtained by carbonization of vinyl pyridine resin at 950^{o}C in argon atmosphere. SCN-3 and SCN-4 were derived from SCN-1 using steam activation to the 20 and 50% burn off, respectively.

4.1.5. Impregnation of Carbon with $FeCl_3$ Solution.

To account for the effect of ash and its iron constituent, the PCB sample (25 ml), which has a very small amount of iron, was impregnated with 0.050 M solution of $FeCl_3$ x $6H_2O$ (100 ml), left on the stirrer for 20 hours, heated at 200 ºC for 3 hours and washed with water in a Soxhlet apparatus to remove excess of iron and chloride. The obtained sample was mixed for 5 hours with a small volume of 0.010 M NaOH to increase the pH to the level where dissociation of CH_3SH is enhanced. Final sample is designated as PCB/Fe.

4.2. Methods.

4.2.1. Adsorption of MM.

Dynamic tests were carried out at room temperature to evaluate the capacity of the sorbents for CH_3SH removal under wet conditions. The schematic view of the experimental set-up is presented in Figure 6. Adsorbent samples were ground (1-2 mm particle size) and packed into a glass column (length 370 mm, internal diameter 9 mm, bed volume 6 cm^3) and prehumidified with moist air (relative humidity 80 % at 25^oC) for one hour. The amount of water adsorbed was estimated from the increase in the sample weight. Moist air (relative humidity 80 % at 25^oC) containing 0.3 % (3,000 ppm) CH_3SH was then passed through the column of adsorbent at 0.5 L/min. The breakthrough of CH_3SH was monitored using a Micromax monitoring system (Lumidor) with an electrochemical sensor calibrated with MM. The test was stopped at the breakthrough concentration of 50 ppm.

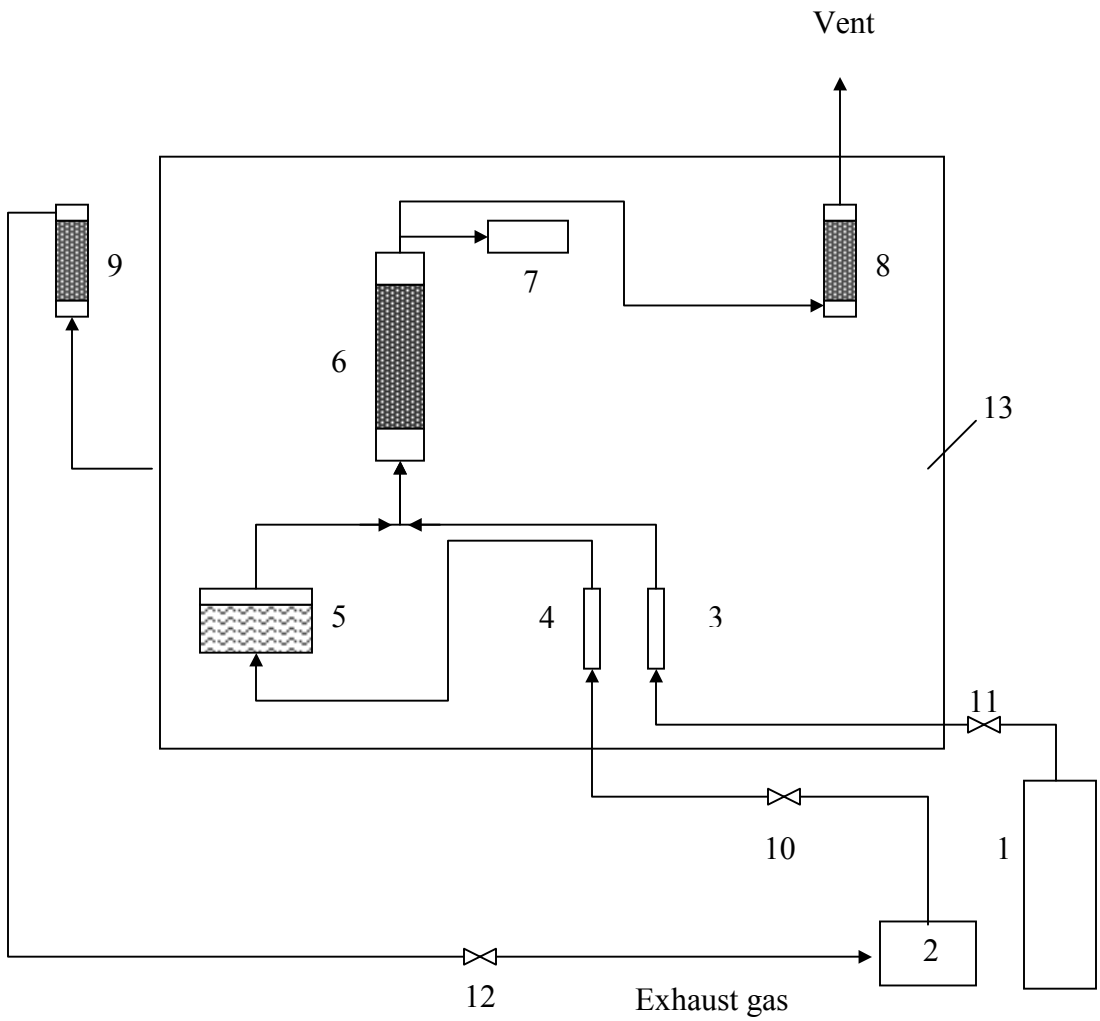

Figure 6. Schematic for the breakthrough capacity test apparatus (1 - MM cylinder, 2 - air pump, 3 - MM flowmeter, 4 - air flowmeter, 5 - water container (humidifier), 6 – carbon column for MM, 7 - MM sensor, 8,9 - carbon columns (IVP 4x6 with NaOH) for exhaust gas, 10,11,12 – valves, 13 - experimental chamber).

The adsorption capacity of each sorbent (A) in terms of mg of CH_3SH per g of carbon was calculated by integration of the area above the breakthrough curve, and from the CH_3SH concentrations in the inlet flow (C_{inlet}) and outlet flow (C_{outlet}), flow rate (Q), breakthrough time (t_{brthr}), and mass of sorbent (m_s).

$$A = [Q*(C_{inlet} - C_{outlet})*t_{brthr}] / m_s \quad (4.1)$$

For each sample the CH_3SH test was repeated at least twice. The determined capacities agreed to within 4 %.

4.2.2. Adsorption of DMDS at Saturated Conditions.

A beaker with 30 mL of DMDS was placed in a dessicator along with several 10 mL weighing dishes containing 0.2 g of powdered carbon samples each. The samples were kept in an atmosphere saturated with DMDS vapors for 4 days (vapor pressure of DMDS at 20°C is equal to 22.1 Torr [182]). It was assumed that the adsorption equilibrium was reached.

4.2.3. Boehm Titration.

One gram of carbon sample was placed in 50 mL of the following 0.050 N solutions: sodium hydroxide, sodium carbonate, sodium bicarbonate and hydrochloric acid. The vials were sealed and shaken for 24 hours. 10 mL of each filtrate, excess of base or acid, were titrated with HCl and NaOH, respectively. The number of acidic sites of various types was calculated under the assumption that NaOH neutralizes carboxylic, phenolic, and lactonic groups, Na_2CO_3 carboxylic and lactonic groups, and $NaHCO_3$

only carboxylic groups [26]. The number of surface basic sites was calculated from the amount of hydrochloric acid used for neutralization.

4.2.4. Potentiometric Titration.

Potentiometric titration measurements were performed with a DMS Titrino 716 automatic titrator (Metrohm) [94, 95, 183]. The instrument was set to the equilibrium pH mode. Subsamples of the carbons of about 0.100 g in 50 mL 0.01 M $NaNO_3$ were placed in a container thermostated at 25°C and equilibrated overnight with the electrolyte solution. To eliminate the influence of atmospheric CO_2, the suspension was continuously purged with N_2. The carbon suspension was stirred throughout the measurements. Volumetric standard NaOH (0.10M) was used as a titrant. The experiments were done in the pH range of 3-10. Each sample was titrated with base after acidifying the carbon suspension. The titration curves were then transformed into proton binding isotherms *Q (pH)*, by using the proton balance equation [94]. It was assumed that the system consists of acidic sites characterized by their acidity constants, K_a. The fraction of sites, which are protonated at certain *pH*, *q (pH, pK_a)*, depends on their pK_a value according to the following form of the Langmuir equation:

$$Q\ (pH, pK_a) = 1/[1+10^{(pH-pKa)}] \qquad (4.2)$$

The population of sites can be described by a continuous pK_a distribution, *f (pK_a)*. The proton binding isotherm, *Q (pH),* incorporating the experimental results and representing the total amount of protonated sites is related to the pK_a distribution by the following integral equation:

$$Q(pH) = \int_{-\infty}^{\infty} q(pH, pK_a) f(pK_a) dpK_a \quad (4.3)$$

The integral is solved numerically using SAIEUS (solution of adsorption integral equation using splines) procedure [95, 184]. The SAIEUS software is designed to take more information from titration data than can be done by simple mathematics and permits calculation of the pK_a of acidic sites with different acidities. SAIEUS has been tested using simulated data and experimental titration data of organic standards, and it was demonstrated that this method could completely resolve peaks that are less than 1 pK_a unit apart.

4.2.5. Thermal Analysis.

Thermal analysis was carried out using TA Instruments Thermal Analyzer (New Castle, DE, USA). The instrument settings were: heating rate 10^{o}C/min in either air or nitrogen atmosphere at 100 ml/min flow rate. Three sets of data were collected with respect to temperature. These are weight (TG), derivative of weight (DTG), and derivative of temperature (DTA) between the sample and the blank scale. The latter provides information about the type of reaction (exothermic or endothermic) that is taking place at specific temperature.

4.2.6. Inverse Gas Chromatography (IGC) at Infinite Dilution.

IGC is a variation of a classical chromatographic method. The term “inverse” indicates that the stationary phase, not solute, is under investigation [110, 185]. In our case IGC is applied to the investigation of solid surface (carbon) properties.

When the experiment is carried out at infinite dilution, the small amounts of solutes are injected and it is assumed that the Henry’s law governs the adsorption. The lateral interactions are considered to be negligible due to the extremely low concentration of the adsorbate. This assumption leads to the calculation of the Henry’s constant, which is important for the prediction of the adsorption isotherms.

The chromatographic experiments were performed with an SRI gas chromatograph equipped with a flame ionization detector. The stainless steel columns (20 cm long, 2.17 mm in diameter) were filled with carbon particles of size ranging from 0.2 to 0.4 mm. Helium was used as a carrier gas with a flow rate of 33-340 cm^3/min, and methane was used as a non-retained species. The samples were conditioned at 200 ºC in the chromatographic column under helium gas flow for 18 h prior to the measurement. The injection volume was in the range of 0.6 to 1.0 ml of 0.5% mixture of CH_3SH in nitrogen. The range of experimental temperatures was 150-200ºC (10ºC steps). Under these conditions, all chromatographic peaks were symmetrical and retention times did not depend on the amount injected.

Retention volume V_N is a fundamental quantity measured in this method. It is independent of the amount injected and can be calculated by the formula:

$$V_N = J^*(t_R - t_m)^*F_c \qquad (4.4)$$

where J is a the James-Martin compressibility factor which is dependent upon the pressure drop along the chromatographic column [191], t_R and t_m are the retention times for adsorbate and non-retained species, respectively, and F_c is the flow rate of the carrier gas estimated for the column temperature.

V_N is also directly related to the standard free energy of adsorption:

$$\Delta G = -R*T*ln\ (B*V_N / S*m) \tag{4.5}$$

where R and T are the gas constant and the temperature of the measurement, B is the constant related to the standard states of gas and adsorbed phases, and m and S are the mass and specific surface of the adsorbent.

Another quantity used to derive thermodynamic parameters of the adsorption process is the specific retention volume, V_S, which is calculated from the equation:

$$V_S = V_N\ / S*m \tag{4.6}$$

The isosteric heat of adsorption Q_{st} at zero surface coverage can be easily calculated from the measurements of V_S or V_N at various temperatures:

$$Q_{st} = R*[\partial\ ln\ (Vs/T) / \partial\ (1/T)] \tag{4.7}$$

4.2.7. Gas Chromatography-Mass Spectrometry (GC/MS).

GC/MS study was done using Shimadzu Gas Chromatograph /Mass Spectrometer model QP 5050. The separation was done on Shimadzu XTI- 5 column (bonded 5 % phenyl) 30 m long and 0.25 mm internal diameter. The column temperature was programmed from 30^{o}C to 250^{o}C at 10-deg/min. The column was held for 10 min at 250^{o}C. The injector temperature was 60^{o}C.

The results were analyzed using an unrestricted library search. The samples for analysis were extracted by placing 1.2 ml of carbon in a vial where 2 ml of methanol were added. Then the suspensions were heated at 60^{o}C for 1 hour. After separation of liquid phase from carbon, 0.5 μl of extracted solution was injected to the GC column. The mass spectra were collected for M/Z ranging from 12 to 500.

4.2.8. Ash Content Analysis.

Total ash content was evaluated as a residue left after heating the sample in air at 10^{o}C/min to 1000 ºC using TA Instruments Thermal Analyzer.

4.2.9. Elemental Analysis.

The content of carbon, hydrogen, and nitrogen was determined by Huffman Laboratories, Golden CO.

4.2.10. Sorption of Nitrogen.

Nitrogen isotherms were measured using an ASAP 2010 (Micromeritics) at -196^{o}C. Before the experiment the samples were heated at 120^{o}C and then outgassed overnight at this temperature under a vacuum of 10^{-5} Torr to a constant pressure. The

isotherms were used to calculate specific surface areas (S), micropore volumes (V_{mic}), volume of pores less than 10 Å and less than 50 Å, total pore volumes (V_t), average micropore sizes (L_{mic}) and pore size distributions. All these parameters were obtained using density functional theory, DFT [80-83]. Characteristic energy of adsorption (E_o) was calculated from Dubinin-Radushkevich (DR) approach [186, 187].

DFT method is based on the description of the density profile of the adsorptive as a single inhomogeneous phase near the surface of the adsorbent. The free energy of this inhomogeneous phase can be expressed as a function of the local concentration, ρ(r), where r is the generalized coordinate vector.

The adsorption isotherm reflects the net adsorptive energy distribution of the material, which is a function of its geometry. For the activated carbon it is assumed that (1) carbon has slit pore geometry, (2) the aspect ratio of pore length to pore width is large, and (3) the concentration of surface functional groups is low and can be disregarded. With these assumptions, pore size distribution *f (H)* of the sorbent involves the solution of the adsorption integral [80, 81, 84]

$$Q(p) = \int dH\, q(p, H)\, f(H) \tag{4.8}$$

where *Q (p)* is the total quantity of adsorbate per gram of adsorbent at pressure *p*, *q (p, H)*, the kernel function, describes the adsorption isotherm for an ideally homoporous material characterized by pore width *H* as quantity of adsorbate per square meter of pore surface, and *f (H)* is the desired pore surface area distribution function with respect to *H*.

Since we are usually only interested in the numerical values of *f (H)*, equation (4.8) can be rewritten as a summation [80, 81, 84]

$$Q(p) = \sum_{i} q(p, H_i) f(H_i) \tag{4.9}$$

where $Q(p)$ is an experimental adsorption isotherm interpolated onto a vector p of pressure points, $q(p, H_i)$ is a matrix of values for quantity adsorbed per square meter, each row calculated for a value of H at pressures p, and $f(H_i)$ is the solution vector whose terms represent the area of surface in the sample characterized by each pore width H_i.

Adsorption isotherms obtained from the deconvolution result in equation (4.9) are fitted to the preexisted adsorption isotherms until the best fit is found. Two independent constraints can be used to stabilize the solution. One is the physical requirement that each f_i be non-negative, that is, only positive values of pore area and pore volume are allowed. The second regularization constraint is to require that for any real sample, the pore distribution should be smooth.

By fitting the set of hybrid models constructed as the function $q(p, H_i)$ to the experimental adsorption isotherms $(Q(p))$ differential and cumulative pore volume and pore area distributions by pore width could be obtained.

The characteristic energy of adsorption, E, can be found from DR equation [187]

$$V(p, T) = V_0 * \exp\left[-(A / E)^n\right] \tag{4.10}$$

where V is the adsorption amount as a function of pressure, p, and temperature, T; V_0 is the limiting volume of adsorption or the volume of the micropores; parameter n is equal to 2; and A is the change of Gibbs free energy on adsorption, defined by

$$A = -\Delta G = R * T * \ln(p_0 / p) \tag{4.11}$$

where R is the gas constant and p_0 is the saturation pressure of an adsorbate.

Moreover, if E_0 is the characteristic energy of adsorption of a standard vapor (usually of benzene on active carbon), then the characteristic adsorption energy E of another vapor or gas is given by the expression [186]

$$E = \beta * E_0 \tag{4.12}$$

where β is a similarity coefficient of the characteristic curves calculated as a ratio of parachors ($\beta = p / p_0$).

Then, the equation (4.10) can be rearranged in the following form:

$$V(p, T) = V_0 * \exp\{- [2.303 * R / E_0]^2 * [T / \beta]^2 * \log^2 (p / p_0)\} \tag{4.13}$$

where:

$$B = [(2.303 * R) / E_0]^2 \tag{4.14}$$

This parameter can be determined experimentally by plotting the adsorption isotherm of $\log V$ versus the $\log^2 (p_0 / p)$ in its linear form [186] and then used for the calculation of E_0 and E.

4.2.11. X-Ray Fluorescence Analysis (XRF).

XRF analysis was applied to study the elements present in carbon. For this purpose SPECTRO Model 300T Benchtop Multi-Channel Analyzer from ASOMA Instruments, Inc. was used. It contained a titanium (Ti) target X-ray tube with Mo-2mil filter and high-resolution detector without a filter. A home-developed method was selected to identify the metals. Acquisition conditions were the following: voltage 24 kV, current 80μA, count time 40 sec, and warm-up 4 min. Instrument reference temperature was 20 ˚C; background conditions: lower ROI – 12.000, upper ROI – 17.000. The amount of iron in carbon was determined based on the calibration curve.

4.2.12. pH of the Carbon Surface.

Carbon powder (0.4 g) was placed in 20 ml of water and equilibrated during the night. Then the pH of the suspension was measured.

5. RESULTS AND DISCUSSION

5.1. Surface Chemistry Characterization.

The surface chemistry of activated carbons can be characterized in terms of the number and strength of acidic and basic groups present on their surface. This information could be found from the results of Boehm titration [26] and should be related to the pH of the carbon surface.

First, initial carbons were water washed and characterized by Boehm titration. Then their modified counterparts obtained by oxidation with hydrogen peroxide and urea treatment were analyzed by Boehm titration. These results are presented in Table 1 [189, 192, 193]. For the Centaur® carbon as well as for the urea treated carbons, due to the presence of nitrogen-containing functionalities, only the total number of basic and acidic species is reported.

Among the initial carbons, BAX carbon is the one with the largest amount of groups on its surface. Its number of acidic groups is exceeding the number of basic groups, which is also reflected on a lower pH value compared to other carbon samples. Centaur®, BPL and S208 carbons with the pH values of 6.66, 6.97 and 7.47, respectively are slightly more basic than BAX with the pH of 6.00. PCB carbon is the most basic with the highest amount of basic groups and the highest pH value of 7.74.

Table 1. Results of Boehm Titration [mmol/g] and pH of the Carbon Surface Before and After MM Adsorption.

Sample	Carboxylic	Lactonic	Phenolic	Acidic	Basic	All	pH	pHE
BAX	0.20	0.21	0.49	0.90	0.35	1.25	6.00	5.46
BAX-O	1.20	0.05	1.15	2.40	0.60	3.00	4.07	3.30
BAX-U450	NA	NA	NA	0.80	0.90	1.70	6.18	5.45
BAX-U950	NA	NA	NA	0.70	0.65	1.35	7.43	4.88
BPL	0.00	0.05	0.45	0.50	0.40	0.90	6.97	4.20
BPL-O	0.10	0.20	0.20	0.50	0.40	0.90	6.60	3.92
BPL-U450	NA	NA	NA	0.50	0.55	1.05	7.84	5.98
BPL-U950	NA	NA	NA	0.35	0.60	0.95	8.46	3.67
S208	0.00	0.05	0.30	0.35	0.45	0.80	7.47	5.94
S208-O	0.10	0.10	0.15	0.35	0.45	0.80	8.13	5.75
S208-U450	NA	NA	NA	0.38	0.55	0.93	8.49	6.56
S208-U950	NA	NA	NA	0.30	0.65	0.95	9.41	6.77
PCB	0.00	0.00	0.25	0.20	0.50	0.70	7.74	5.51
PCB-O	0.05	0.18	0.28	0.51	0.35	0.86	6.35	4.57
PCB-U450	NA	NA	NA	0.50	0.60	1.10	8.81	7.26
PCB-U950	NA	NA	NA	0.35	0.60	0.95	9.07	7.35
Centaur®	NA	NA	NA	0.25	0.40	0.65	6.66	3.42

Hydrogen peroxide is considered to be a weak oxidant, slightly changing the amount of oxygen-containing groups on the surface but preserving the carbon pore structure [188, 189]. Indeed, in the case of BPL, PCB, and S208 carbons, only small changes in the amount of oxygen-containing groups were noticed. These changes are demonstrated mainly by the increase in the number of carboxylic and lactonic groups. For BPL-O and S208-O a decrease in the number of phenolic groups is found, whereas the total number of groups is unchanged. For PCB-O the amount of acidic groups increased and the amount of basic groups decreased, which is also reflected by a significantly lower pH value (Table 1).

On the other hand, the BAX carbon is very susceptible to oxidation [189-191], which results in a significant increase of oxygen-containing groups on the surface. Thus, a 2-fold increase in the number of basic groups and a 3-fold increase in the number of acidic groups (mainly carboxylic and phenolic) were observed. Therefore, this carbon material still remains acidic and its surface pH is decreased compared to the initial sample.

Urea treatment introduces nitrogen-containing groups into the carbon matrix. Urea-treated samples heated at 450°C have nitrogen bonded to the surface in the form of -CN, -NH, $-NH_2$, or NH^{4+} species, which decompose at high temperature [37, 43]. On the other hand, urea-treated carbon samples carbonized at 950°C result in a majority of nitrogen incorporated into the carbon matrix in a pyridine-like or "quaternary" configuration [43, 47, 49-51, 105] (Figure 7). Introduction of these species raises the basicity of the carbon surface and this effect is more pronounced for the high temperature

treated samples [192]. This is shown in Table 1 by an increase in the amount of basic groups on the surface as well as by a quite significant raise in pH.

The results of elemental analysis are presented in Table 2 [192]. Urea modification increases the percentage of nitrogen in the carbon matrix, which is higher for low temperature treated samples. Changes in the degree of carbonization are expressed in Table 2 by changes in the carbon and hydrogen content.

Table 2. Results of Elemental Analysis for the Carbon Materials Studied.

Sample	% C	% H	% N
BAX	73.80	3.64	0.19
BAX-U450	75.02	2.46	9.30
BAX-U950	75.44	2.31	3.05
BPL	91.23	0.47	0.44
BPL-U450	86.36	0.73	3.65
BPL-U950	86.61	0.75	1.14
S208	79.01	0.67	0.12
S208-U450	85.92	1.27	1.67
S208-U950	89.69	0.89	0.93
PCB	90.88	1.09	0.11
PCB-U450	89.95	1.06	0.70
PCB-U950	89.65	1.02	0.43
Centaur®	90.60	0.70	1.10

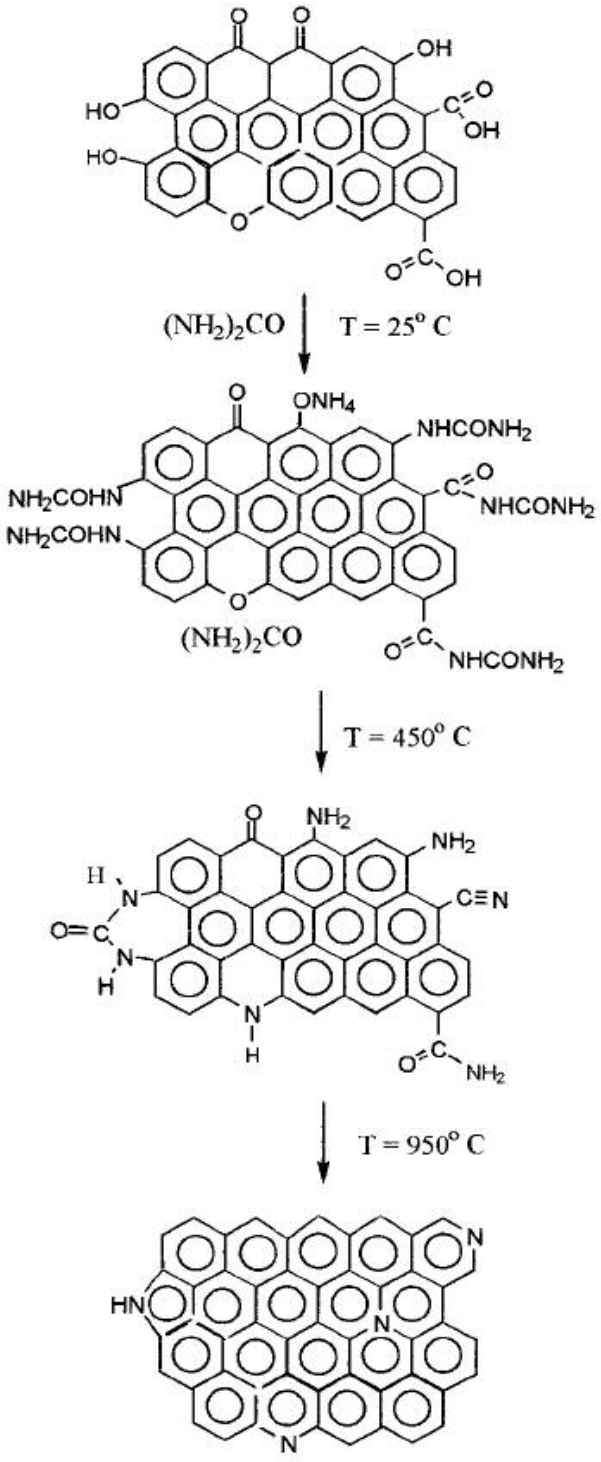

Figure 7. Changes in the surface chemistry of carbons due to saturation with urea and heat treatment [43].

The nitrogen content for the Centaur® sample, which is commercially produced by impregnation with nitrogen-containing species, is the closest to that of BPL-U950, which is interesting in terms of comparing the effect of nitrogen on their MM adsorption abilities. Nevertheless, BAX-U950 has even higher nitrogen content than Centaur® carbon, which is likely the result of differences in the degree of carbonization of the initial carbons and their surface areas. BAX is a low temperature carbon with a high content of different surface groups. Its high surface area [43, 189, 192] increases the accessibility of the crystallite edges to incorporate nitrogen.

Potentiometric titration is another method used to see the changes in acidity of the carbon surface. The proton binding curves can be calculated as described in section *4.2.4*. They are analyzed from the point of view of proton uptake (basic) and proton release (acidic) and indicate significant changes in the chemical character of the surface.

The proton binding curves for the initial and oxidized carbon samples are presented in Figure 8. Only a slight increase in acidity, represented by a decrease in the amount of protonated sites (Q values) is noticed for PCB, S208, and BPL carbon samples. On the other hand, a drastic change is found for the BAX carbon, which acidity significantly increased. These changes in acidity after oxidation are consistent with the results of the Boehm titration. An exception is the BPL carbon, whose total acidity according to the Boehm titration has not been changed. Nevertheless, the decrease in pH of this carbon likely caused by the increased amount of strong acidic groups on its surface may also be represented as a decreased amount of protonated sites on the proton-binding curve.

More detailed information about the species present on the carbon surface can be obtained from the pK_a distributions. These can be calculated using the SAIEUS procedure [94, 95, 183, 184, 189], which applies a stable numerical method for the solution of the adsorption integral (equation 4.3).

The proton binding curves for the initial and oxidized carbon samples are shown in Figure 9 [189] in the range of acidity constants between 3 and 11. The common feature for the initial carbons is the presence of the first three peaks at pK_a*'s* about 4.6, 6.0 and 7.5, which correspond to carboxylic acids and their derivatives [94]. For example acetic acid has a pK_a of 4.76 and malonic acid a pK_a of 5.70 [193]. Peaks with pK_a values higher than 8 are referred to phenols and their derivatives [94]. One of these peaks is placed in the pK_a range of 8.3 to 9.7 and another one in the range of 10 to 10.4 (pK_a of phenol is 9.95 [193]).

After oxidation with hydrogen peroxide a slightly larger number of groups is detected for all the samples. More specifically, for BPL carbon the main increase was found in the number of carboxylic groups having pK_a*'s* of 4.7 and 7.5 and instead of two peaks at pK_a 9.0 and 10.0 only one peak at pK_a 9.7 is displayed. This is consistent with the results of the Boehm titrations, which show an increase in the number of carboxylic groups and a decrease in the number of phenolic groups after oxidation. For S208 carbon an increase was found in intensity of all the peaks. The only discrepancy with the Boehm titration for this carbon was in the amount of phenolic groups, the number of which has decreased according to the Boehm titration. The most visible changes for the PCB carbon have happened in the pK_a range of 7 to 8.The peak at pK_a 7 disappeared and a broader peak at pK_a about 8 is found. The disappearance of the first peak is likely related to the

removal of some species after H_2O_2 treatment. However, the broadening of the second peak could be due to the formation of more species with pK_a about 8.

Finally, as it was noticed before, oxidation had a significant impact on the acidity of the BAX carbon. Noticeable differences exist between the distributions obtained for BAX and BAX-O. Although the peaks have similar positions (similar pK_a), the number of acidic groups considerably increased after oxidation, especially in the range of carboxylic acids, which was also observed from the Boehm titration results.

Proton binding curves for the urea-treated carbon samples are presented in Figure 10 [192]. They clearly show that after modification with urea and heat treatment at 950°C all carbons became much more basic than their initial counterparts. It is interesting that nitrogen incorporated into the carbon matrix at 450°C makes BPL-U450 and BAX-U450 look slightly more acidic than the initial samples. This fact is possibly related to the protonation of amine- and cyano- type groups. These groups may not be detected by Boehm titration resulting in a discrepancy between these two methods. On the contrary, S208-U450 and PCB-U450 have become slightly more basic, which is in agreement with the results of the Boehm titration. These distinctions between the samples suggest some differences in nitrogen incorporation caused by different degrees of aromatizaton of the carbons studied.

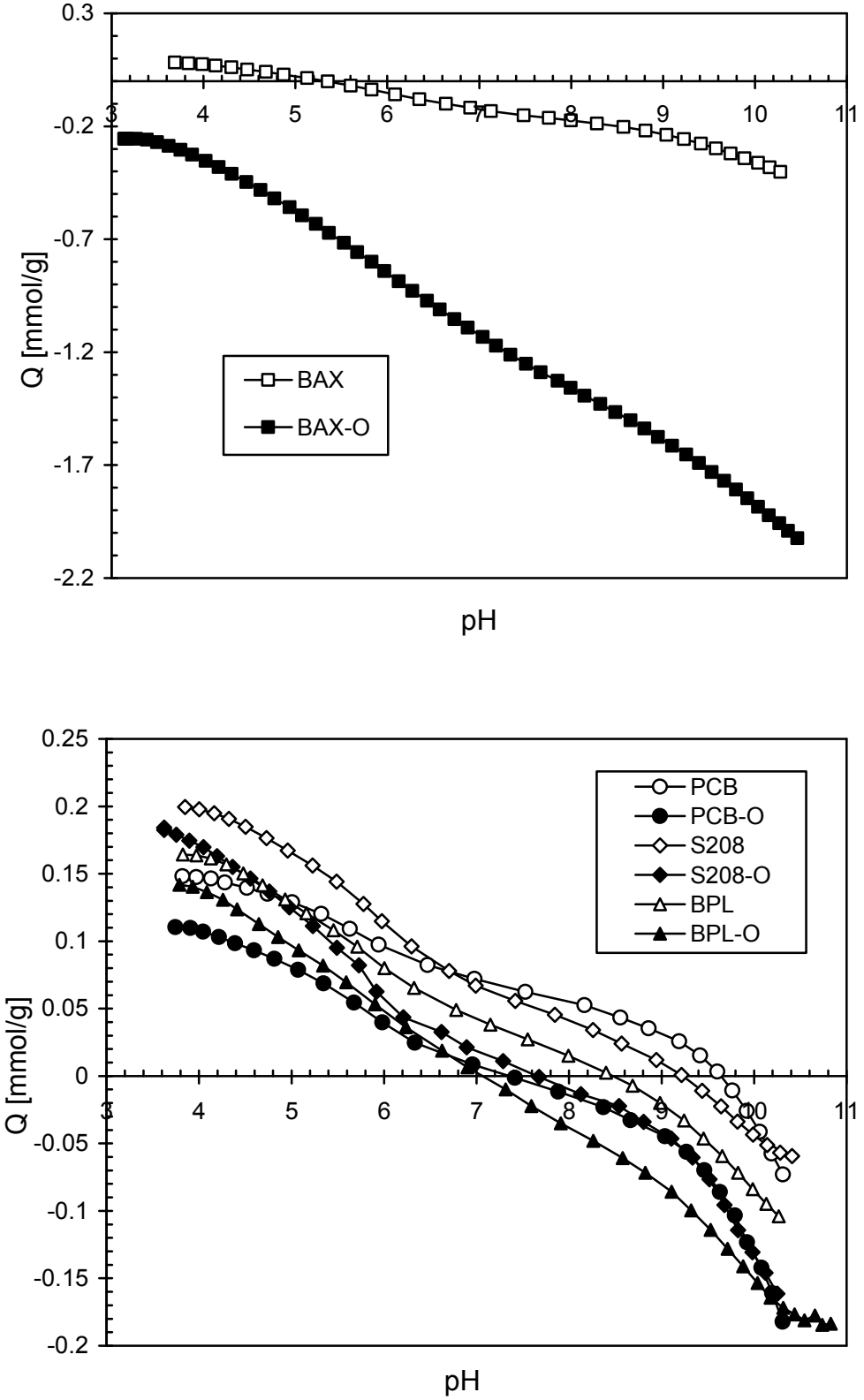

Figure 8. Proton binding curves for the initial and oxidized carbon samples.

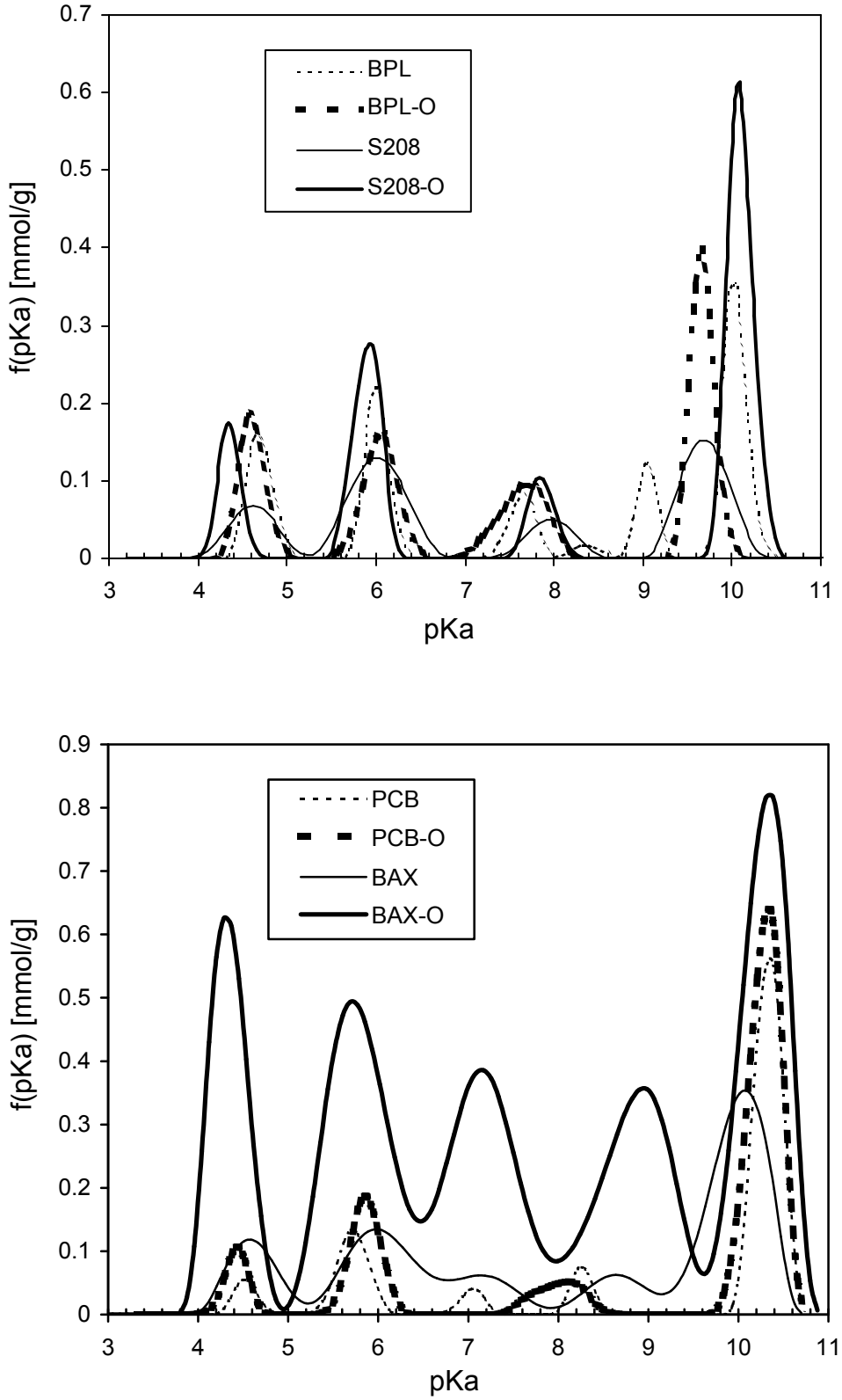

Figure 9. pK_a distributions for the initial and oxidized carbon samples.

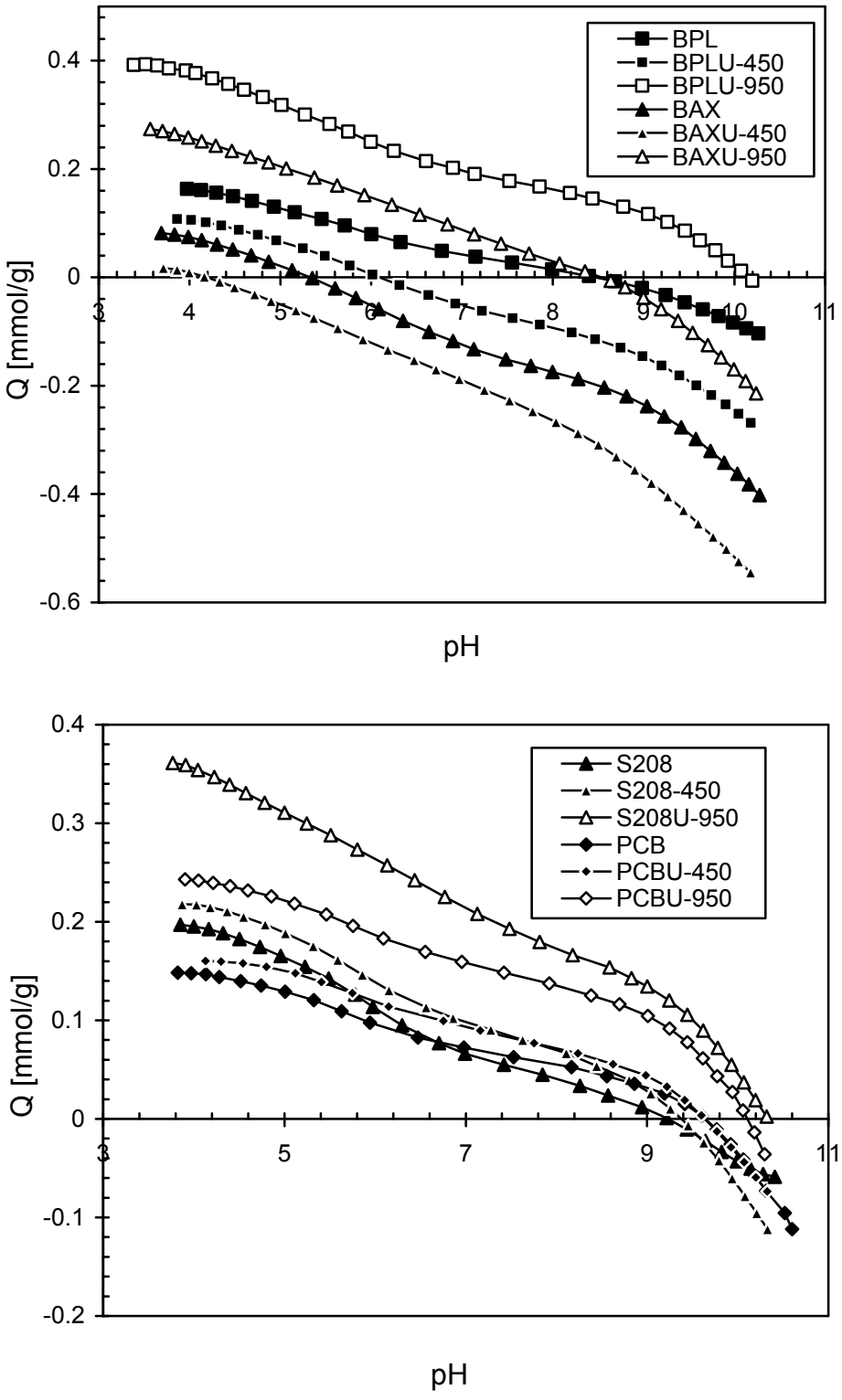

Figure 10. Proton binding curves for the initial and urea-modified carbon samples.

The inorganic phase (ash) present in all of the carbon samples may also contribute to the overall basicity of the carbon surface and influence the MM adsorption /oxidation process. That is why ash was evaluated for the initial samples using thermal gravimetry as described in section *4.2.8* [43, 191, 194]. As seen from Table 3, BPL carbon has the highest amount of ash and S208 carbon the lowest amount. For BAX, PCB and Centaur® samples, the percentage of ash is about the same.

For more detailed analysis, the quality and relative quantities of different metals present in ash were evaluated. This was carried out by the XRF technique and the results are presented on Figure 11 [194].

The most predominant metals found in ash are aluminum, potassium and iron. Moreover, BPL, which has the highest ash content, appears to be rich in iron. The amount of iron in BPL was estimated to be ≈ 0.45 %, which is similar only to that of Centaur® (Table 3). S208 carbon has a much smaller content of iron but has a significant amount of potassium, a natural component of its coconut shell precursor. The other two samples, PCB and BAX, contain only scanty amounts of all the detected metals, even though the amount of ash for both carbons is higher than that for S208 carbon. The plausible explanation for this could be the presence of other metals in these two samples, which are not detected by XRF in the energy range studied.

However, not all of the metals will catalytically enhance the adsorption of MM. From previous research on adsorption of MM [152] it was hypothesized that iron present in activated carbons could catalytically participate in the adsorption/oxidation process. If this proves to be true, BPL and Centaur® carbons are expected to have higher MM adsorption capacities than other carbons. Besides, it was proven by some researchers

[178, 179] that activated carbons impregnated with potassium species have higher MM adsorption capacities than their initial counterparts. This fact could favor the adsorption of MM on S208 carbon and result in a significant capacity value. In such a case, PCB and BAX carbons are expected to have lower capacities than other three samples.

Nonetheless these assumptions are true only if the presence of such catalytically active metals as iron and potassium is a primary factor for the effective MM removal. Otherwise such factors as the amount of basic and acidic groups on the surface, surface pH, structural parameters and the presence of water may all influence the adsorption of MM on activated carbons.

Table 3. The Amount of Ash Content for the Initial Carbon Samples.

Sample	Ash content [%]	Fe [%]
BAX	2.11	0.04
BPL	8.96	0.45
S208	1.22	0.09
PCB	2.76	0.07
Centaur®	2.90	0.36

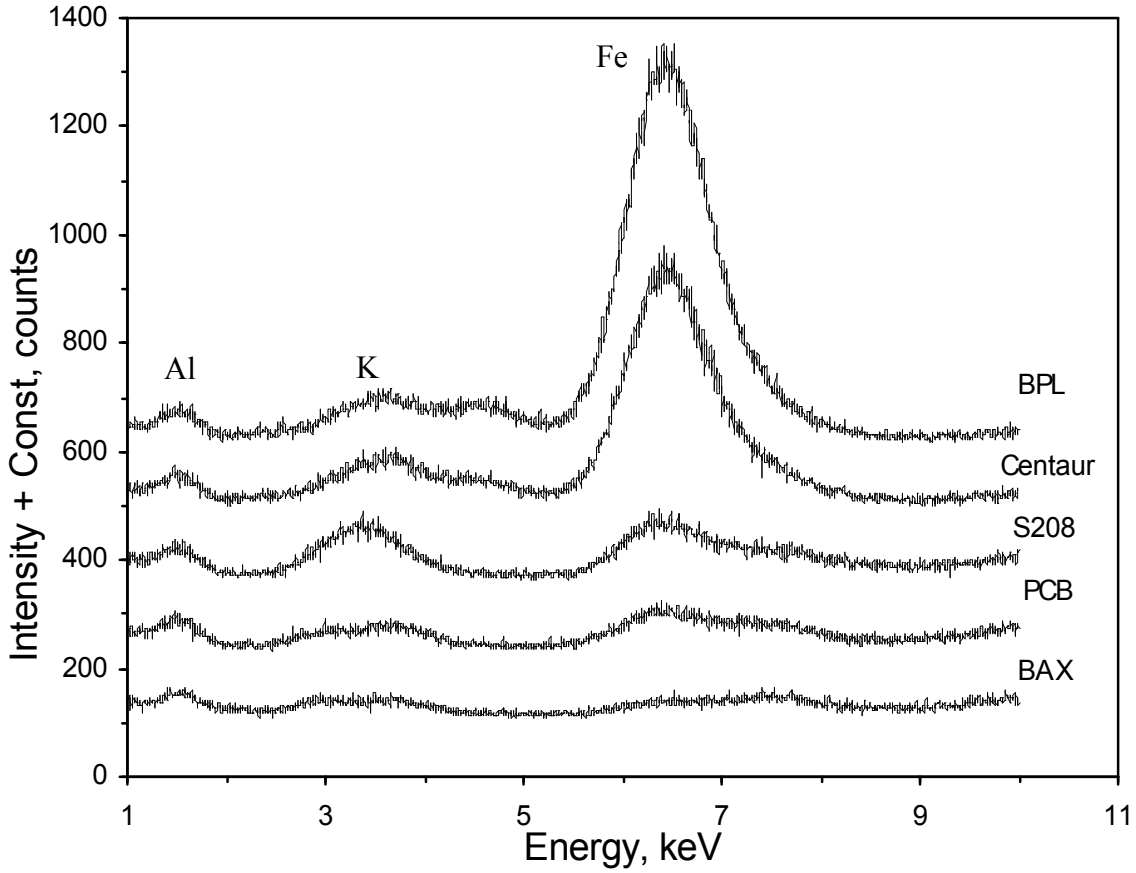

Figure 11. Results of XRF analysis for the initial carbon samples.

5.2. Structural Parameters of Activated Carbons.

Large surface area and developed pore structure are highly important for the effective adsorption/oxidation process. The products of surface reactions are stored inside the carbon pores and the process is more effective the closer are the dimensions of the pore to the size of the adsorbed molecule. For the pores that are no more than a few molecular diameters in width, the potential fields from neighboring walls will overlap and the interaction energy of the carbon with a gas molecule will be correspondingly enhanced.

Structural parameters of different carbons depend both on the carbon precursor and the method of its activation. Therefore each carbon has a different pore structure, which could be either favorable or unfavorable for a particular type of molecule.

Nitrogen adsorption isotherms for the carbons studied were measured at the boiling point of nitrogen at –196ºC and for the initial carbon samples are presented on Figure 12. From this figure it is clear that BAX carbon follows the type IV isotherm with a characteristic hysteresis loop [2]. This type of isotherm indicates the presence of mesoporosity, which causes an increase in adsorption. This increase could be explained by the capillary condensation theory [2]. According to this theory, adsorption is restricted to a thin layer on the walls along the initial part of the isotherm until the inception of the hysteresis loop brings the beginning of capillary condensation in the finest pores. As the pressure is progressively increased, the capillary condensation spreads to wider and wider pores until at the saturation pressure the entire system is full of condensate.

PCB, S208 and Centaur® carbons all follow the type I isotherm characteristic of a microporous solid [2]. Interpretation of this type of isotherm accounts for the fact that the uptake does not increase continuously but comes to a limiting value displayed by a plateau, which is nearly or quite horizontal. Many type I isotherms exhibit no hysteresis at all (Centaur®), while others display a definite loop, which may or may not persist to the lowest pressures.

Unlike other four carbons, BPL carbon cannot be characterized by a single type of isotherm, it has features of both type I and type IV isotherms, thus exhibiting the characteristics of both meso- and microporous carbons.

These structural patterns are also preserved for the oxidized and urea treated carbon samples, which are characterized by the same type of isotherms as their initial counterparts (Figures 13 and 14). The most significant differences are noticed for the BAX-O and BAX-U950 carbon sample, which clearly became more microporous and now structurally resemble the BPL carbon. It is also worth mentioning that in general the surface areas of all the carbons were reduced after their modifications.

The more detailed information can also be obtained from the pore size distributions (PSDs) presented in Figure 15 and 16 [189, 192]. From Figure 15 it is seen that PCB, S208 and Centaur® carbons are all homogeneous in terms of their porosity with most of the pores being micropores (≤ 20 Å). Among them Centaur® has the lowest volume of pores and both S208 and PCB have high volume of pores, with the majority of the S208 carbon's pores being less than 10Å.

On the other hand, BAX carbon is structurally very heterogeneous and has a high volume of both meso- and micropores. In comparison to BAX, BPL carbon has approximately half of its pore volume but the pore size distribution patterns of these two carbons are very similar to each other.

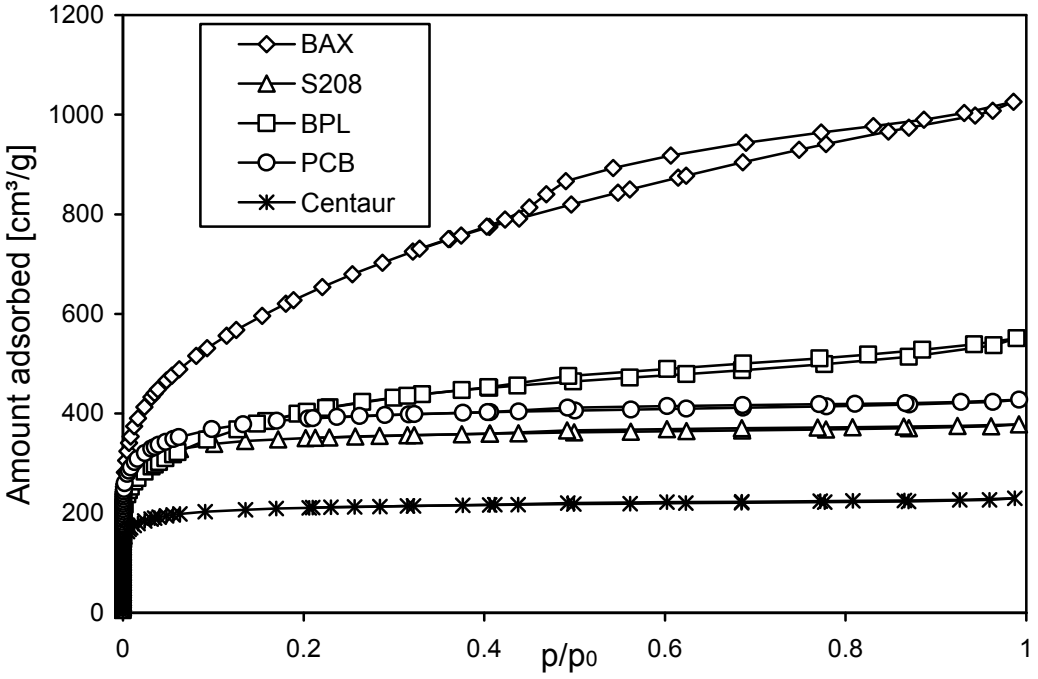

Figure 12. Nitrogen adsorption isotherms measured at –196°C for the initial carbons.

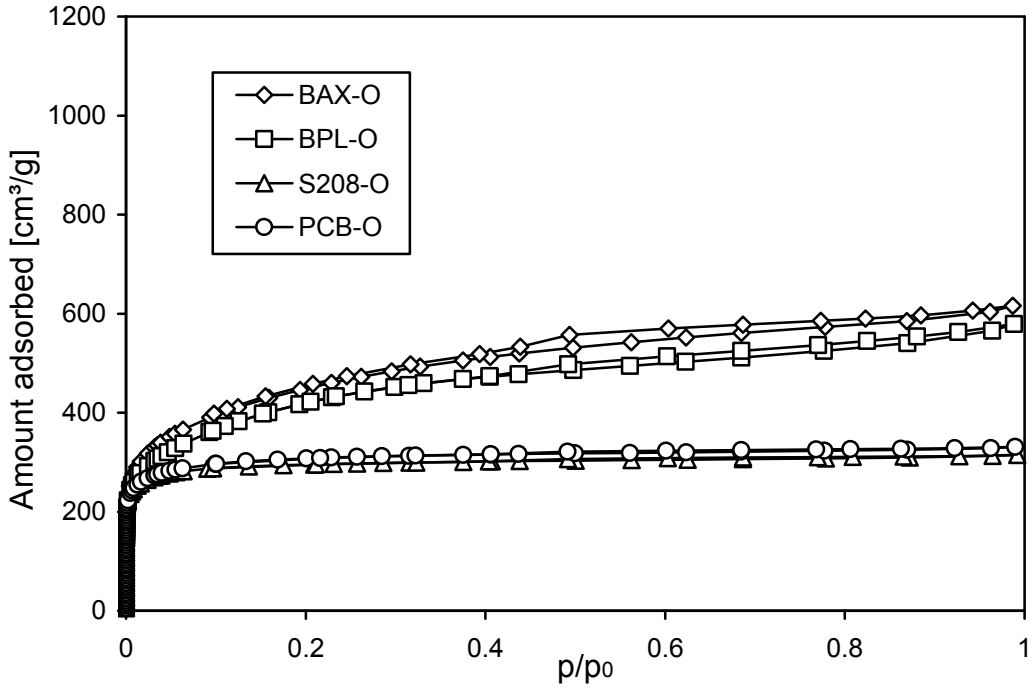

Figure 13. Nitrogen adsorption isotherms measured at –196°C for the oxidized carbons.

a)

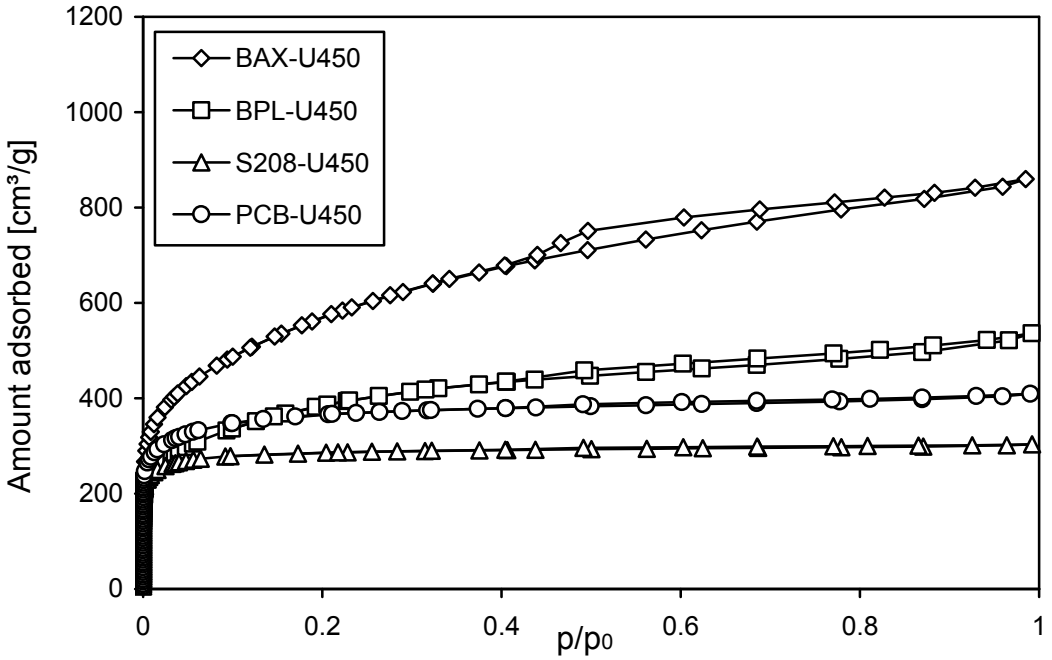

b)

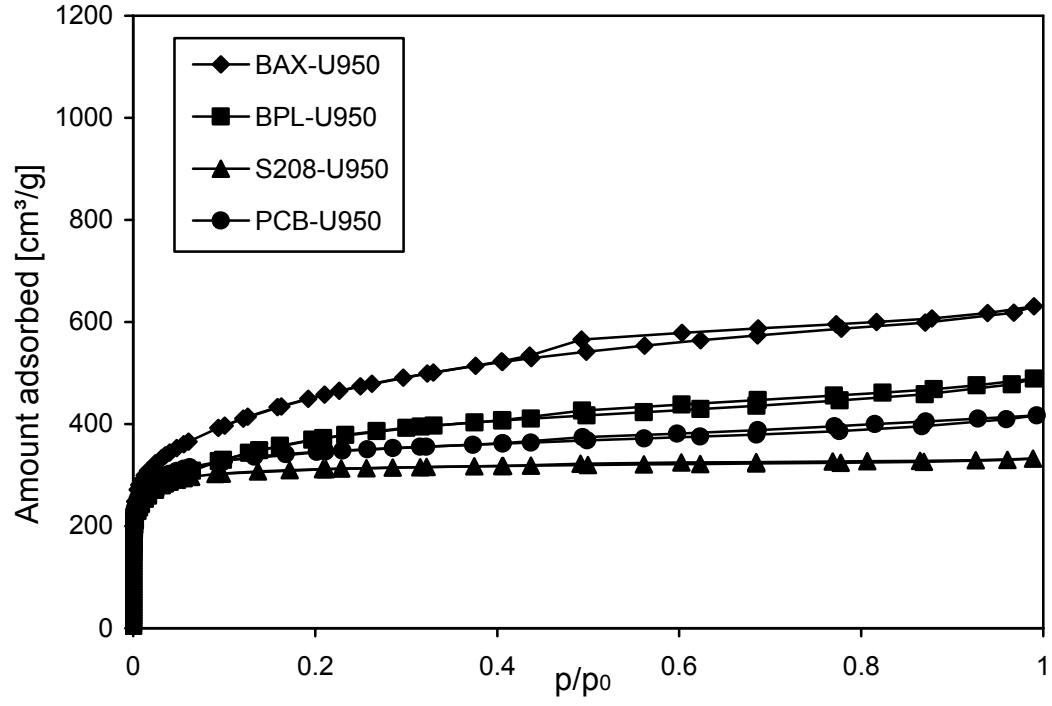

Figure 14. Nitrogen adsorption isotherms measured at –196°C for the urea-treated carbons carbonized at a) 450ºC and b) 950ºC.

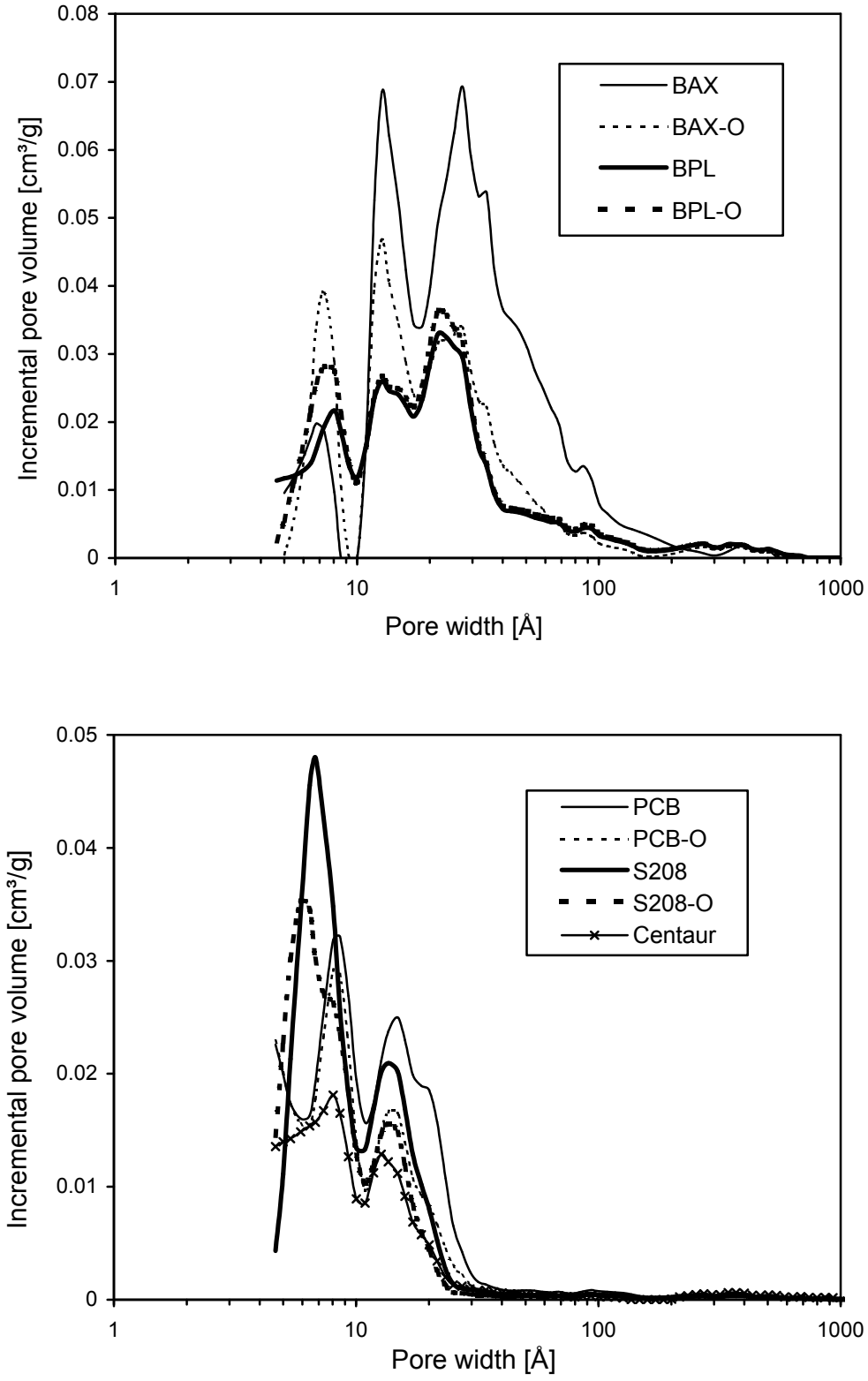

Figure 15. Pore size distributions (PSDs) for the initial and oxidized carbon samples.

The structural parameters of the carbons were calculated from the nitrogen adsorption isotherms at –196ºC by applying the DFT approach. The results of these calculations are collected in Table 4 [189, 192, 194]. They show that the BAX carbon has the highest surface area and the largest volume of pores among the carbons studied, which however may not be enough for the efficient MM removal. Taking into account the small size of the MM molecule (4.19Å [147]) pores smaller than 10 Å should be the most active in the MM adsorption process. The volume of these pores for the BAX carbon is very small, which in addition to its large average micropore size and correspondingly small energy of adsorption makes this carbon unfavorable for the adsorption of MM.

S208 carbon is more microporous than PCB and as was already shown in the PSDs it has the highest volume of pores less than 10 Å. Moreover, from Table 4 it is seen that the average micropore size (L_{mic}) of S208 carbon is smaller than that of PCB but slightly higher than that for Centaur®. The latter carbon has a low surface area and a small volume of pores but its relative microporosity (V_{mic}/V_t) is high and a very small L_{mic} value found for this carbon leads to the high energy of adsorption. These characteristics could make Centaur® carbon very effective in terms of its porosity for the adsorption of MM.

Finally, BPL carbon has about the same volume of meso- and micropores, which makes it not quite as microporous as S208, PCB and Centaur® but more microporous than BAX carbon. Its volume of pores less than 10 Å is higher than that for the BAX carbon, which in combination with a much smaller L_{mic} value makes BPL structurally more favorable than BAX for MM adsorption.

As it was mentioned earlier, oxidation with hydrogen peroxide was performed in order to slightly change the surface chemistry of the carbon but to preserve its pore structure. Indeed this task was accomplished with some changes in porosity taking place upon oxidation. The surface areas and total pore volumes of BAX, PCB, and S208 carbons were decreased with a strongest effect noticed for the first two carbons. This effect may be the result of the blockage of some pores with surface oxidation products. In general, BAX carbon became more microporous, as it was observed earlier from its nitrogen adsorption isotherm (Figure 13), with a much higher relative microporosity and a smaller average micropore size. Besides, for the BAX carbon an increase was found in the volume of pores less than 10 Å, which is clearly observed from its pore size distributions (Figure 15). Some changes are also noticed for S208 carbon in the pores less than 10 Å. Even though the volume of these pores for S208-O is about the same as for S208, the distribution of pores in this region was changed and now two peaks instead of one are displayed (Figure 15). The latter fact may also have contributed to a very small L_{mic} value and a very high E_{ads} value for the S208-O sample. The decrease in average micropore size was also noticed for PCB-O carbon and its energy of adsorption went up.

No significant structural changes were noticed for the BPL carbon but unlike other three carbon samples, its surface area increased slightly, which is mainly related to an increase in the volume of pores less than 10 Å and mesopore volume (Figure 15).

Table 4. Structural Parameters of Carbons Calculated from Adsorption of Nitrogen at –196ºC.

Sample	S_{DFT} [m^2/g]	V_{mic} [cm^3/g]	V_t [cm^3/g]	$V_{<10Å}$ [cm^3/g]	V_{mic}/V_t	L_{mic} [Å]	E_{ads} [kJ/mol]
BAX	1351	0.50	1.29	0.10	0.39	13.2	15.8
BAX-O	1055	0.44	0.77	0.15	0.57	12.1	17.4
BAX-U450	1315	0.50	1.09	0.11	0.45	12.5	16.6
BAX-U950	1087	0.40	0.80	0.17	0.50	11.5	19.1
BPL	953	0.37	0.69	0.16	0.54	11.7	18.1
BPL-O	1016	0.40	0.72	0.18	0.56	11.7	17.5
BPL-U450	901	0.35	0.68	0.15	0.52	11.7	18.1
BPL-U950	1024	0.39	0.76	0.17	0.52	11.7	17.8
S208	1084	0.44	0.46	0.30	0.93	9.7	21.4
S208-O	990	0.37	0.39	0.28	0.95	8.8	23.1
S208-U450	892	0.34	0.39	0.25	0.88	9.0	23.3
S208-U950	1038	0.40	0.42	0.28	0.95	9.0	22.5
PCB	1018	0.43	0.55	0.25	0.79	10.6	20.9
PCB-O	853	0.34	0.37	0.23	0.91	9.7	22.8
PCB-U450	1118	0.44	0.52	0.28	0.86	9.9	21.1
PCB-U950	928	0.38	0.54	0.23	0.70	10.2	21.4
Centaur®	617	0.24	0.29	0.16	0.83	9.5	22.8

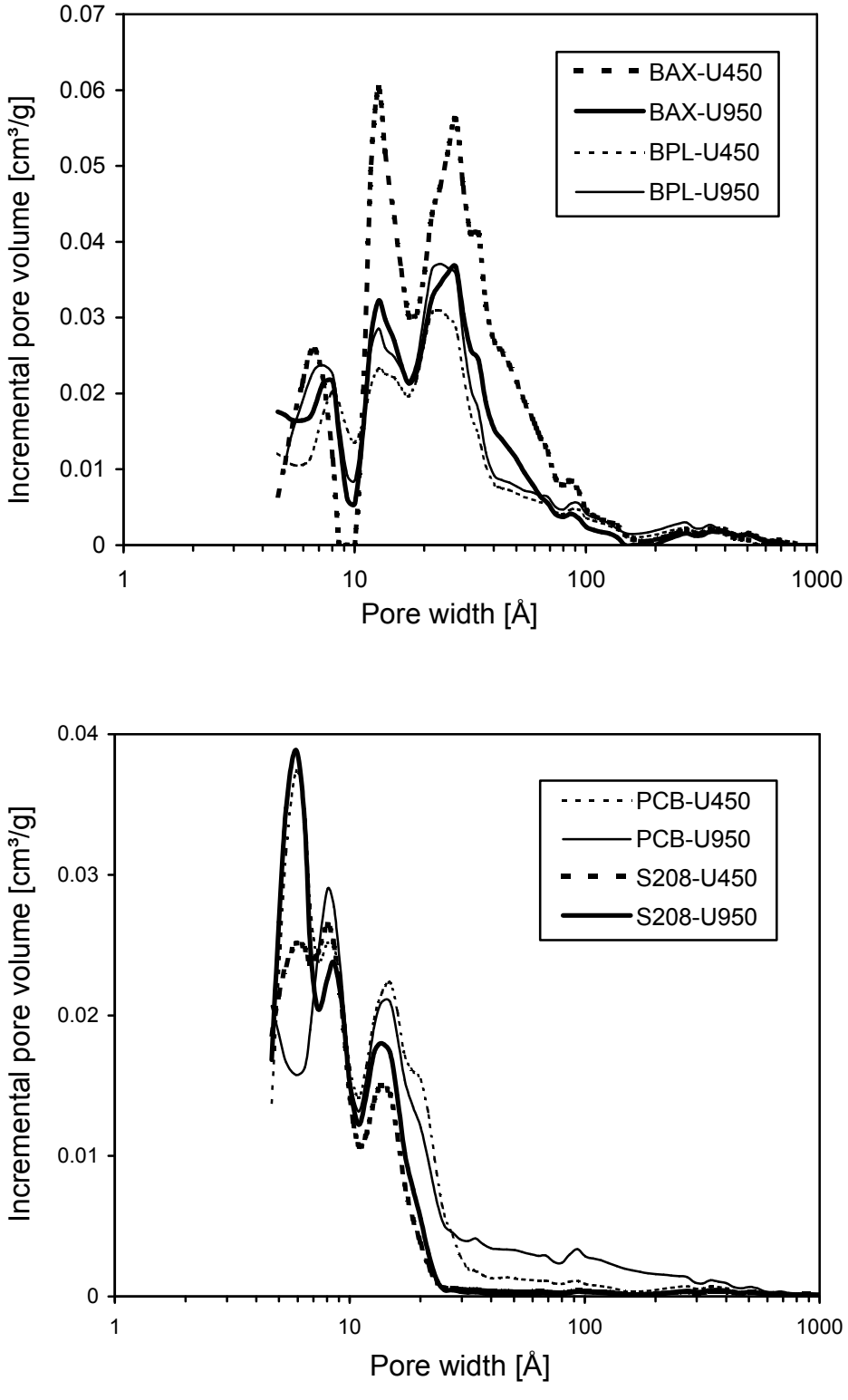

Figure 16. Pore size distributions (PSDs) for the urea-treated carbon samples.

Urea treatment introduced nitrogen functionalities into the carbon matrix, which for the most of the samples caused a decrease in the surface area and pore volumes. Carbonization of the urea-treated samples at 450ºC had a very small effect on the structural parameters of the carbon samples. Almost nothing changed for the BPL carbon but for the other three carbons the main change occurred in the average micropore size, which became smaller. What is interesting is that there is a change in distributions of pores smaller than 10 Å after urea treatment and carbonization at 450ºC for the microporous carbons S208 and PCB (Figure 16). The same effect was noticed earlier for the S208-O sample, which tells us about the possible incorporation of oxygen- and nitrogen-containing functionalities inside the very small pores and the formation of new pores.

Carbonization at 950ºC had a considerable effect on the urea-treated BAX sample. As for the BAX-O sample the surface area and pore volumes of BAX-U950 decreased but $V_{<10Å}$ and relative microporosity significantly increased. Modifications also resulted in a decrease of L_{mic}, which became even smaller than that for the BPL carbon and elevated the characteristic energy of adsorption. The average micropore size of S208-U950 became smaller as well. This carbon again shows two peaks in the region of pores less than 10 Å but unlike its 450ºC heated counterpart the peak with a maximum at 6 Å is of a higher intensity than the peak with a maximum at 9 Å (Figure 16). As for the PCB-U950, its structural parameters remained almost unchanged except for L_{mic}, which became slightly smaller and elevated the energy of adsorption.

5.3. CH_3SH Adsorption and Breakthrough Capacities.

Table 5. Adsorbate Parameters.

Parameter	H_2O	MM	DMDS
Boiling Point (ºC)	100	6	109.6
Saturated Vapor Pressure at 25ºC (kPa)	3.17	202.3	3.83
Liquid Density at 25ºC (g/cm^3)	1	0.87	1.06
Critical Temperature (ºC)	374	470	570
Critical Pressure (kPa)	2240	5530	4280
Critical Volume (cm^3/mol)	56	145	290
Critical Density (g/cm^3)	0.32	0.33	0.32
Parachor	52.6	121	212
LJ Parameters:			
Molecular Diameter, σ_{ff} (Å)	3.48	4.19	5.27
Well Depth, ε_{ff} (K)	271	422	511

Assuming that DMDS is the main product of MM adsorption/oxidation on the carbon surface [152, 177-180], the predicted amounts of MM and DMDS adsorbed can be calculated based on the DR approach [187, 195]. It is also implied that due to a larger size and higher boiling point of DMDS (Table 5) it will adsorb more strongly on the carbon surface than MM [147].

Three specific carbons used in this study, S208, BAX, and Centaur® were chosen and the predicted isotherms are presented in Figure 17 [195].

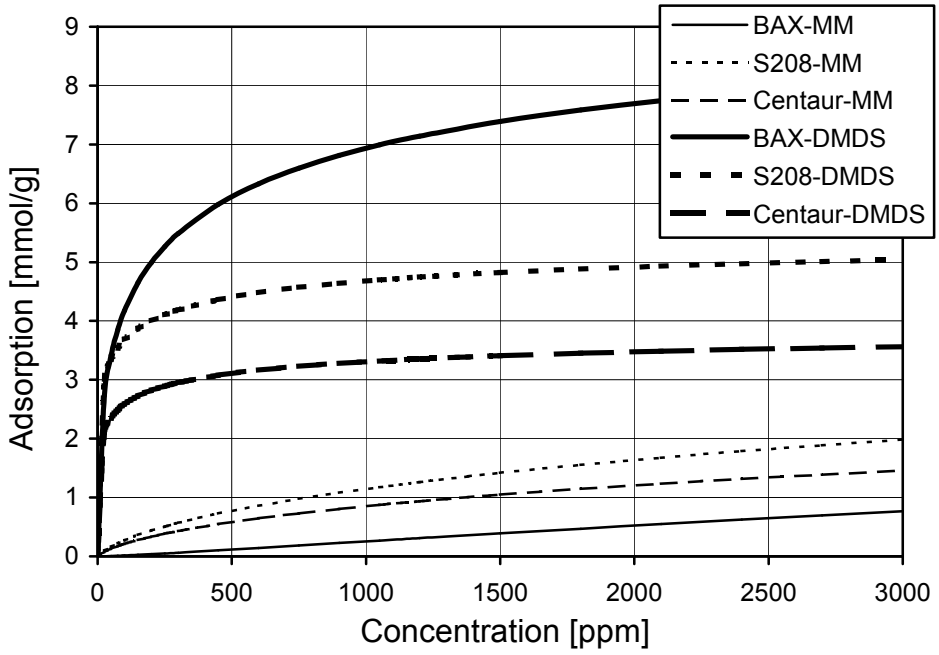

Figure 17. Predicted isotherms of MM and DMDS adsorption on the chosen carbons.

The amount of vapor, A, adsorbed at pressure P and temperature T can be calculated from the DR equation [186, 187, 195]:

$$A = V_0 * d_L * \exp\{-[R*T*\ln(P_S/P)/\beta*E_0]^2\} \quad (5.1)$$

where V_0, E_0, β, d_L and P_S are the volume of micropores, characteristic energy of adsorption of standard gas (benzene), the affinity coefficient for vapor adsorbed, density of liquid adsorptive and its saturation pressure at temperature T, respectively. The properties of the adsorbents required for the calculations were determined from nitrogen adsorption isotherms at -196^{o}C. Parameters of the adsorbates are given in Table 5. The affinity coefficients were estimated from the parachor values [186, 187]. They are equal to 0.580 for MM and 1.018 for DMDS.

However, the highest amount of MM adsorbed at 3000 ppm is expected on S208 carbon due to its high volume of small micropores (Table 4), BAX seems to be more efficient in adsorbing DMDS than the other two carbons. It is important to mention that this prediction is done assuming physical adsorption of DMDS and MM. This could be different from the actual experimental results, where adsorption of MM and its oxidation to DMDS is the matter of several factors. Thus, high acidity of the BAX carbon and the lack of catalytically active centers on its surface may result in its poor MM adsorption capacity. On the other hand, Centaur® carbon, due to its excellent overall characteristics may prove to work efficiently towards adsorption of MM and its conversion to DMDS.

5.3.1. CH_3SH Adsorption in Wet Conditions.

To investigate the ability of activated carbons to adsorb MM, breakthrough tests were carried out at room temperature in the presence of moisture and air. Methyl mercaptan breakthrough curves obtained for the initial carbon samples are collected in Figure 18a [194]. Based on the breakthrough times the performances of the carbons differ significantly. MM adsorption capacities for the carbons along with the amount of water preadsorbed are presented in Table 6 [189, 192, 194]. The highest amount adsorbed was found for the Centaur® carbon even though the breakthrough test had to be stopped at 26 ppm. This happened due to inability of the sensor to detect DMDS formed as a result of a fast oxidation of MM based on the strongly catalytic nature of this carbon. The capacities of BPL and S208 carbons are also high compared to those found for BAX and PCB carbons. To understand what governs the process of MM adsorption on different carbon

samples, a comparison has to be done between the carbons under investigation and their surface and structural features.

Table 6. MM Breakthrough Capacities and Preadsorbed Amount of Water for the Carbon Materials Studied.

Sample	Amount of water preadsorbed [mg/g]	Amount of MM adsorbed [mg/g]
BAX	163.4	28.2
BAX-O	168.8	23.0
BAX-U450	161.1	30.0
BAX-U950	145.5	299.0
BPL	98.3	172.6
BPL-O	99.6	104.3
BPL-U450	129.4	321.1
BPL-U950	102.0	440.6
S208	92.6	162.2
S208-O	98.1	203.2
S208-U450	93.9	221.9
S208-U950	68.9	272.9
PCB	78.2	85.5
PCB-O	94.5	72.9
PCB-U450	81.7	203.5
PCB-U950	75.7	192.3
Centaur®	98.3	400.0

a)

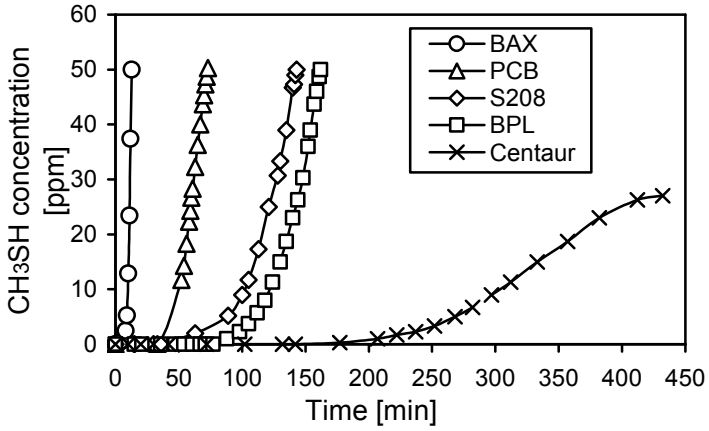

b)

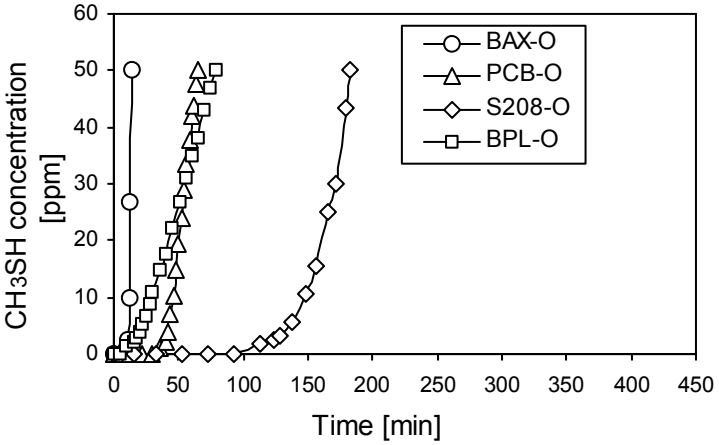

c)

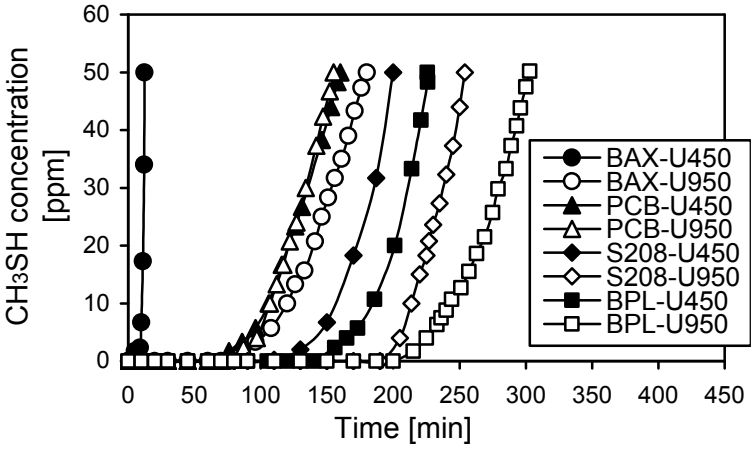

Figure 18. MM breakthrough curves for a) initial, b) oxidized, and c) urea-treated carbon materials.

Going back to the carbon surface characterization (Table 1), the importance of the surface basicity for the effective MM removal could be evaluated. As was mentioned earlier, the basicity of the carbon surface is the result of the presence of oxygen-containing surface groups of pyrone-type and/or oxygen-free Lewis basic sites [31-35]. Pyrone-like structures are combinations of carbonyl and etheric non-neighboring oxygen atoms at the edges of the basal plane and are formed by air re-exposure of heat-treated carbons [32]. Such basic oxygen-containing groups on the carbon surface could affect the dissociation of MM and oxidation of thiolate ions to disulfides [4, 177-180, 189, 194, 196]. They may also attract MM via weak acid-base interactions. To see this effect, the density of surface groups was calculated taking into account the number of groups and the specific surface areas reported in Table 4. Figure 19 shows the dependence of MM adsorption capacity on the density of basic groups for the initial carbon samples [194]. It is interesting that a good correlation is found for all the samples except PCB. Both BPL and S208 samples are very active towards the adsorption of MM even though they are less basic than PCB. This suggests a contribution of other factors, such as catalytically active ash, to the adsorption/oxidation process.

The amounts of ash are reported in Table 3 [194]. Since the amount of ash in PCB is similar to that found for the other carbon samples, the “crude” ash content analysis for this carbon fails to explain its deviation from the general trend in Figure 19 [194]. The more detailed analysis of ash by XRF showed the obvious lack of catalytically active metals for PCB carbon (Figure 11). This led to the suggested earlier hypothesis about the crucial role of catalytically active metals.

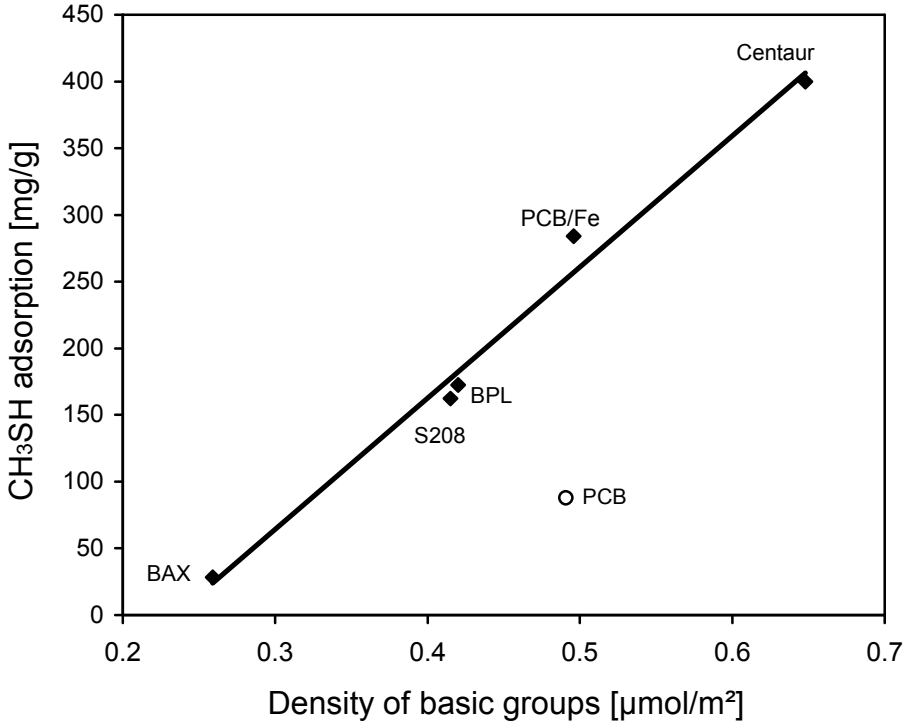

Figure 19. Dependence of MM adsorption capacity on density of basic groups for the initial carbon samples.

One of the metals, iron, seems to be especially important, since two carbons with the highest iron content, BPL and Centaur® (Table 3), have the highest MM adsorption capacities. To check this hypothesis, the PCB sample was impregnated with iron chloride, which, as a result of treatment described in section *4.1.5,* was mainly converted to oxides. The impregnation process was designed not to significantly affect the pore sizes of the material. In fact, the main change after the modification process has occurred in large micropores (Table 7). The iron content in PCB carbon after modification with iron was considerably increased and according to XRF results became a little higher (≈ 0.53 %) than that for BPL coal-based carbon (≈ 0.45 %) [194]. On the other hand, the total ash content of the iron-modified PCB sample became lower than that in the initial

PCB carbon (Table 7). This apparent inconsistency may be the result of dissolution of some silica or alumina components in NaOH during the surface neutralization process. An increase in the iron content positively affected the performance of PCB carbon for the adsorption of MM. Its MM capacity increased 3.3 times and now follows the trend of dependency on the surface basicity generally observed for the other carbons (Figure 19) [194].

The extremely small capacity of the BAX carbon, despite the theoretical prediction (Figure 17), may be primarily due to the acidic nature of this carbon. Even though the pH of BAX is only slightly smaller than the pH of BPL and Centaur® carbons it may be below the threshold value for dissociation of methyl mercaptan on activated carbons [113, 191, 195]. In addition to this, the large amount of acidic oxygen-containing groups on the surface and the lack of catalytically active metals may also contribute to the small MM adsorption capacity on this carbon.

Although it is understandable that the surface chemistry has complex and significant effects on the performance of activated carbons as MM adsorbents, the process of adsorption/oxidation cannot be effective without a developed pore structure where the products of surface reactions have to be stored. The predictable main product of MM adsorption/oxidation on the activated carbon surface is DMDS [152, 177-180, 189, 192, 194, 196], the adsorbed amount of which was evaluated under saturation conditions where only vapors of DMDS are present (section *4.2.2*). It is plotted in Figure 20 against the volume of pores smaller than 50 Å [195] to show the significance of the pore volume for MM adsorption. A very good linear agreement with the slope equal to 0.997 and correlation coefficient equal to 0.89 is found.

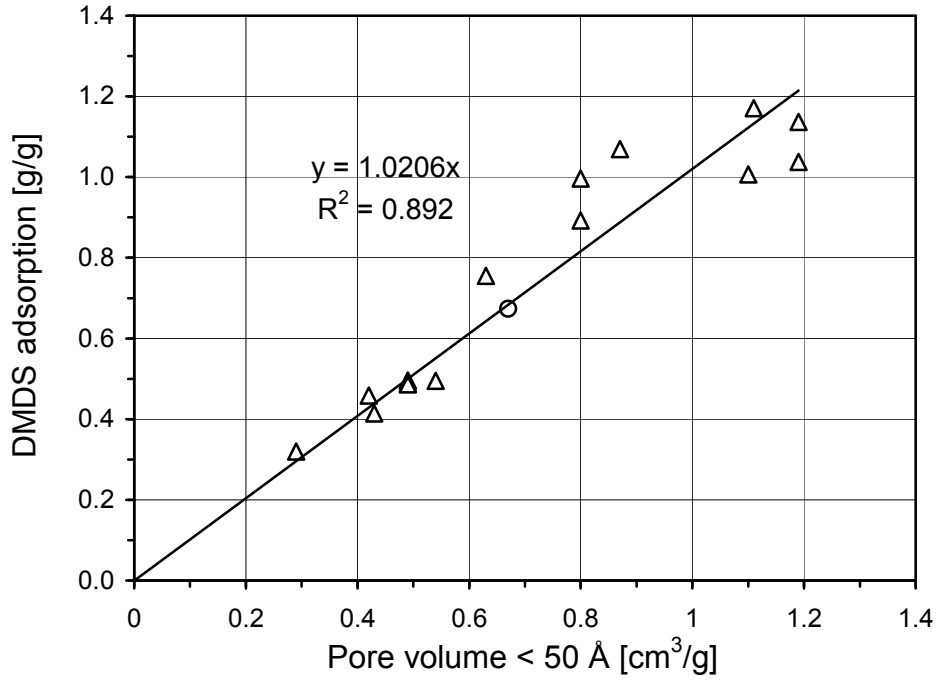

Figure 20. Dependence of the amount of DMDS adsorbed at saturation conditions on the volume of pores smaller than 50 Å.

While the structural parameters of the BAX carbon indicate that it has the superior porous structure, its MM removal capacity is very small. Besides the disadvantages of this carbon mentioned above, another reason for its poor performance lies in its insignificant volume of pores smaller than 10 Å and its large average micropore size. On the other hand, in the case of BPL whose volume of small pores is not exceptionally high as well, the most likely explanation for the high MM adsorption capacity is in its surface chemistry and the presence of iron, which acts as a catalyst in the oxidation process. As indicated above, a lack of chemically active centers on the PCB carbon surface is an important factor suppressing the oxidation process and its high microporosity is not able to compensate for that. After introduction of iron into this carbon, no significant changes in the volume of very small pores were noticed (Table 7).

However, its average micropore size was considerably decreased. This may somewhat contribute, in addition to the catalytic participation of iron, to the increase in MM adsorption capacity of this carbon.

Centaur® carbon is the only carbon with all the characteristics needed for the efficient MM removal. This carbon has a catalytic nature, which includes nitrogen and iron and is supported by a large relative volume of micropores and very small size of micropores [42, 43].

Table 7. Surface and Structural Characteristics of PCB Carbon and its Iron Modified Counterpart.

Sample	pH	Ash Content [%]	Basic Groups [mmol/g]	Amount of MM Adsorbed [mg/g]
PCB	7.74	2.76	0.50	85.5
PCB-Fe	7.80	0.84	0.45	284.0

Sample	S_{DFT} [m^2/g]	V_{mic} [cm^3/g]	V_t [cm^3/g]	$V_{<10Å}$ [cm^3/g]	L_{mic} [Å]
PCB	1018	0.43	0.55	0.25	10.6
PCB-Fe	907	0.35	0.45	0.24	9.4

MM breakthrough curves for the oxidized carbon samples are presented in Figure 18b [189]. Based on the breakthrough times, there are some differences in the performance between the initial and the oxidized carbon samples. It is interesting that for S208–O an increase in the breakthrough time is found in comparison with the initial

sample. The breakthrough times for BAX-O and PCB-O remain almost unchanged compared to their initial counterparts whereas for BPL-O a decrease is found.

From Table 6 it is seen that after treatment with hydrogen peroxide the MM breakthrough capacity of the S208 sample increased about 25 %, while for BPL-O the capacity became 1.6 times smaller compared to the initial sample. As indicated above, a small decrease in the MM breakthrough capacity is also found for PCB-O. These changes in capacity are likely related to the changes in pH of the carbon surface. As it was found for hydrogen sulfide, high pH facilitates the dissociation of H_2S molecule as well as its oxidation to elemental sulfur [191]. The same can be true in the case of MM, which at high pH can dissociate and then be oxidized to DMDS [189, 194, 195]. Indeed the pH of S208-O increased compared to that of the initial sample, whereas the pH of BPL-O and PCB-O decreased. More so, an increase in the number of carboxylic and lactonic groups after oxidation was higher for BPL and PCB carbons than that for S208 carbon, which also may have affected the surface pH. In case of the BAX carbon the most noticeable changes in the surface chemistry occurred after oxidation and they resulted in a decrease of more than 2 units in the pH value of the surface. Nevertheless, already negligible capacity of the initial sample was only slightly reduced after oxidation.

Another important factor affected by oxidation is the amount of water adsorbed during prehumidification, which increased for all the samples. This is due to an increase in the degree of hydrophilicity of the carbon surface caused by formation of new oxygen-containing groups [197].

From the point of view of porosity (Table 4), no significant changes were noticed for the BPL carbon. Although the average micropore size of the BPL-O is the same as of

the BPL, the energy of adsorption on the oxidized sample was reduced, which could be the reason for the decrease in its MM adsorption. On the other hand, a large decrease in L_{mic} and an increase in E_{ads} for the S208 carbon may contribute to a significant rise in the adsorption capacity of this carbon. Finally, despite even higher microporosity and energy of adsorption for the BAX-O and PCB-O samples than those for their initial counterparts, their MM capacities became smaller. This observation could be the result of the increased acidity of both carbons after oxidation (Table 1).

Methyl mercaptan breakthrough curves for the urea-treated carbons are presented in Figure 18c [192]. They indicate that after impregnation with urea and heat treatment the adsorption capacities of the carbons studied increased from 1.4 to 10 times depending on the carbonization temperature. From experimental data collected in Table 6 it is also seen that the higher the heat treatment temperature after impregnation with urea the more methyl mercaptan is adsorbed on the carbon surface. High capacities were found for BPLU-950, BPLU-450, BAXU-950 and S208U-950 while the lowest capacity was recorded for BAXU-450. The greatest effect of urea modification was observed for BAX carbon carbonized at 950ºC, whose adsorption capacity for MM increased ten-fold compared to the initial sample. On the other hand, for the same carbon but carbonized at 450ºC no effect of urea treatment was found and a very small amount of MM was immobilized on the surface. As for the PCB carbon series, the capacity of PCBU-450 is only slightly higher than that for PCBU-950 making PCB urea treated sample not very sensitive to the carbonization temperature.

Although an increase in MM adsorption capacities of the carbons after urea modification is strongly related to an increase in their surface basicity (Table 1 and

Figure 10) the effect of nitrogen could also be significant for MM adsorption. Thus, for example, the BPL-U950 carbon sample was found to have the same amount of nitrogen as Centaur® carbon (≈1.1 %), which could possibly explain their similar MM adsorption capacities (Table 6). Therefore, in order to see the effect of nitrogen, the normalized MM capacity (with respect to the surface area of materials) was plotted versus the ratio of atomic content of nitrogen to carbon determined from elemental analysis (Figure 21) [192].

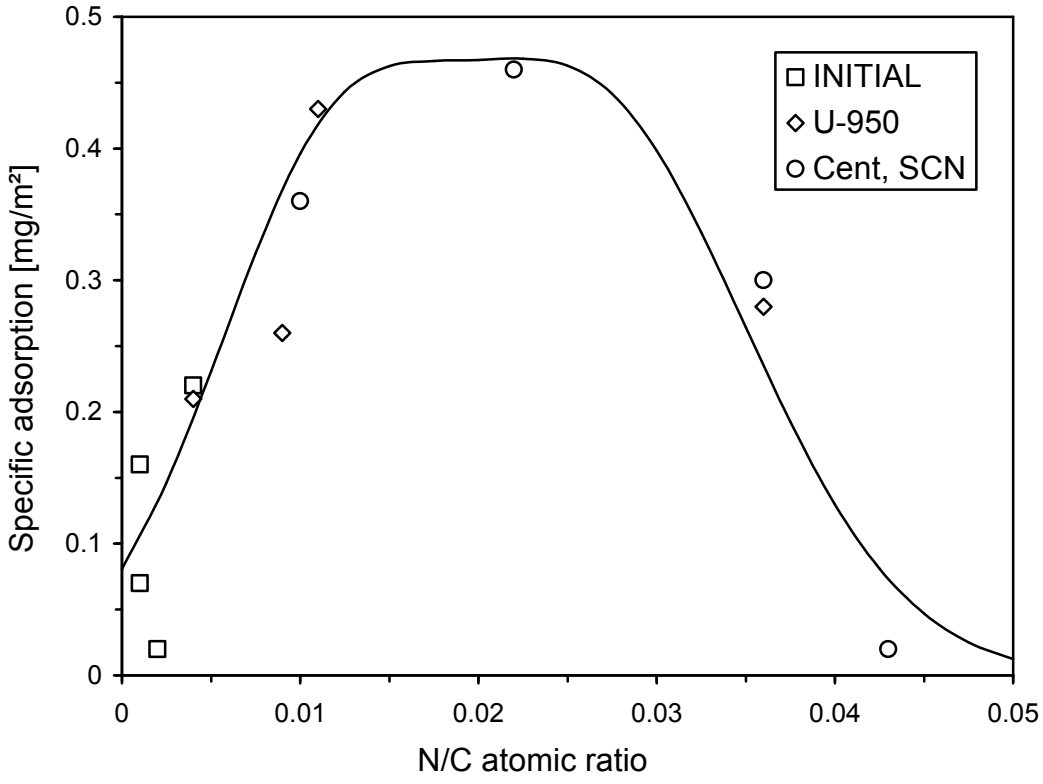

Figure 21. Dependence of the normalized MM breakthrough capacity on N/C atomic ratio in carbon matrixes.

For this analysis only initial carbons and those modified with urea at 950^{o}C were taken into consideration to ensure that nitrogen is in similar chemical form as a result of high temperature heat treatment [47, 49, 105]. Data for polymeric based carbons (SCN series) [49, 50, 192] is also included for the sake of comparison. The obtained dependence presented in Figure 21 shows the maximum in the capacity at N/C content about 0.02. It confirms the results obtained by Strelko and coworkers [53] who found, using the quantum chemical calculations of model nitrogen containing carbon clusters that at the atomic concentration of nitrogen within the carbon matrix between 2-3 % the minimum in the band gap occurs. The lowest width of the band gap, ΔE, indicates the highest catalytic activity in electron transfer reactions [53]. In the case of the carbons studied the maximum specific capacity is related to the high catalytic activity and it occurs for BPL carbon modified with urea at 950^{o}C. As found by Strelko and coworkers [53], ΔE further increases with an increase in the nitrogen content. Indeed, in this study the decrease in catalytic activity is observed for such carbons as BAX-U950 and some of the polymeric based carbons. Moreover, the results of quantum chemical calculations showed that carbons with quaternary nitrogen-containing groups at the edges of carbons layers have the highest charge mobility in a carbon matrix and the best donor-acceptor properties [53].

The contribution of porosity to MM adsorption is also significant for some of the carbons. Since the presence of small pores is critical for the effective MM removal, an increase in the volume of these pores and a decrease in their size are desirable. Thus for BAX-U950 a significant increase in the volume of pores smaller than 10 Å is noticed. Moreover its average micropore size is considerably smaller than that for the initial

sample and there is more than 3 units increase in the energy of adsorption. These factors, in addition to the increased basicity of BAX-U950, could explain a much higher capacity (10 times) of this carbon than that for its initial counterpart. On the other hand, although for the BAX-U450 carbon a slight improvement in microporosity is found, its capacity still remains very low. The main reason for this could be the low pH of BAX-U450 (Table 1), which was not increased much in comparison to the initial sample and it is probably too low for the MM to dissociate and be oxidized to DMDS.

For both BPL-U450 and BPL-U950 samples the volume of pores less than 10 Å was reduced and L_{mic} stayed the same. It follows that for both of these samples the same tendency exists as for their initial counterpart, which is the superiority of the surface chemistry over the porosity in the MM adsorption process.

Even though the volume of pores smaller than 10 Å decreased for both of the S208 modified samples (Table 4), it is worth mentioning the significance of the pore size, which can be directly related to an increase in MM adsorption capacity. Modification of S208 carbon resulted in a visible decrease of L_{mic} and in an increase of E_0.

In the case of the urea-treated PCB carbon samples, the higher volume of pores smaller than 10 Å as well as a smaller L_{mic} for the PCB-U450 sample than for the PCB-U950 sample resulted in a slightly better performance of the former one for MM adsorption. Nevertheless, as was mentioned earlier, the carbonization temperature does not seem to significantly affect the MM adsorption capacity of PCB carbon.

5.3.2. CH_3SH Adsorption in Dry Conditions.

To throw some light on the process of methyl mercaptan adsorption/oxidation on the surface of the carbons studied, the experiments were also performed in dry conditions, either in air (-A) or nitrogen (-N). The measured capacities are shown in Table 8 [196] in comparison to the capacities of the same carbons obtained in wet conditions. The latter ones were as received carbons without washing with water. The results are shown for four of the carbons and it is seen that for all the carbons, except BAX, the capacities in dry conditions were at least twice smaller than those measured in the presence of moisture. Moreover, except for Centaur®, the amounts of MM adsorbed in dry air and in nitrogen do not differ significantly. However the results suggest that water facilitates the adsorption process, it is not the case for BAX carbon, where adsorption in dry conditions was higher than that in wet conditions. For this carbon the amount of water adsorbed was the greatest (Table 6), which may suggest the competition for adsorption sites between water and MM molecules and/or surface reaction products. The unchanged amounts adsorbed in dry air and nitrogen indicates the lack of participation of oxygen from air, not chemisorbed or bonded, to the surface reactions.

Table 8. MM Breakthrough Capacities for the As Received Carbon Samples Obtained in Wet and Dry Conditions.

Sample	Amount of MM adsorbed [mg/g]
BAX	0
BAX-A	27.9
BAX-N	29.3
BPL	251
BPL-A	48.1
BPL-N	36.6
S208	349
S208-A	84.9
S208-N	74.6
Centaur®	230
Centaur®-A	99.5
Centaur®-N	57.7

5.4. The Products of CH_3SH Adsorption/Oxidation.

The species present on the carbon surface after adsorption can be characterized using thermal analysis (section *4.2.5*). Differential thermogravimetric (DTG) curves were obtained in nitrogen and are presented in Figures 22-23, 28-30. On DTG curves a weight loss is represented as a peak with area related to the amount of the species removed or decomposed from the surface. This method was used before for the characterization of

the products of hydrogen sulfide oxidation [43, 45, 191], sulfur dioxide adsorption [42], and chemisorption of organosulfur compounds on gold [198]. It is assumed that the peak at a temperature smaller than 100°C represents desorption of weakly adsorbed species, likely water, and the peak between 100 and 300°C may represent desorption of disulfides [192, 196, 198]. Due to its physicochemical properties (CH_3SH is desorbed from the gold surface between -83°C and -50°C [199]), the adsorption of CH_3SH on the carbon surface should be very weak and it is not expected to be present in the adsorbed phase.

For all the carbons after MM adsorption two of the above-mentioned peaks are present. The second peak shows the heterogeneity of species displayed by the presence of a shoulder around 300°C with a sharp decrease in the weight loss. This shoulder is especially clearly pronounced for the microporous carbons (Figure 22b). It may represent decomposition of a surface DMDS-oxygen complex, $CH_3SSCH_3 \cdot nO2$. Oxygen, if present in this form, does not contribute to a decrease in the pH value of the carbon surface after exhaustion. Support for this assumption is the desorption temperature of oxygen complex, which is close to the desorption temperature of weakly adsorbed SO_2 or SO_3 on activated carbons [42, 199]. However, this shoulder may also represent some other products of MM and/or DMDS oxidation by oxygen.

For the initial unmodified carbons (Figure 22), it is interesting that the Centaur® the DTG curve shows the presence of some species that are not found for the other initial carbons. These species could be some nitrogen-containing compounds commercially introduced into this carbon's matrix. Moreover, the intensity and the area of the second peak of the Centaur® carbon is the greatest among the carbons studied, which is in agreement with the breakthrough test results.

a)

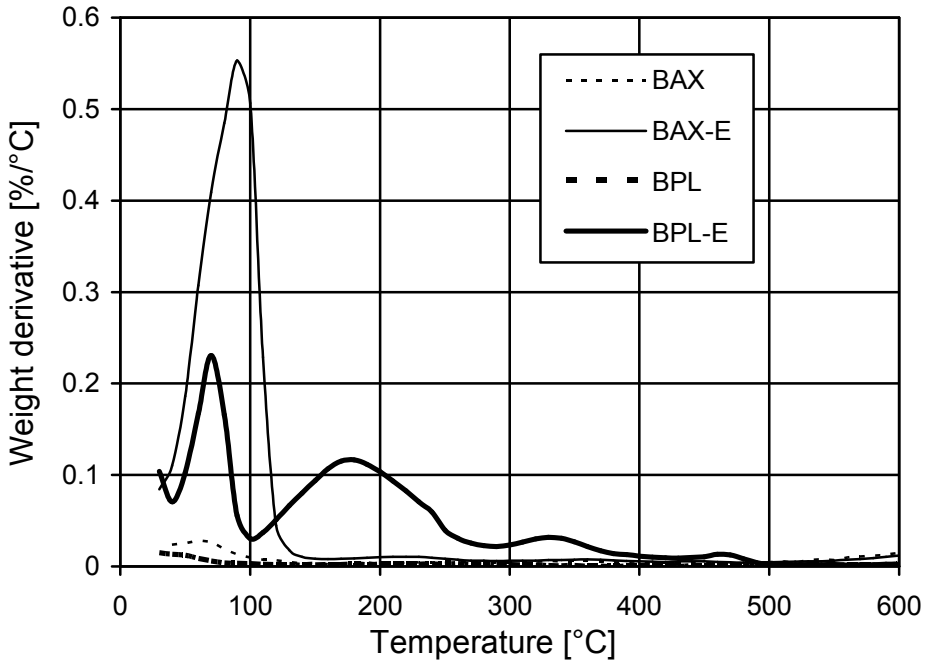

b)

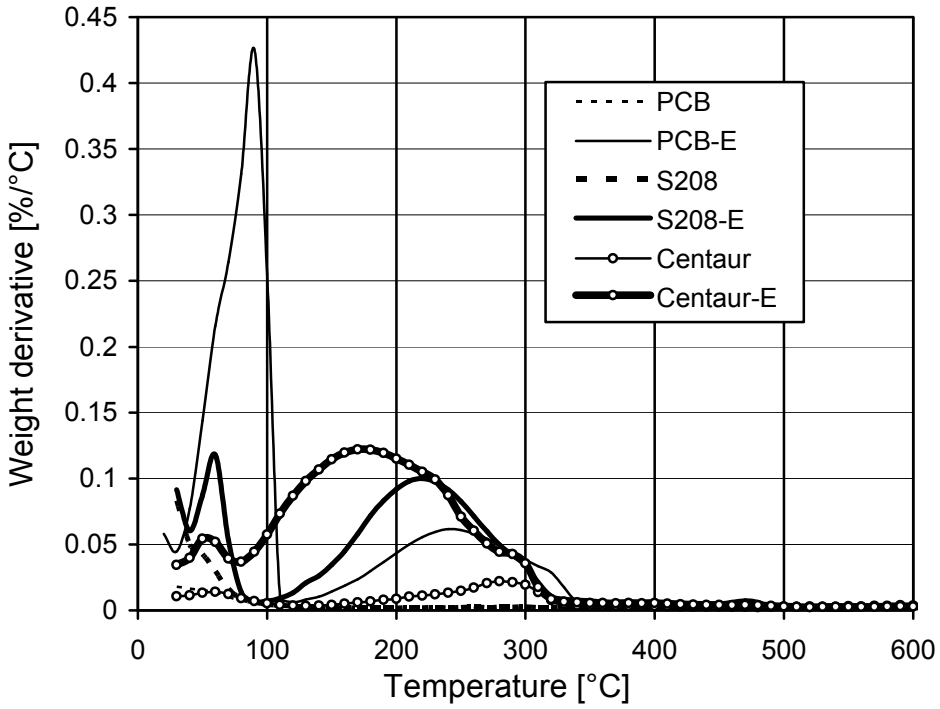

Figure 22. DTG curves for the unmodified initial and exhausted a) BAX and BPL series of samples and b) PCB, S208 and Centaur® series of samples.

a)

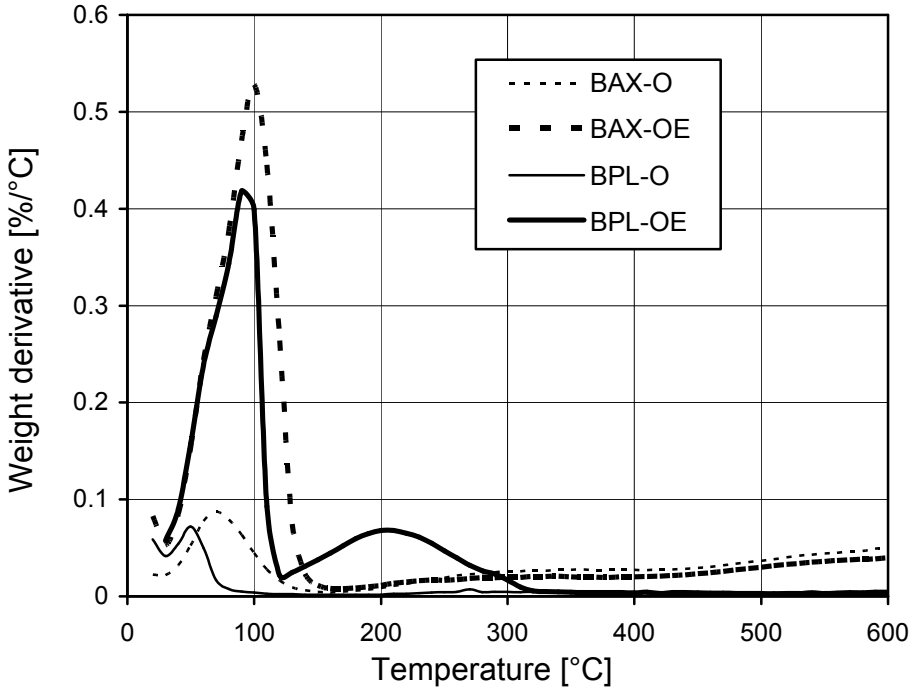

b)

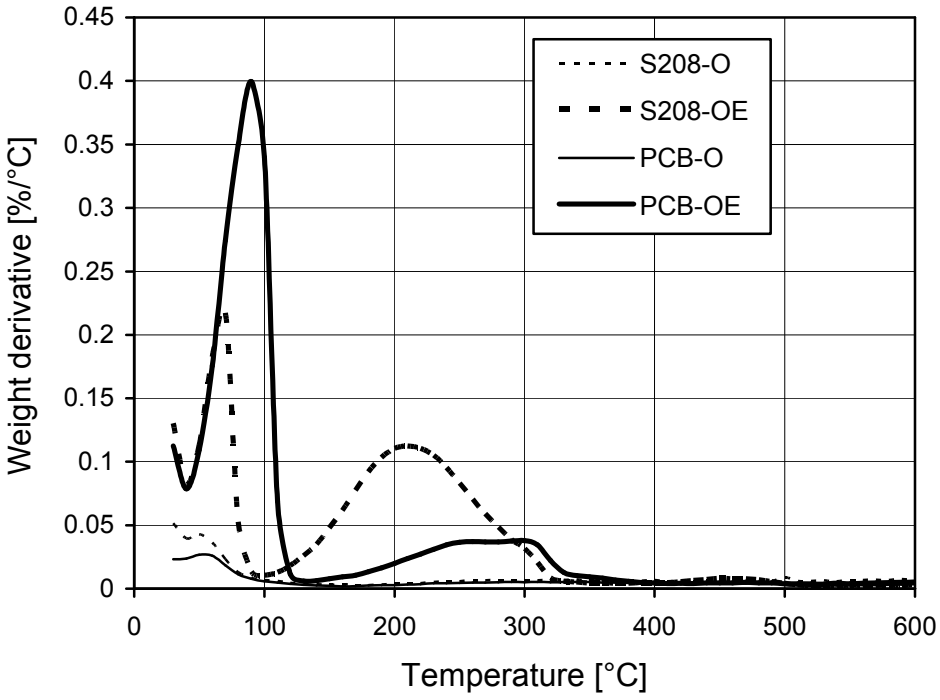

Figure 23. DTG curves for the oxidized initial and exhausted a) BAX and BPL series of samples and b) PCB and S208 series of samples.

The balance of the amount of sulfur species evaluated from TA and the breakthrough test is demonstrated in Table 9 [189, 192] and shows good agreement for all of the carbon samples. The last column in this table lists the amount desorbed corrected for the initial weight of carbon. The validity of TA is also established from the correlation between the adsorbed amounts of MM evaluated from TA and the breakthrough test. This relationship is presented in Figure 24 [195].

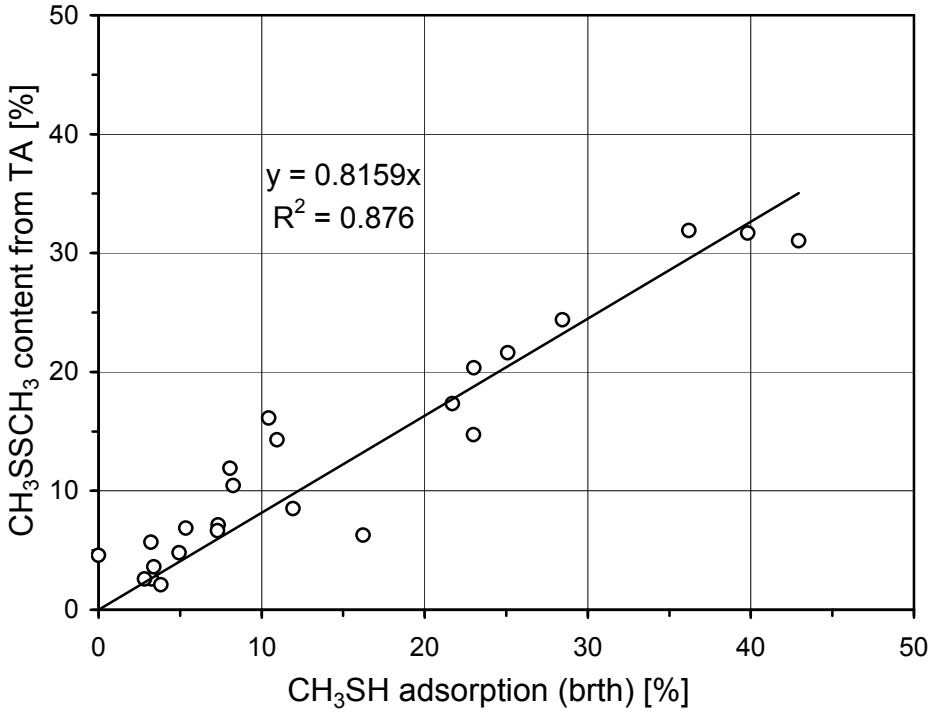

Figure 24. Relationship between the amounts of MM adsorbed estimated from the breakthrough test and thermal analysis (Maxsorb carbon - mesophase pitch based from Kansai and SCN polymer based synthetic carbon [49, 50] are added for the sake of comparison).

Table 9. Balance of Sulfur Species from Breakthrough Tests and Thermal Analysis.

Sample	MM ads (%)	ΔW 100-500ºC (%)
BAX	2.8	1.3
BAX-O	2.6	0
BAX-U450	3.0	2.9
BAX-U950	29.9	27.8
BPL	21.7	22.6
BPL-O	10.4	13.3
BPL-U450	32.1	26.2
BPL-U950	44.1	38.5
S208	16.2	15.9
S208-O	20.4	19.1
S208-U450	22.2	20.4
S208-U950	27.3	22.4
PCB	8.6	5.1
PCB-O	7.3	8.0
PCB-U450	20.4	18.4
PCB-U950	19.2	15.5
Centaur®	39.5	36.0

For the initial S208 and PCB carbons the position of the second DTG peak is shifted to a higher temperature range than that for the BPL carbon (Figure 22). This is due to the differences in porosity between these carbons. As was shown earlier, both S208 and PCB are microporous carbons (Figure 15) with a small average micropore size (Table 4). Therefore a higher temperature is needed to remove adsorbed DMDS from the pores similar in size to the adsorbed molecule than from larger pores as those found in BPL carbon. For Centaur® carbon, which is highly microporous, the desorption of DMDS starts at lower temperatures and continues to higher temperatures, which is due to a high amount of DMDS adsorbed on this carbon.

It is clear that after oxidation the intensity and the shape of the peaks on the DTG curves of the carbons studied have changed (Figure 23). For the S208-O sample, for example, intensities of both peaks increased compared to the initial sample. This is the result of an increase in the degree of hydrophilicity of this carbon after oxidation and its higher affinity for water adsorption.

As mentioned before, the shoulder centered at about 300°C may represent the surface DMDS-oxygen complex, $CH_3SSCH_3 \cdot nO_2$, or some other products of CH_3SH/CH_3SSCH_3 oxidation, such as sulfonic or sulfinic acids [147, 149, 152]. After oxidation the intensity of this peak increased for the PCB carbon and it became about the same as the DMDS peak. Indeed, according to the results of the Boehm titration (Table 1), an increase in the amount of total groups after oxidation for this carbon is higher than that for S208 and BPL carbons, meaning that more oxygen-containing groups on the surface may facilitate further extent of oxidation.

Looking at the DTG curves for BPL-O and PCB-O samples, it is obvious that the intensity of the second peak is smaller after oxidation even though the amount of water is increased. These results are also consistent with the breakthrough test results collected in Table 6. The possible explanation of such phenomenon can be the competition between water and DMDS for the adsorption sites. For the initial carbon samples (Figure 22) the higher the intensity of the DMDS peak, the lower the intensity of the water peak. Thus, Centaur® carbon is the one that preadsorbed enough water during prehumidification (Table 6) but all of it was replaced by DMDS formed in a high amount on this carbon's surface (Figure 22b). On the other hand, both BAX and BAX-O have very high amounts of water on their surface but almost no DMDS (no second peak) (Figures 22a, 23a).

By assuming that either H_2O or DMDS is adsorbed only in pores smaller than 50 Å, the adsorption data can be normalized based on that volume. The relationship between the normalized amount of DMDS and water is shown in Figure 25 [195]. The correlation coefficient and slope are equal to 0.89 and 0.99, respectively. The slope represents the density of DMDS (1.06 g/cm^3). The small discrepancy is likely related to the fact that not all pores are filled by oxidation products owing to the existence of some physical hindrances (blocked pore entrances). The thin line represents theoretical limit of adsorption using the actual densities of DMDS and H_2O. The fact that almost all points are located below this line validates the hypothesis about the "active" pore volume. It is important to mention here that all points represent equilibrium data. If equilibrium conditions, for instance for adsorption of water, are not fulfilled the amount of DMDS is usually small and the point "moves" from the established dependency line.

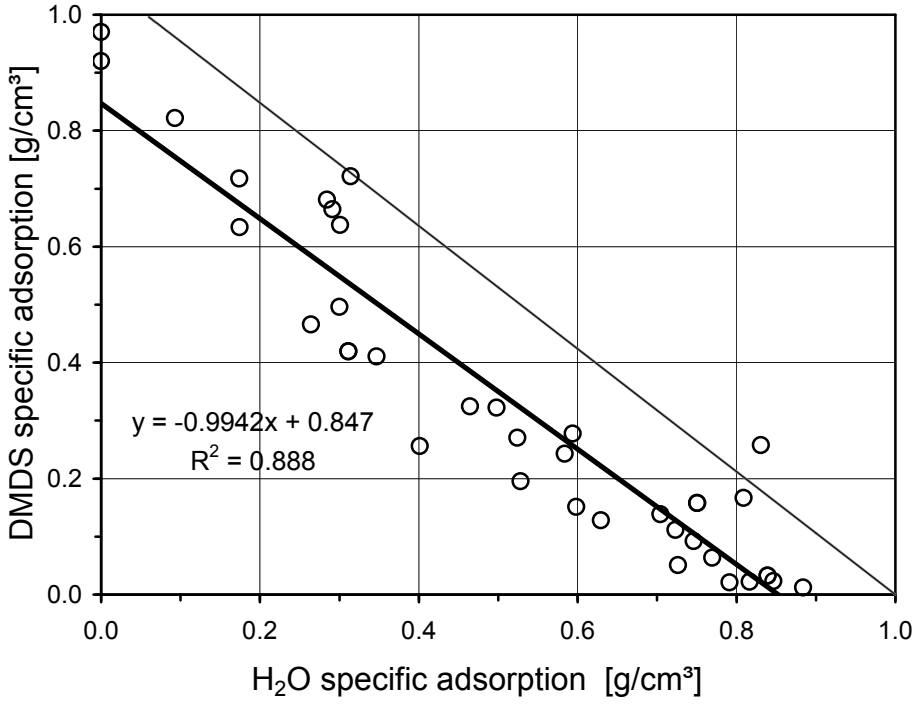

Figure 25. Specific adsorption of DMDS versus specific adsorption of H_2O.Capacities were normalized to the volume of pores smaller than 50 Å.

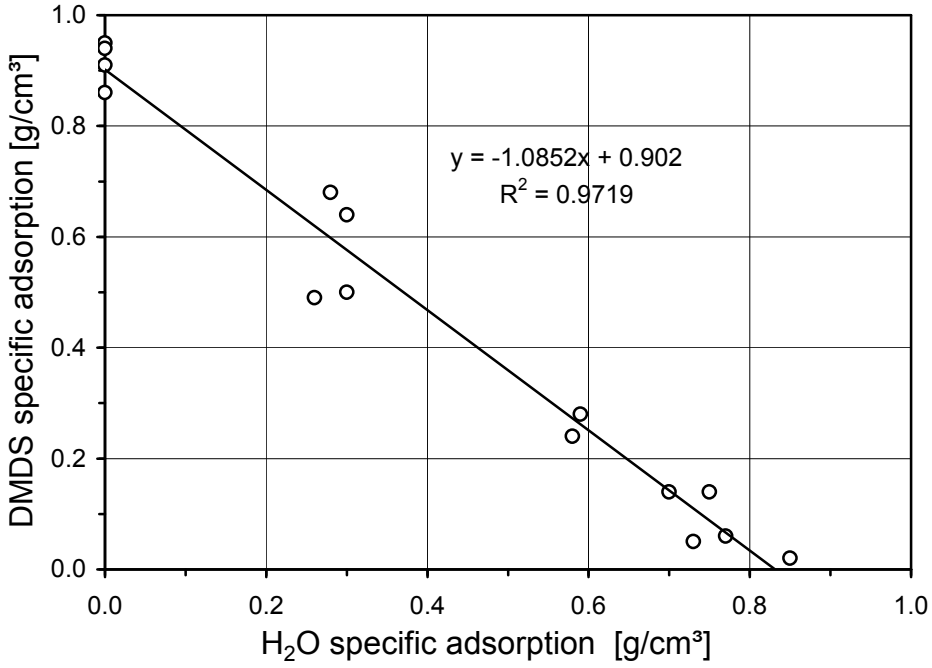

Figure 26. Specific adsorption of DMDS versus specific adsorption of H_2O for S208 carbon.

In order to get closer look at the described phenomena, the data for one carbon, S208 was plotted in Figure 26 [195]. For this carbon the correlation coefficient and slope are equal to 0.97 and 1.08, respectively, which is in agreement with the expected values.

Another supporting factor for the possible competition between water and DMDS for the adsorption sites is their predictable amounts adsorbed on two of the chosen carbons, BAX and S208 (Figure 27) [195]. Prediction of water adsorption was done following the approach of Lodewyckx and Vansant [200] based on application of the Dubinin-Astakhov (DA) equation using an affinity coefficient equal to 0.063 for activated carbons with low content of oxygen-containing groups on the surface. For both carbons at relative pressure P/P_S equal to 0.8 (experimental conditions) the amount of water which can be adsorbed is close to the adsorbed amounts of MM and DMDS. What is even more interesting is that the amount of DMDS adsorbed at very low relative pressure, $P/P_S = 0.05$, corresponding to inlet concentration of MM (3000 ppm) is practically the same as the amount of water adsorbed at $P/P_S = 0.8$. This can be considered as a favorable factor to promote competition for adsorption sites, which results in replacement of water with much stronger adsorbed DMDS molecules.

The DTG curves for the urea-treated carbons are presented on Figures 28 and 29 [192]. An interesting fact is noticed for the BPL carbon treated with urea and carbonized at 950 ºC. Its DTG curve slightly resembles the DTG curve for the Centaur® carbon (Figure 22b), which, just like BPL has a high MM capacity value (Table 6). Besides, both BPL and Centaur® carbons have no peaks corresponding to water desorption, which suggests the competition between water and DMDS for the adsorption sites and complete replacement of water by DMDS.

a)

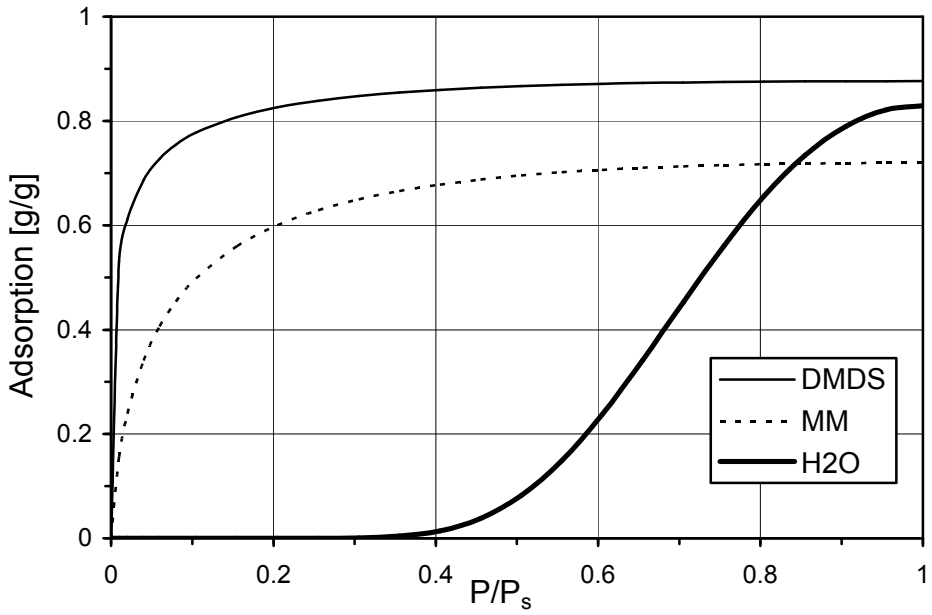

b)

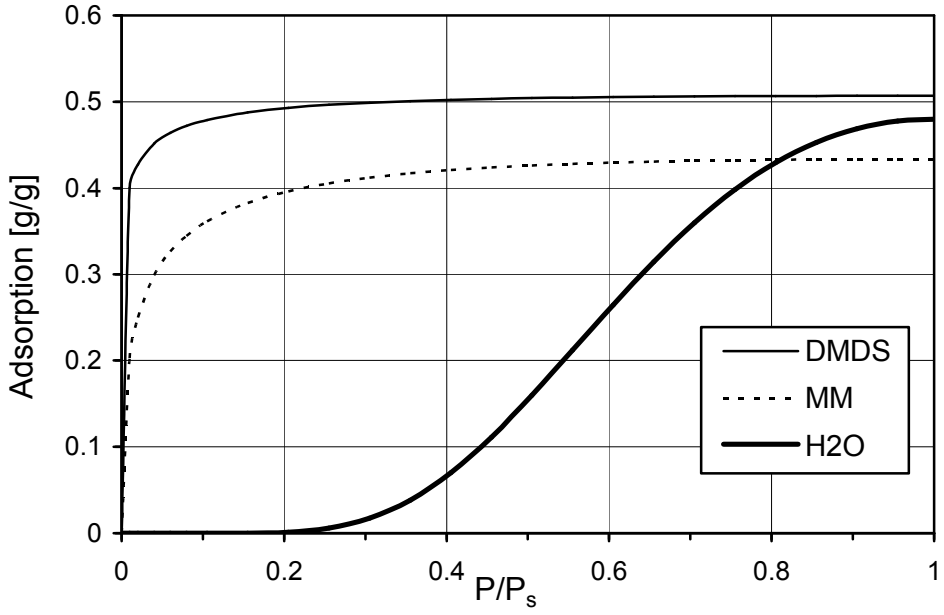

Figure 27. Predicted isotherms of MM, DMDS, and water adsorption on a) BAX and b) S208 carbons.

Moreover, following the fact that the largest amount of MM was adsorbed on the BPLU-950 carbon sample, the intensity of the peak between 80 and 300ºC is the highest for this sample compared to other urea treated samples.

There is also a common tendency noticed for the urea-treated samples. The second peak on their DTG curves is shifted to the lower temperatures of desorption, suggesting weaker adsorption forces. This can be due either to the changes in surface chemistry or to the decrease in the volume of micropores observed for most of the samples (Table 4). Besides, for BAX and BPL urea-treated carbons, which have a significant contribution of larger micropores and mesopores to their structure, DMDS desorption occurs at much lower temperatures than for microporous carbons. In spite of similarities in the PSDs between BAX and BPL carbons, the DMDS seems to be adsorbed stronger on the latter carbon as a result of stronger surface basicity.

The shoulder of the second peak at about 300-350^{o}C varies in intensity after urea modification. While for the S208 sample it became more pronounced, for PCB carbon it almost disappeared and for BPL it remained about the same. This can be related to the formation of some strongly adsorbed compounds or chemisorbed MM. Another high temperature peak, especially noticeable for the BPL series of carbons is centered at about 400 ºC and may represent the formation of elemental sulfur [43].

To see the differences in the products of MM adsorption/oxidation, comparison was done between the exhausted carbons obtained in dry and wet conditions. Figure 30 shows the DTG curves for the as received S208 carbons run at various conditions [196].

a)

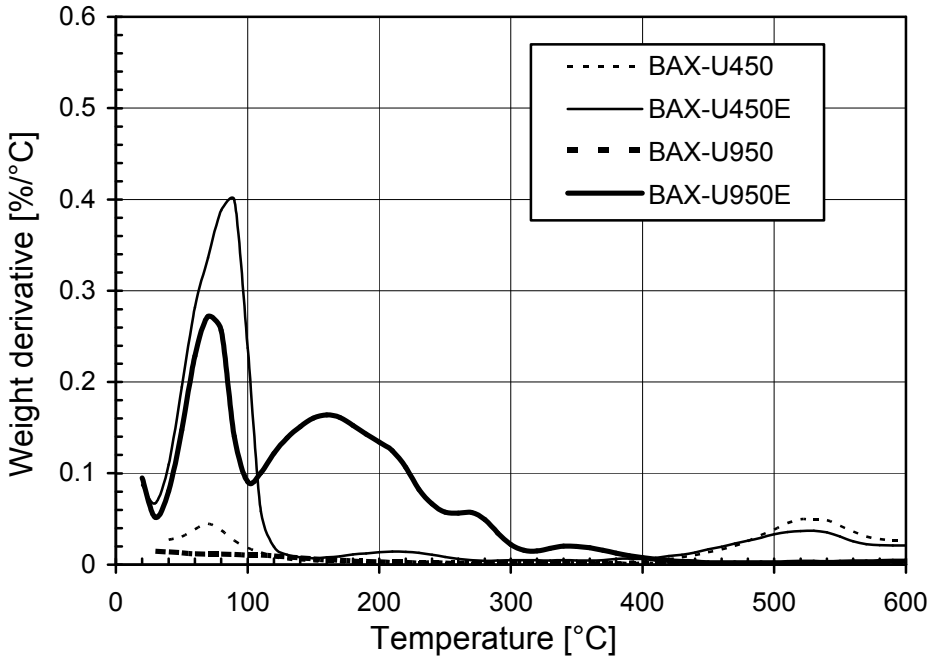

b)

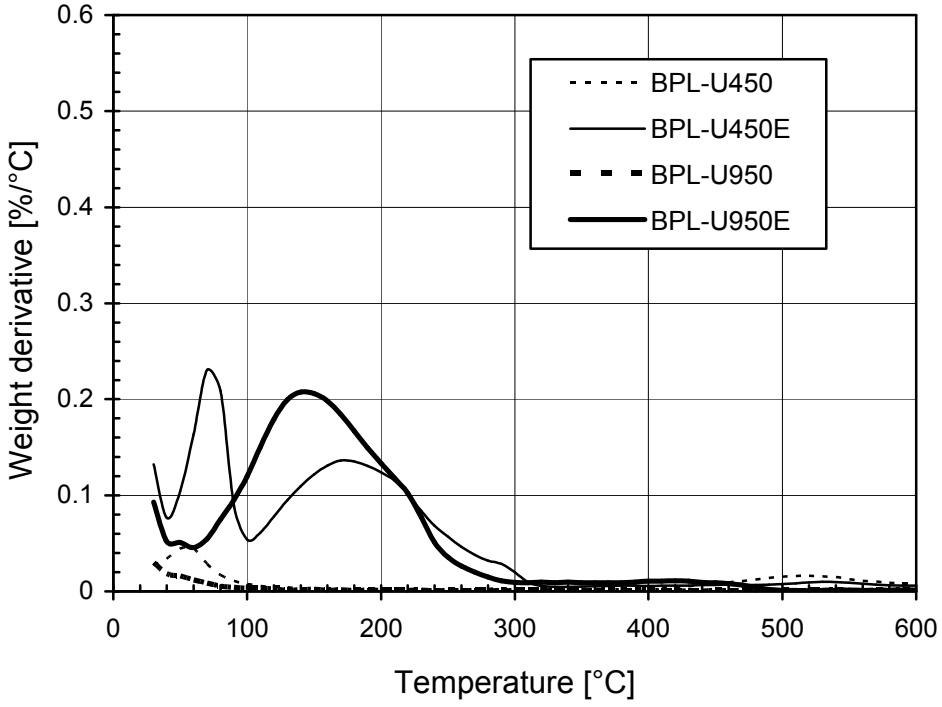

Figure 28. DTG curves for the urea-treated initial and exhausted a) BAX series of samples and b) BPL series of samples.

a)

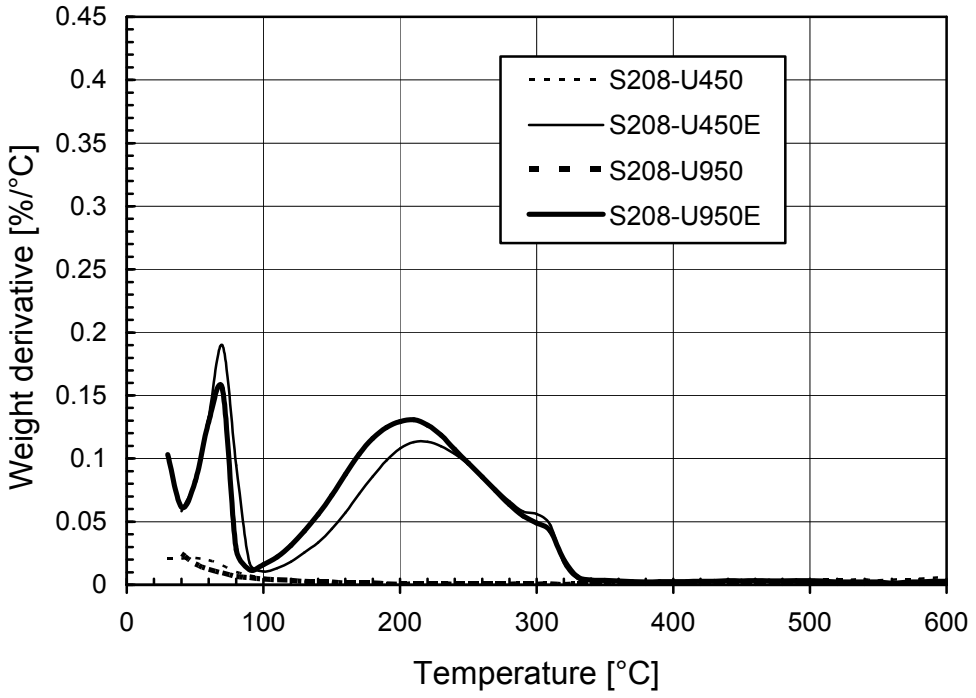

b)

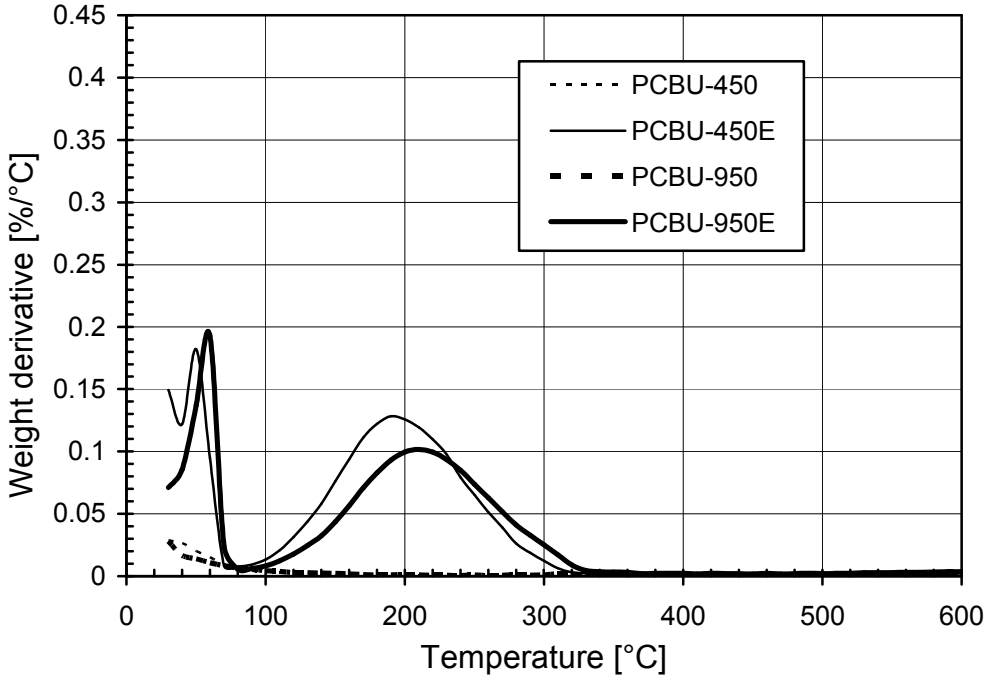

Figure 29. DTG curves for the urea-treated initial and exhausted a) S208 series of samples and b) PCB series of samples.

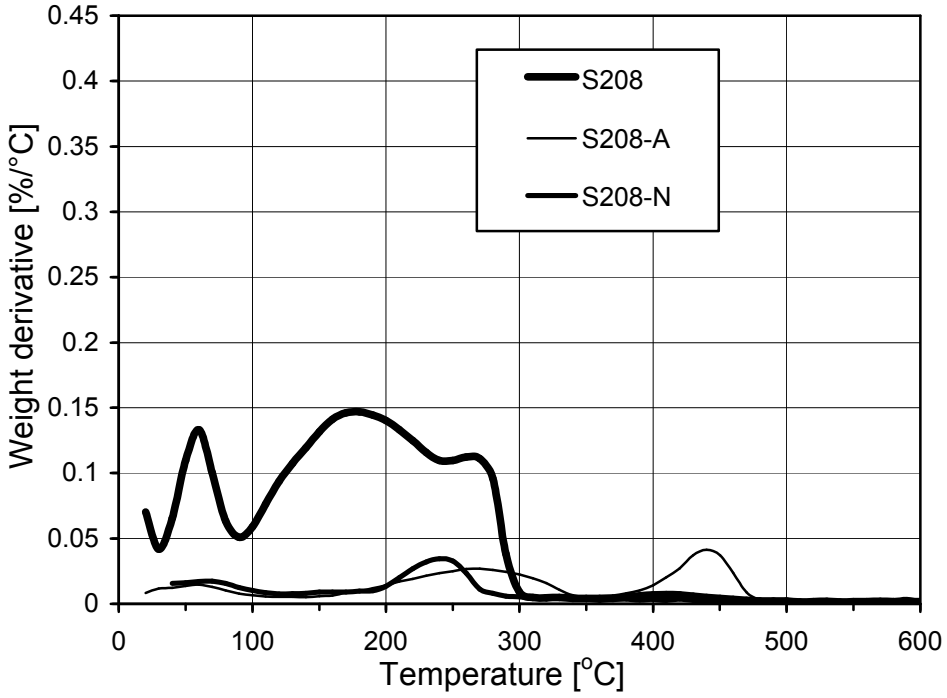

Figure 30. DTG curves for the as received S208 carbons run in moist air, dry air (-A), and dry nitrogen (-N).

In the case of running the breakthrough test in dry conditions, the DTG curve indicates the presence of a small peak starting at about 200°C. When the moisture is absent, the species, which decompose between 100 and 200°C, are not present. The absence of oxygen results in the presence of more homogeneous surface chemistry (the weight loss occurs in a narrow temperature range) than that when oxygen is in the system (the peak expands to 350°C). The broadening of the peak at higher temperatures overlaps with the observed shoulder at 270°C and is likely related to the oxygen bonded to the adsorbed disulfide molecules or to some products of MM/DMDS oxidation by oxygen [147, 149, 152]. It is interesting that when oxygen is in the system, another peak at about

440°C appears. This peak likely represents elemental sulfur [43, 191], which, as well might be formed as a result of oxidation of disulfides by oxygen.

For a more accurate product evaluation GC/MS analysis was used. The products of MM adsorption/oxidation were extracted from the carbon surface with methanol and subjected to the GC/MS analysis. Chromatograms of all the carbon samples studied were obtained, revealing two peaks for the majority of the samples. The retention times of the peaks were 7.8 minutes for the first one and 18.8 minutes for the second one. These peaks were identified as dimethyl disulfide, which is the main product of the surface reaction and methyl methane thiosulfonate (MMTS), which was detected only for the carbons with a significant MM adsorption. Thus, for the initial and oxidized carbons, the highest intensities of the second peak were found for the Centaur®, BPL, S208-O and S208 carbon samples and no peak was detected for the BAX carbon series. For the urea-treated samples, BPLU-950 is the only carbon for which the second peak is well pronounced and its intensity is only twice smaller than of the first peak. Other urea modified carbon samples, for which the second peak was noticed but has a very small intensity, are BPLU-450, BAXU-950, S208U-950 and PCBU-950. The example of the mass spectra for the S208 carbon is shown in Figure 31 [189].

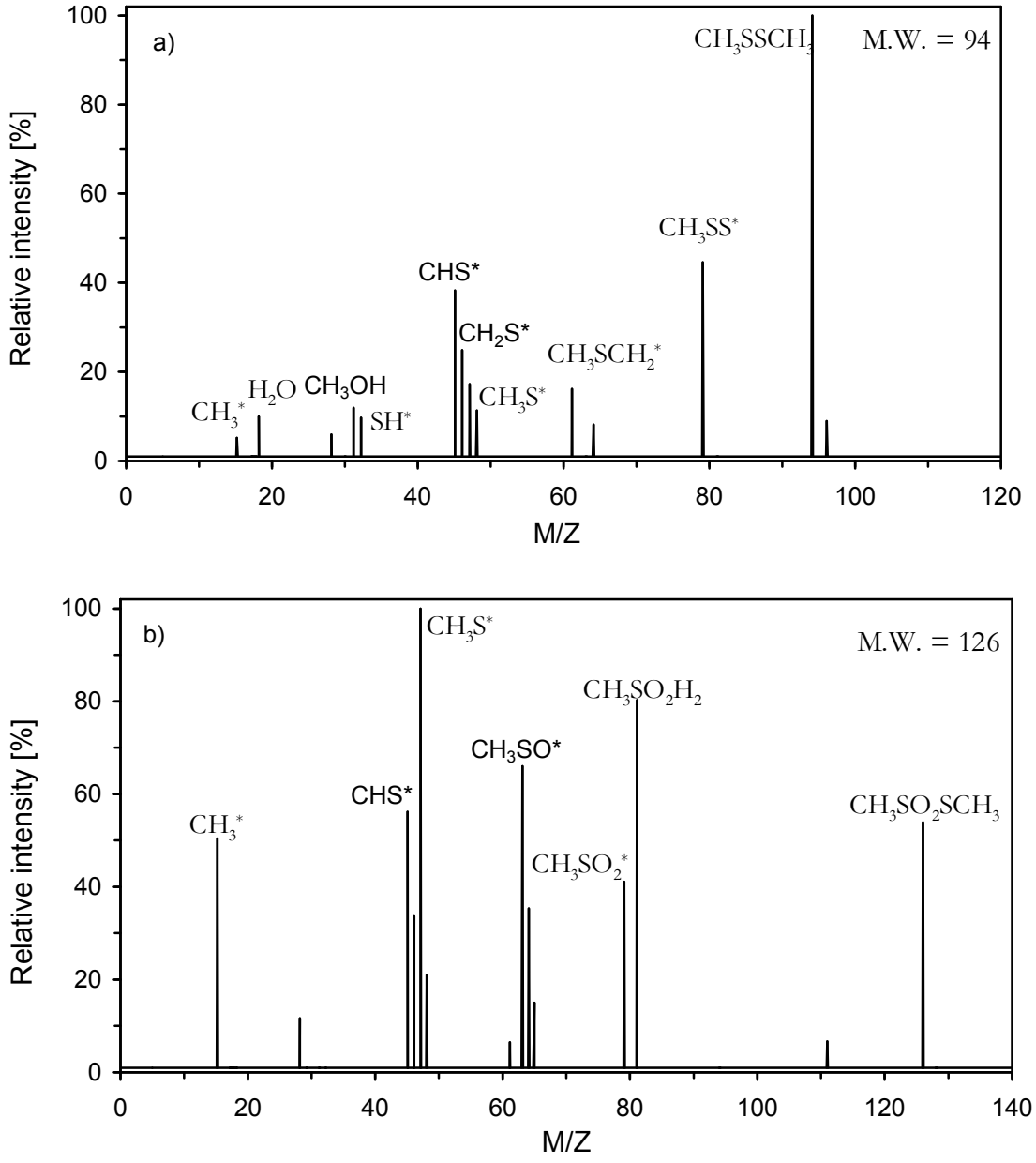

Figure 31. Mass spectra for the species extracted from the exhausted S208 sample: a) dimethyl disulfide, b) methyl methanethiosulfonate.

5.5. Energetic Characteristics of the Carbon Surface.

5.5.1. Theoretical Concept.

At very low pressure (Henry's range), the tendency of different adsorbates to adsorb on the carbon surface can be estimated from the heat of adsorption and the equilibrium constant K_H at infinite dilution [195, 201, 202]. For simplicity, it can be assumed that the species under investigation (water, MM and DMDS) are simple one-center Lennard-Jones molecules, which can interact with uniform flat carbon surface via Van der Waals forces.

For the classical approximation of Henry's constant the following equation can be applied [195, 201]:

$$K_H = \int_0^{\infty} exp\,[(-\Phi / k*T) - 1]\, dz \qquad (5.2)$$

where Φ is the potential energy of molecular interaction with the adsorbent, k is Boltzmann's constant, and z is the distance from the surface in perpendicular direction to it. Detailed calculation methods for the interaction potential of a molecule with the carbon surface are described in literature [86-88, 201-203]. Here the most common approach is used [195, 203], where the adsorbent is modeled as having slit-like pores with two infinite parallel walls separated by a distance H in the z direction. The potential of interaction between a fluid molecule and a pore is given in this case as a sum of potentials, U_s, of fluid-solid interactions with a single wall:

$$\Phi(z) = U_s(z) + U_s(H-z) \qquad (5.3)$$

where z is now defined as a distance between the molecule and the center of the carbon atom on one of the pore walls.

The fluid-carbon wall interactions are described below by the Steele potential [203], which is widely used for modeling interactions of simple molecules with graphite:

$$Us(z) = 2\pi*\rho_c*\varepsilon_{cf}*\sigma_{cf}^{2}*\Delta*\{2/5*[\sigma_{cf}/z]^{10} - [\sigma_{cf}/z]^{4} - [(\sigma_{cf})^{4} / (3*\Delta*(z + (0.61*\Delta))^{3})]\} \quad (5.4)$$

where the density of the carbon is ρ_c =114 nm^{-3}, the separation of the graphite planes is Δ = 0.335 nm, and ε_{cf} and σ_{cf} are the LJ parameters for interaction between carbon atoms and fluid molecule. The carbon-carbon potential parameters are taken as ε_{cc}/k = 28 K and σ_{cc} = 0.340 nm [85-88, 203].

Fluid-solid cross parameters are calculated using the Lorentz-Berthelot rules:

$$\varepsilon_{cf} = (\varepsilon_{cc} * \varepsilon_{ff})^{1/2} \quad (5.5)$$

$$\sigma_{cf} = (\sigma_{cc} + \sigma_{ff}) / 2 \quad (5.6)$$

The LJ parameters of fluid-fluid interactions in formulas (5.2) and (5.3) were determined from the critical parameters of gases under investigation by the method of "corresponding" states [204]. For the polar molecules without hydrogen bonding (methyl mercaptan and dimethyl disulfide):

$$\sigma_{ff} = 36.9*(V_{cr})^{1/3} \quad (5.7)$$

$$\varepsilon_{ff}/k = 0.897* T_{cr} \quad (5.8)$$

and with hydrogen bonding (water):

$$\sigma_{ff} = 36.9*(V_{cr})^{1/3} * (Z_{cr})^{2.75} \quad (5.9)$$

$$\varepsilon_{ff}/k = 0.00331* T_{cr} / (Z_{cr})^{4} \quad (5.10)$$

where $Z_{cr} = P_{cr}*V_{cr} / R*T_{cr}$ and V_{cr}, T_{cr} are the critical volume and critical temperature of studied gases.

The critical parameters of fluid-fluid interactions calculated by equations (5.7)-(5.10) and are given in Table 10.

Table 10. Heats of Adsorption and Henry's Constants for the Molecules Studied.

Species	Q_{st} (kJ/mol)	K_H
H_2O	19.8	3.83×10^3
MM	33.1	7.81×10^4
DMDS	59.9	4.61×10^{10}

The plots for the interaction potential profiles of H_2O, MM and DMDS molecules with a 7 Å width graphitic slit micropore, calculated by equations (5.2) – (5.3), are shown in Figure 32.

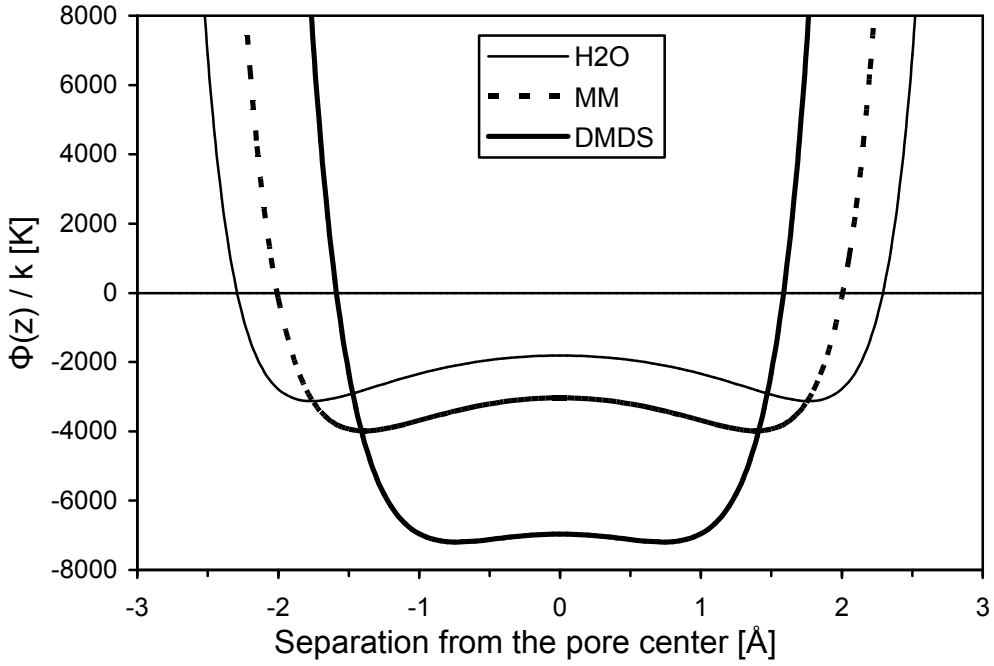

Figure 32. The calculated interaction potential profiles for adsorption of MM, DMDS, and water in a model 7 Å pore.

The effective pore width, L, is defined as the distance between the centers of surface atoms corrected for the diameter of a carbon atom in the graphite lattice:

$$L = H - 3.45\ Å \tag{5.11}$$

It is clearly seen in Figure 32 that MM and especially DMDS molecules interact much stronger than water with a single carbon pore wall. The overlapping effect of the molecule-pore wall interactions in the center of a 7 Å micropore is the strongest for DMDS, which should lead to a higher value of the heat of adsorption for DMDS molecule than for MM and water molecules. The heat of adsorption was calculated from the minimum of the potential well depth, $\Phi(z_0)$, by expression:

$$Q_{st} = -R*\Phi\ (z_0) \tag{5.12}$$

The calculated values of Q_{st} are collected in Table 10 and, as expected, the highest value was obtained for DMDS. The heat of adsorption of water is in agreement with the value reported by Kiselev obtained for a flat carbon surface based on chromatographic experiments [201].

The Henry's constants determined by numerical integration of equation (5.4) for a model 7Å pore are also collected in Table 10. The K_H value for MM is 20 times larger than for water, while for DMDS and H_2O they differ by about seven orders of magnitude. The data received from statistical-molecular calculations also confirms that in an activated carbon – water – DMDS system in an equilibrium state, DMDS tends to substitute water in the adsorbed state. Moreover, if carbon porosity drives the adsorption process then the highest capacity for DMDS adsorption will be found for microporous carbons.

5.5.2. Experimental Approach.

Isosteric heats of MM adsorption can also be determined experimentally from IGC. Using this technique it is possible to better understand the effect of surface functionality (presence of surface oxygen) on the adsorption process and the effect of the small pores on the enhancement of the energetics of the process. Only those pores can play a significant role when the IGC at infinite dilution is carried out [185].

In the absence of water and air mainly physical forces are expected to play a role in the immobilization process. All the chromatograms obtained by IGC (section *4.2.6*) contained only one peak likely arising from the physically adsorbed MM. As expected,

retention volume increased with a decrease in temperature. For different carbons different retention volumes were obtained depending on the strength of asorbate-asorbent interactions.

From the slope of the dependence of $ln\ (V_N/T)$ on $1/T$ (Figure 33) the heats of adsorption were calculated (Table 11). The correlation coefficients were in all cases higher than 0.99. The heat of MM adsorption in the case of all carbons used in this study was higher than 60 kJ/mol. Average values from several measurements are reported with a percentage error less than 5 %. It is interesting that these values are 1.9 to 2.3 times higher than the theoretically predicted Q_{st} value for MM (Table 10). This increase in the Q_{st} value could be the result of the presence of pore shapes other than slits. Besides, experimental Q_{st} values received for MM can be compared to those received for H_2S on the similar carbon samples [205]. These values were from 38 to 47 kJ/mol, and taking into consideration additional methyl group, which contributes about 9 kJ/mol on a nonporous carbon black [201] and twice more on a porous carbon, the values for MM should be in the range of 60 kJ/mol. The highest value was found for the Centaur® carbon, which reflects strong adsorption of MM molecule on this carbon's surface. On the other hand, BAX carbon exhibited the smallest value of the heat of adsorption indicating that weak adsorption forces are taking place.

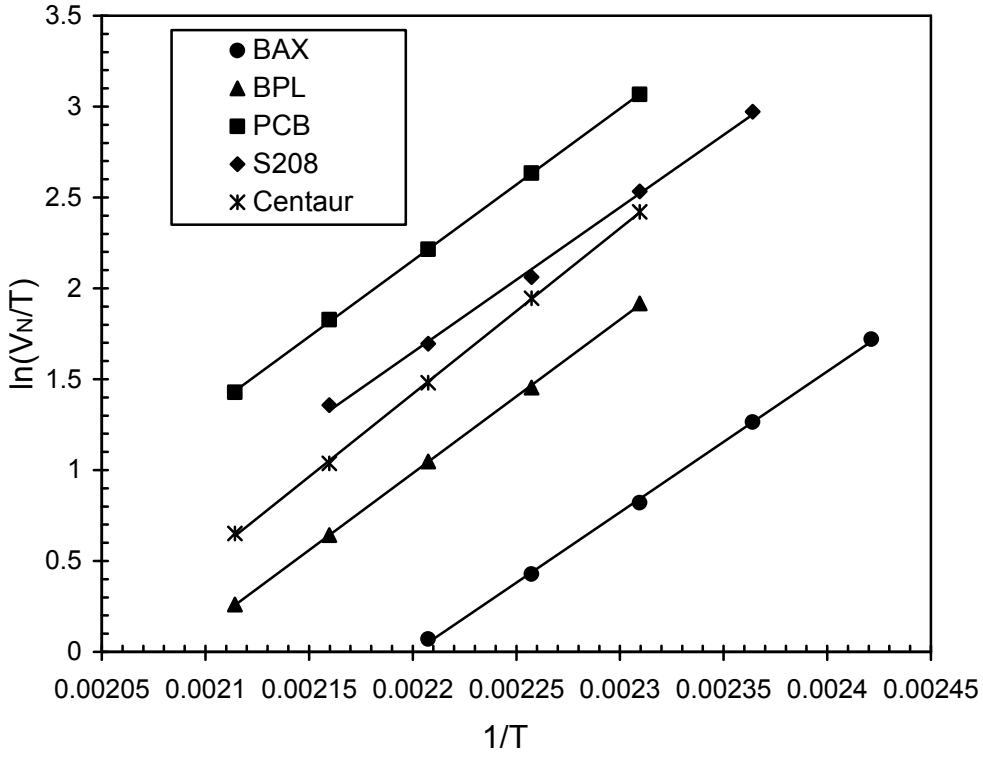

Figure 33. Dependence of the retention volume on temperature.

Table 11. Isosteric Heats of Adsorption for the Carbons Studied.

Sample	Q_{st} [kJ/mol]
BAX	63.7
BPL	70.7
S208	69.5
PCB	70.0
Centaur®	75.8

To find out which carbon features determine the magnitude of the heat of adsorption, the relationship between the heat of adsorption and the surface and structural characteristics of the carbons studied was explored.

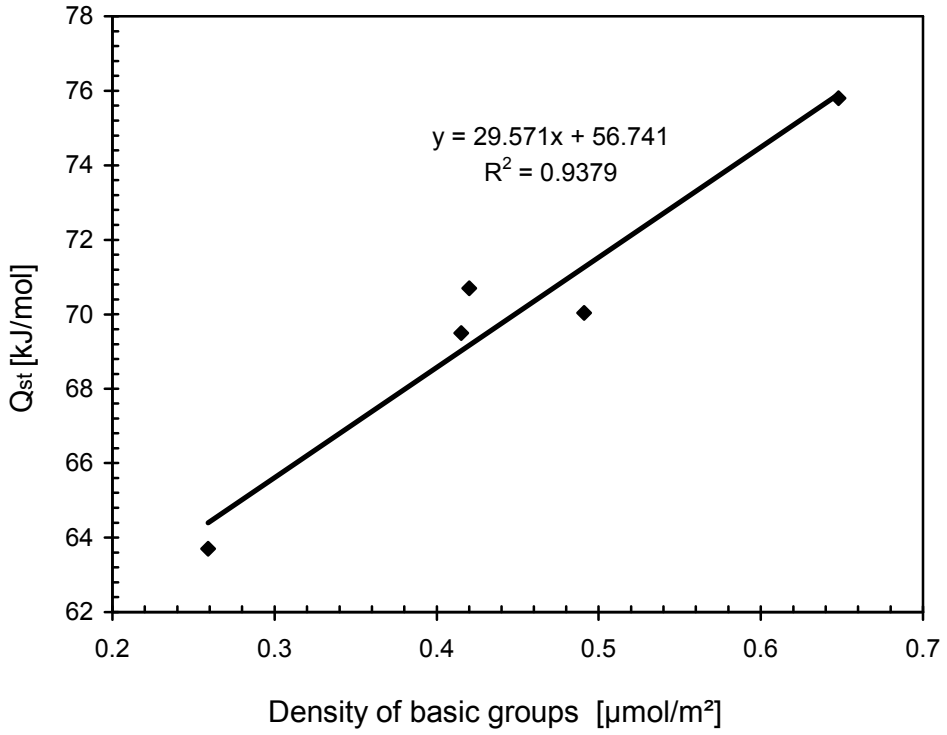

Figure 34. Dependence of the isosteric heat of adsorption on the density of basic groups.

To understand the impact of surface chemistry on the heats of MM adsorption in the temperature range studied, isosteric heats of adsorption were plotted versus the density of basic groups and the results are shown in Figure 34. The correlation coefficient of 0.9379 indicates that oxygen from surface basic groups is the contributor to MM adsorption. Since oxygen-containing pyrone-type structures are possibly the ones responsible for the overall basicity of the carbon surface, the interactions of these groups with MM in dry conditions can be Lewis type acid-base interaction, considering MM as a

weak acid. No dependency was found on the oxygen-containing acidic groups, indicating their minor role in the process of MM adsorption.

Analysis of the thermodynamic functions obtained under the conditions of infinite dilution provides information about the interactions with the surface only, since interactions between adsorbed molecules are neglected. It is known that the characteristic energy of adsorption calculated using Dubinin-Radushkevich approach is related to the average size of micropores [54, 186] (Table 4). It was also demonstrated that the initial heat of adsorption evaluated from IGC experiments is linked to the adsorption energy in micropores [110]. Theoretical calculations of the dependence of energetic parameters of adsorption on pore sizes at low surface coverage showed a significant enhancement in the adsorption energy and heat of adsorption due to the overlapping of the adsorption potentials in pores of molecular size [111].

Since physical adsorption in very small pores is the most likely a mechanism of the adsorption process at infinite dilution, the dependence of Q_{st} on the characteristic energy of adsorption is plotted in Figure 35. Although linear correlation between the heat of adsorption and carbon microporosity was found in the case of H_2S adsorption (R^2 = 0.943) [43, 205], only a general trend is noticed for CH_3SH adsorption (Figure 35). Probably, wider range of Q_{st} and E_{ads} values could have given some better understanding of this relationship.

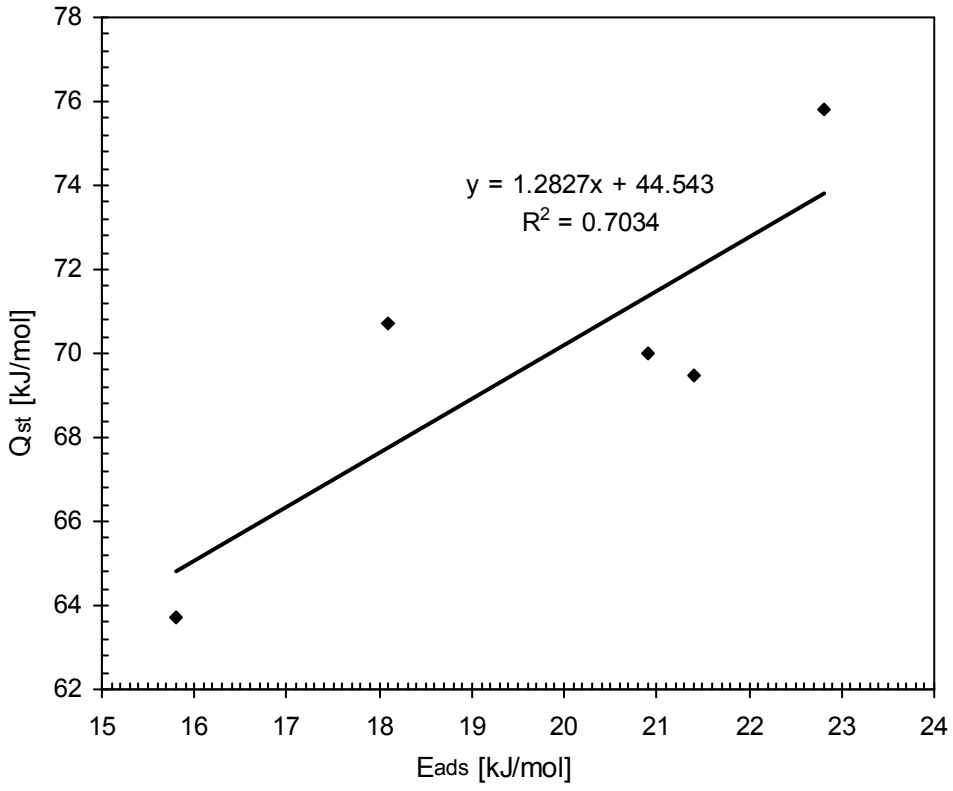

Figure 35. Dependence of the heat of adsorption on the characteristic energy of adsorption.

5.6. The Role of Surface pH and the Proposed Mechanism of CH_3SH Adsorption/Oxidation.

As was found in the case of H_2S [191], pH of the carbon surface plays a significant role in the adsorption process. The same effect is expected for the adsorption of MM. Due to the presence of water, CH_3SH is expected to dissociate to CH_3S^- and H^+ ions. The pK_a for this process is reported to be 10.3 [147, 149, 150], which may suggest that dissociative adsorption of CH_3SH may occur only on a very basic carbon surface. As seen from Table 6, the capacity of Centaur® is large despite its almost neutral pH (Table 1). On the other hand, the capacity of BAX is close to nil, although its average pH is very close to that of Centaur®. Moreover, the large capacity is reported for BPL carbon whose pH is not much higher than that of BAX. In discussing these data it should be taken into consideration that the pH reported in Table 1 is the average pH of the carbon surface, which could be different from the "local" pH inside the carbon pores, especially when these pores are small and they have functional groups present at their entrances [43, 113]. Besides, manufacturing technology should also be taken into consideration. Thus, the pH of BAX carbon is likely the result of surface neutralization with base after activation with phosphoric acid, which usually results in carbons with acidic pH [190, 191].

From the above it follows that the higher the pH the higher should be the amount of MM adsorbed. This is reflected in Figure 36 [195] by the increased intensity of the second peak. It is also seen from the DTG curves that by increasing the pH of the carbon surface the amount of DMDS increases, while the amount of water adsorbed decreases. The possible reason for this behavior is the above-mentioned (Figure 22) incompatibility of these two species and the differences in their driving forces for adsorption.

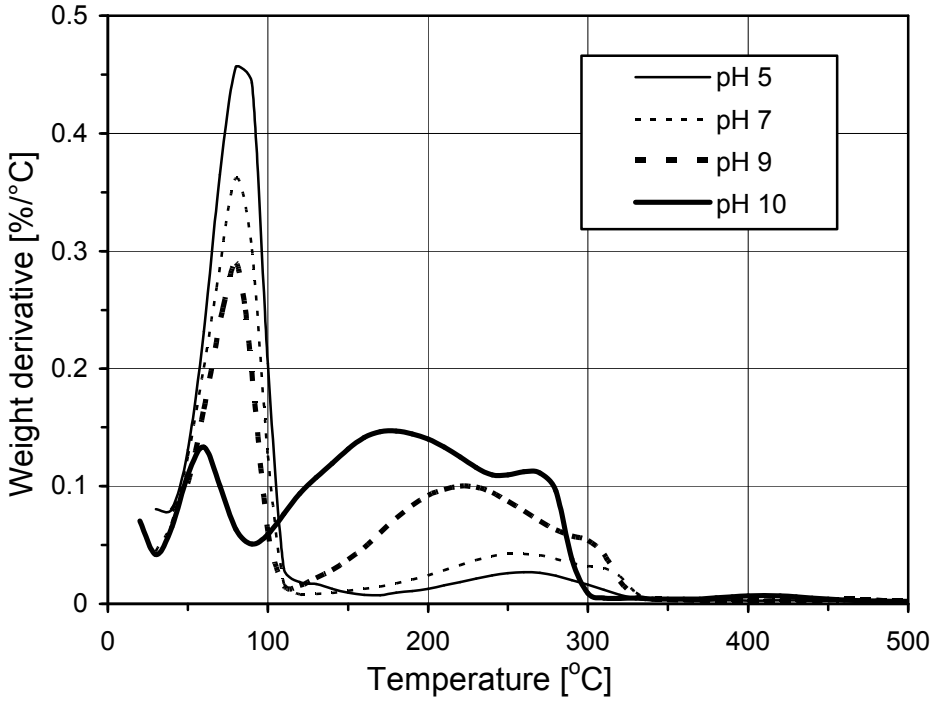

Figure 36. DTG curves of the exhausted S208 carbons with various surface pH.

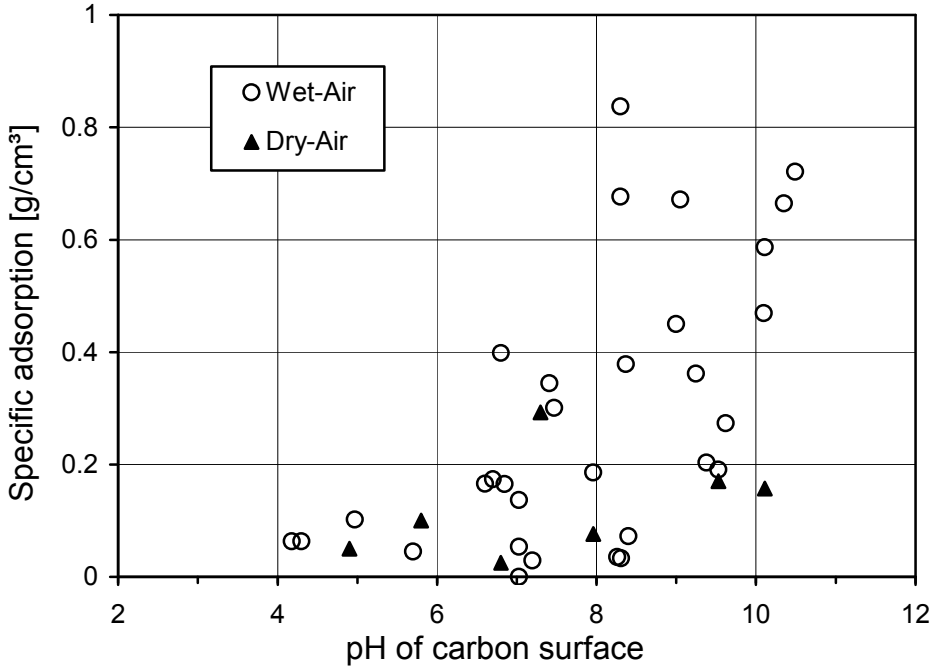

Figure 37. Dependence of the amount of MM adsorbed on surface pH of the carbons studied.

The dependence of the amount of MM adsorbed (normalized to the pore volume of the carbons studied) on the surface pH was also found and is presented in Figure 37 [195]. To broaden the spectrum of pH, some carbons were acidified with HCl [190, 191] and impregnated with NaOH [206]. In the case of microporous carbons the volume of micropores was used, whereas for carbons with a large contribution of mesopores the volume of pores smaller than 50 Å was chosen. It was assumed that only those pores are active in the adsorption process. This choice was justified knowing that: 1) at a small concentration of adsorbent in a gas mixture it is likely that only micropores and small mesopores are active in the adsorption process [2]; 2) molecular simulation studies of water adsorption suggested that at 80% humidity (our conditions) 50 Å and smaller pores are filled with water molecules [207]; 3) if the normalization is done using only the volume of micropores the density of adsorbed species is higher than liquid density of DMDS. Moreover, pore volume has to be a limiting factor for the adsorption capacity since the products of adsorption/oxidation should be stored inside the pores [113, 208]. Although the data is scattered due to the complexity of the system the maximum boundary of the adsorption capacity can be determined. A similar phenomenon was described for adsorption of hydrogen sulfide on activated carbons [113, 208].

Normalized capacity dependence on the surface pH is also shown as an example on the S208 carbon series (Figure 38) [195]. Samples were acidified to broaden the pH spectrum [113, 190]. As indicated in the legend, the points were obtained under various conditions. The circles represent data for the samples run in moist air and squares - data for the samples run in moist nitrogen. For the samples run in moist air the dependence on the pH is apparent, which supports the hypothesis about the importance of the dissociation step. On the other hand, all samples run in wet nitrogen have more or less

similar capacity. These results clearly indicate the existence of two regions related to two different phenomena. When oxygen is not present, only small amount of DMDS is adsorbed. DMDS is likely the product of oxidation of MM with chemisorbed oxygen. Since that oxygen is a limiting factor, the amount of DMDS formed is the same for all the samples, in spite of their various pH. When oxygen from air is present in the system it facilitates the oxidation process and much more DMDS is formed, consuming MM. This ensures high efficiency of MM removal.

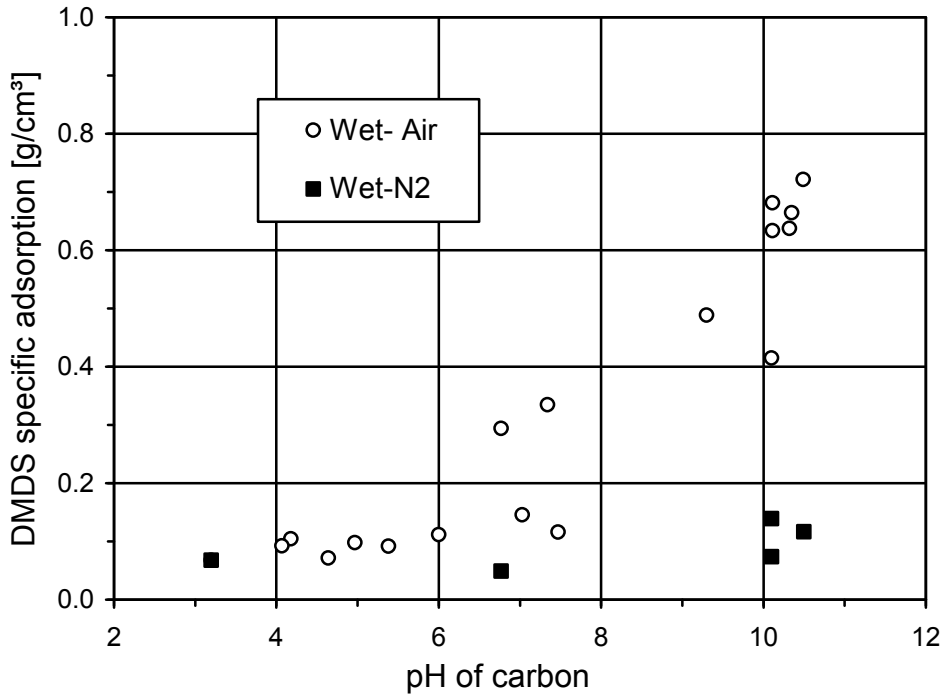

Figure 38. Dependence of the specific adsorption of DMDS on surface pH of the S208 carbon series.

To explain the apparent dependence of MM breakthrough capacity on the surface pH, two different mechanisms of adsorption/oxidation process are taken into consideration. In both cases it is supposed that adsorbed MM reacts with oxygen and than it is stored in the pore system in the form of DMDS. Taking into account the chemical nature of MM, the removal mechanism should be different in dry conditions ("dry" mechanism) and in wet conditions [195].

In the "dry" mechanism it is assumed that MM and oxygen are adsorbed from a gas phase on the dry carbon surface, where reaction takes place. Water and DMDS are the reaction products [195]. The latter species is adsorbed on the carbon surface while the former one is desorbed (Figure 39).

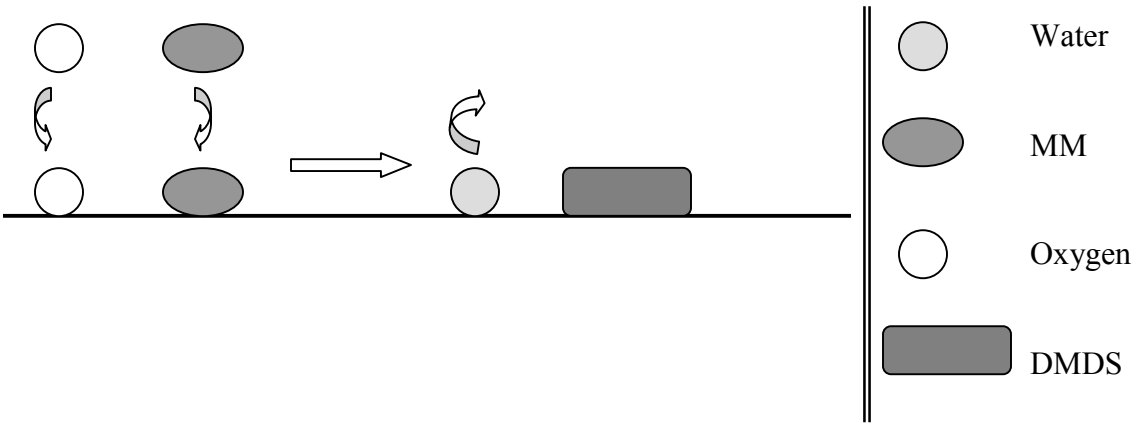

Figure 39. "Dry" mechanism of MM adsorption/oxidation on activated carbon surface.

Based on the proposed mechanism the following reactions are likely to take place [195]:

$$CH_3SH_{\,g} \rightarrow CH_3SH_{\,ads} \qquad K_{HM} \quad (5.13)$$

$$O_{2\,ads} \rightarrow 2\,O_{\,ads} \qquad K_{HO} \quad (5.14)$$

$$2\,CH_3SH_{\,ads} + O_{\,ads} \rightarrow CH_3SSCH_{3\,ads} + H_2O_{\,g} \qquad K_{R1} \quad (5.15)$$

where K_{HM}, K_{HO} and K_{R1} are equilibrium constants for MM adsorption, oxygen adsorption and surface reaction respectively.

In wet conditions water adsorbed on the carbon surface is able to create water clusters or small water islands. The adsorption of MM may occur either on the dry carbon surface or in the water clusters ("island" mechanism) [195]. The schematics of the "island" mechanism are shown in Figure 40. Methyl mercaptan and oxygen are first dissolved in the molecular form in these water clusters and later, depending on the pH, MM can dissociate to thiolate ions. Oxidation occurs due to the surface reaction between adsorbed thiolate ions and dissociatively adsorbed oxygen in water "islands" and/or between adsorbed MM and oxygen on a dry part of the carbon surface. The product of reaction, DMDS, is adsorbed in a molecular form on the carbon surface.

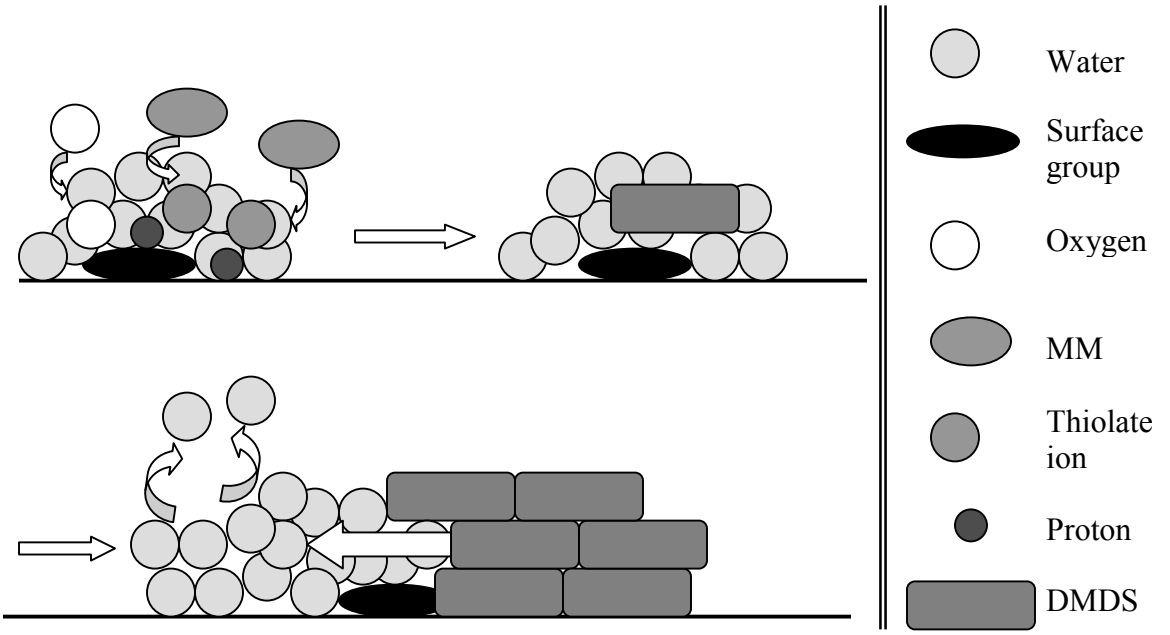

Figure 40. "Island" mechanism of MM adsorption/oxidation on activated carbon surface.

The following reaction pathways can describe the proposed mechanism [195]:

$$H_2O_g \rightarrow H_2O_{ads} \quad (5.16)$$

$$O_2 \rightarrow O_{2\ ads} \quad (5.17)$$

$$O_{2ads} \rightarrow 2\ O_{\ ads} \quad (5.18)$$

Then on the dry part of the surface:

$$CH_3SH_{\ g} \rightarrow CH_3SH_{\ ads} \quad K_{HM} \quad (5.19)$$

$$2\ CH_3SH_{\ ads} + O_{\ ads} \rightarrow CH_3SSCH_{3\ ads} + H_2O_g \quad K_{R1} \quad (5.20)$$

While on water islands:

$$O_2 \rightarrow O_{2\ L} \quad (5.21)$$

$$O_{2\ L} \rightarrow 2\ O_{\ ads\text{-}L} \quad (5.22)$$

$$CH_3SH_{\ g} \rightarrow CH_3SH_{\ L} \quad K_S \quad (5.23)$$

AtpH > pK_a

$$CH_3SH_{\ L} \rightarrow CH_3S^-_{\ L} + H^+ \quad K_a \quad (5.24)$$

$$CH_3S^-_{\ L} \rightarrow CH_3S^-_{\ ads\text{-}L} \quad K_I \quad (5.25)$$

$$2\ CH_3S^-_{\ ads\text{-}L} + O_{\ ads\text{-}L} \rightarrow CH_3SSCH_{3\ ads\text{-}L} + O^{2-} \quad K_{R1} \quad (5.26)$$

$$O^{2-} + 2\ H^+ \rightarrow H_2O \quad (5.27)$$

At pH < pK_a

$$CH_3SH_{\ L} \rightarrow CH_3SH_{\ ads\text{-}L} \quad K_L \quad (5.28)$$

$$2\ CH_3SH_{\ ads\text{-}L} + O_{\ ads\text{-}L} \rightarrow CH_3SSCH_{3\ ads\text{-}L} + H_2O \quad K_{R2} \quad (5.29)$$

where subscripts g, ads, and ads-L are concentrations of species in gas, adsorbed, and liquid phases, respectively, K_{HM}, K_I, K_S, K_a, K_L, K_{R1} and K_{R2} are equilibrium constants for related processes (adsorption from a gas phase on the dry surface, adsorption of the ionic form, gas solubility, dissociation, adsorption of the liquid form and surface reaction constants), and O_{ads} is dissociatively adsorbed oxygen.

The formation of MMTS ($C_2H_6O_2S_2$) detected by GC/MS could take place through the oxidation of DMDS:

$$CH_3SSCH_3 + 2\ O_{ads} \rightarrow CH_3SOSCH_{3\ ads} + O_{ads} \rightarrow CH_3SO_2SCH_{3\ ads} \quad (5.30)$$

Another possible scenario for the formation of MMTS is through the disproportionation of sulfinic acid [147]:

$$3\ CH_3SO_2H \rightarrow C_2H_6S_2O_2 + CH_3SO_3H + H_2O \quad (5.31)$$

Although sulfonic acid was not detected on the surface of the carbons by GC/MS, if it is formed it can be stored deep inside the carbon pores, thus explaining a noticeable decrease in pH for all carbons after MM adsorption (Table 1). Sulfonic acid is a strong acid and its effect on pH should be greater than a decrease of 3 or 4 pH units.

Since water is present in the system and the carbon surface is able to produce and sustain active oxygen radicals and hydroxyl radicals [149, 152] further oxidation of disulfides to α-sulfinic acid, CH_3SO_2H, and formation of methane sulfonic acid is possible (Figure 41):

$$CH_3SSCH_{3\,ads} + 2\,O_{ads} + H^+ \rightarrow CH_3SO_2H_{ads} + CH_3S^*_{ads} \quad (5.32)$$

$$CH_3S^*_{ads} + 3\,O_{ads} + H^+ \rightarrow CH_3SO_3H_{ads} \quad (5.33)$$

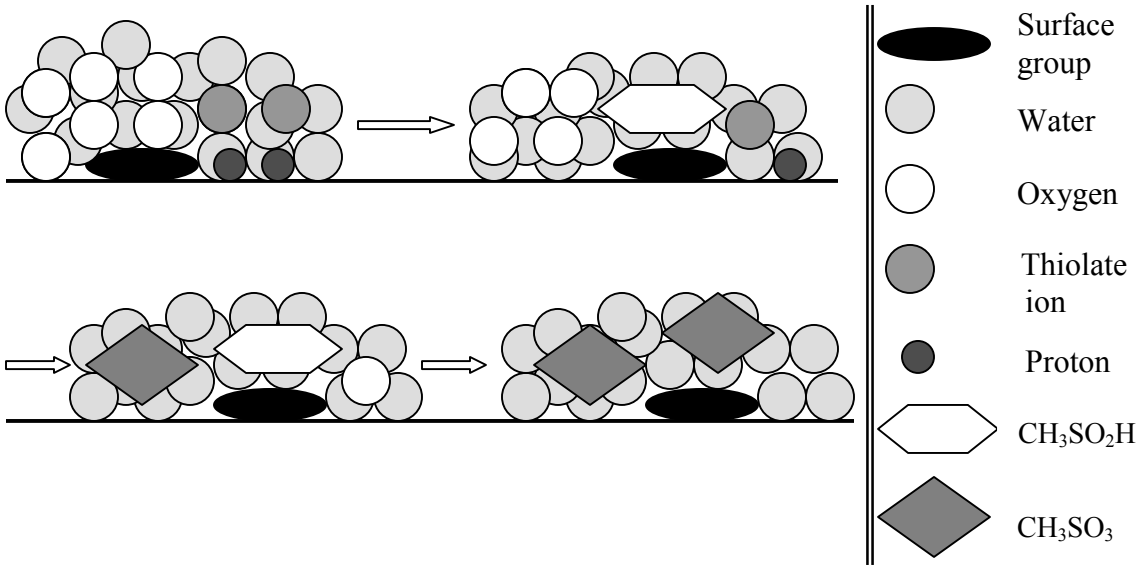

Figure 41. Oxidation mechanism of DMDS to α-sulfinic acid (CH_3SO_2H) and methane sulfonic acid (CH_3SO_3H).

To find the total concentration of MM in the adsorbed state (in molecular and ionic forms) the following relationship can be applied [195]:

$$[CH_3SH_{ads}] + [CH_3S^-_{ads\text{-}L}] = K_{HM} * [CH_3SH_g] * (1 - \theta_W) + K_S * K_a * K_1 * \theta_W * [CH_3SH_g]/[H^+] \quad (5.34)$$

where θ_W is the surface coverage by water.

From the equation (5.13) the concentration of MM in the adsorbed state would be determined in the following way:

$$[CH_3SH_{ads}] = K_{HM} * [CH_3SH_g] \quad (5.35)$$

where $[CH_3SH_g]$ is the concentration of MM in a gas phase.

From the examination of equations (5.13) – (5.15) and (5.35) it is clear that for the dry mechanism one cannot expect any pH dependence for the adsorption capacity due to the lack of water on the surface.

The "island" mechanism proposes two scenarios, which can coexist. While the first one, on the dry part of the surface, is similar to the "dry" mechanism, the second scenario is definitely pH-dependent due to the presence of a dissociation step. It follows that in the case of MM adsorption on activated carbons, though the pH dependence is expected due to the chemistry of adsorbate it cannot be so clearly seen as in the case of hydrogen sulfide removal [113, 190]. In fact this explains the "scattering" of the experimental points seen in Figure 37.

The precise expression for MM capacity dependence on the carbon surface pH can be obtained by solution of the set of equations, describing adsorption-oxidation of MM from wet air in dynamic conditions. Another goal is an estimation of the pH threshold value where the sharp change in capacity can occur [113, 190]. From equation (5.34), the dependence of the predicted capacity on the pH has a step-like shape, which is in agreement with the experimental data trend. To find a pH range where transition in capacity may occur, the second term in equation (5.34) has to be analyzed [195].

$$[CH_3S^-_{ads\text{-}L}] = K_S * K_a * K_I * \theta_W * [CH_3SH_g]/[H^+] \quad (5.36)$$

$$log\,([CH_3S^-_{ads\text{-}L}]) = log\,(K_S) + log\,(K_I) + pK_a + log\,(\theta_W) + pH + log\,([CH_3SH_g]) \quad (5.37)$$

Solubility of pure CH_3SH at 25°C in water is 0.813 mol/L [147, 209], which corresponds to K_S = 9.9 [209]. The distribution coefficient for the ionic form, K_I, depends on the interaction of CH_3S^- with carbon and should be determined independently as a ratio of $[CH_3S^-_{ads\text{-}L}]$ to $[CH_3S^-_L]$. For the evaluation it was assumed that $[CH_3S^-_{ads}]$ is not higher than static anion-exchange capacity of activated carbon, which is determined by the amount of basic groups on the carbon surface. The amount of basic groups measured by Boehm method for the carbons studied is in the range of 0.1 to 0.5 mmol/g [43, 113, 191]. For 3,000 ppm of CH_3SH in the gas phase, taking into account solubility constant and condition for complete dissociation, it follows that $[CH_3S^-_L]$ will be not larger than 1.2 mmol/L. Then K_I will be in the range from 42 to 208, with average value equal to 125. The constant for MM dissociation in water, K_a, is equal to $5.0*10^{-11}$ [147]. The water surface coverage was estimated from the amount of water preadsorbed and its cross-sectional area (10.5 Å^2). The values of θ_W are varied from 0.26 to 0.69 depending on the type of carbon and the average value is equal to 0.43. Substitution of K_S, K_I, K_a and θ_W values in equation (5.37) gives:

$$log\,([CH_3S^-_{ads\text{-}L}]) = -7.6 + pH + log\,([CH_3SH_g]) \qquad (5.38)$$

By plugging in the above-mentioned constants and the value for $[CH_3SH_g]$ into expression (5.37), predicted dependencies between the amount of MM adsorbed and surface pH were calculated and are presented in Figure 42 [195]. The thick line represents the process on activated carbon (dissolution, dissociation and adsorption) and the thin line - the process of oxidation in the volume of water (dissolution, dissociation).

However the comparison of experimental and calculated results (Figures 37 and 42) reveals similar trends, there are samples, which have small normalized capacities in spite of their high pH. This may be related to coexistence of both mechanisms of MM removal, pH-dependent and pH-independent.

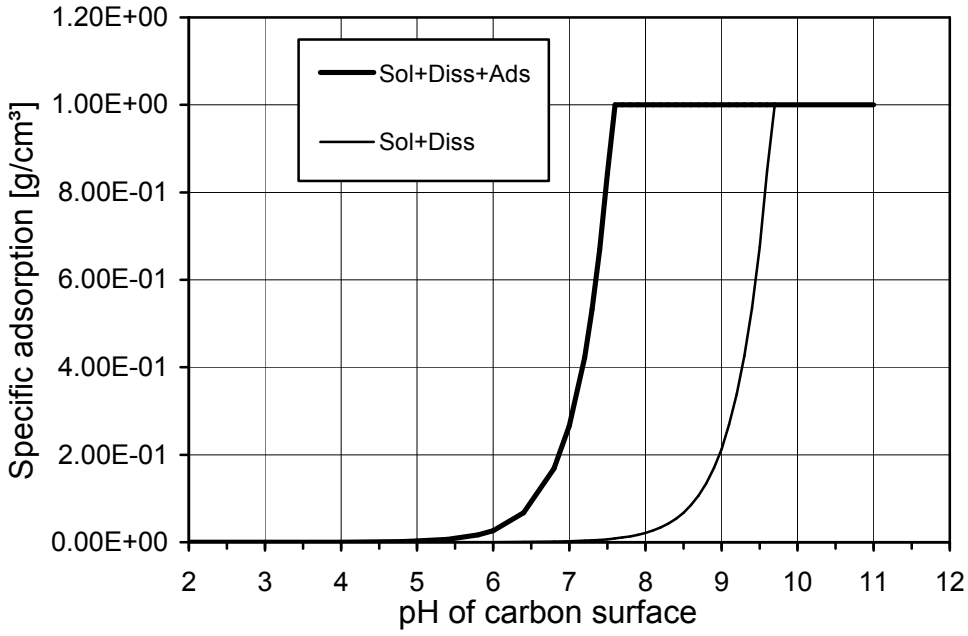

Figure 42. Predicted dependencies of the amounts of MM adsorbed on the surface pH of the carbons studied (thick line – dissolution, dissociation, adsorption; thin line – dissolution, dissociation).

This simplified expression (5.38) suggests that for all carbons with the average surface pH greater than 7.6, concentration of CH_3S^- in the adsorbed state will be equal to CH_3SH in a gas phase (100% dissociation + adsorption), which is required for effective CH_3SH removal. It is about 2.7 pH units less than for simple dissociation in water. These results support the significance of the activated carbon surface and its effect on physicochemical processes taking place in the pore system.

Although for most of the carbons studied the pH of the surface is below 7.6

(Table 1), they still exhibit significant MM capacity values. In this case it should be taken into consideration that the pH values reported in Table 1 are the ones that are characteristic for the carbon surface (section *4.2.12*) and can deviate from the ones found inside the carbon pores. Nonetheless, the pH of the BAX carbon is the lowest among the initial carbons studied and may be just below the threshold value for the effective MM removal. This could be one of the reasons for the poor performance of this carbon towards the adsorption of MM.

To explain the influence of iron on the adsorption of CH_3SH, its catalytic abilities have to be explored. It is possible that besides the mechanism described above, the following reactions promoted by Fe^{3+} occur in the presence of moisture and oxygen form air [194]:

$$2\ CH_3SH \rightarrow 2\ CH_3S^- + 2\ H^+ \quad (5.39)$$

$$Fe^{3+} + 2CH_3S^- \rightarrow Fe^{2+} + 2CH_3S^{\bullet} \quad (5.40)$$

$$Fe^{2+} + O_2 \rightarrow Fe^{3+} + O_2^{-\bullet} \quad (5.41)$$

$$O_2^{-\bullet} + 2H^+ \rightarrow H_2O_2 \quad (5.42)$$

$$2\ CH_3S^{\bullet} \rightarrow CH_3SSCH_3 \quad (5.43)$$

$$2\ CH_3SH + H_2O_2 \rightarrow 2\ CH_3S^{\bullet} + 2\ H_2O \quad (5.44)$$

As seen from the above reactions, the role of iron is to promote the formation of very active thiolate radicals and superoxide species. The formation of these species is likely to occur through the electron transfer mechanism, taking into account the

conductivity of activated carbons [52, 53]. In such a mechanism the electron is first transferred from sulfur to iron to form thiolate radicals and then from iron to oxygen to form superoxide species. As a result the iron sites are reduced from Fe^{3+} to Fe^{2+} but are regenerated after further reexposure to oxygen. Furthermore, very active superoxide species could participate in the formation of other radicals either in wet or dry conditions. More so, the formation of hydrogen peroxide is also possible, which can further react with CH_3SH to form more thiolate radicals.

The schematic representation of this mechanism is shown below.

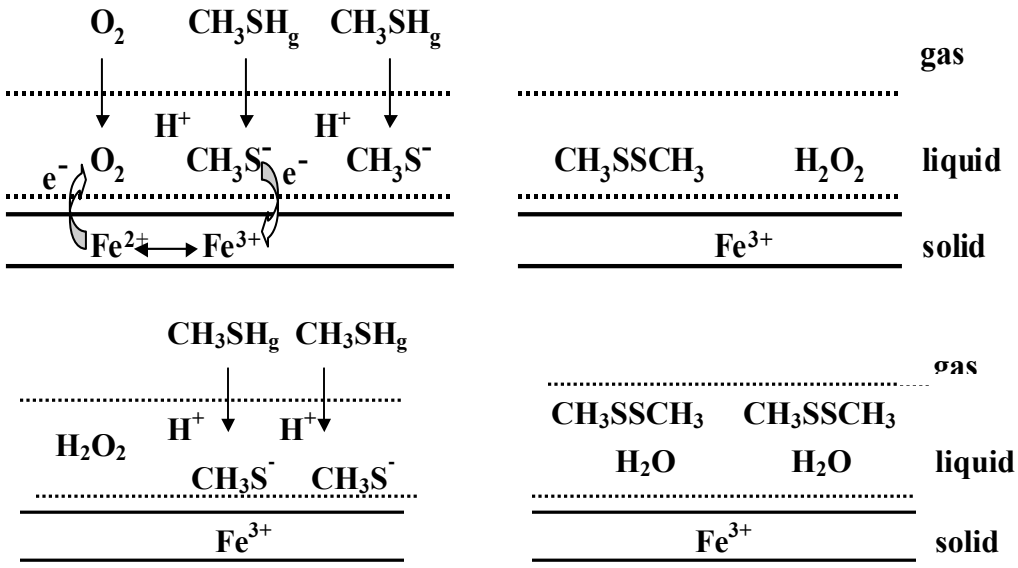

Figure 43. The mechanism of catalytic participation of iron in the process of MM adsorption/oxidation.

Another element found to catalytically enhance the process of MM adsorption/oxidation on the activated carbons is nitrogen [192]. Taking into account this fact and the ability of CH_3SH to dissociate the mechanism for MM adsorption/oxidation on the nitrogen containing carbons is proposed (Figure 44) [192]. Since after high

temperature treatment the majority of nitrogen is in pyridinic and quaternary configurations the following mechanism will involve these types of nitrogen. The role of nitrogen in this mechanism is similar to that of iron and infers the formation of thiolate radicals and superoxide species. MM is first adsorbed from the gas phase on the carbon surface, where, due to the presence of the water film, it is dissolved and then, depending on the pH it can dissociate with the formation of thiolate ions and protons; 2) since the positively charged quaternary nitrogen enhances the ion-exchange properties of activated carbons, thiolate ion is adsorbed in the vicinity of the nitrogen center; 3) then nitrogen accepts an electron from sulfur and transfers it to the oxygen adsorbed on the surface; 4) as a result, thiolate radicals and superoxides ions O_2^- can be formed with the latter triggering the formation of hydroxyl radicals; 5) the final step of the oxidation process is the formation of DMDS and water. All of this should gradually happen in a confined pore space where the reaction products are stored. The reaction will proceed until all the pores with positively charged nitrogen centers are filled with the reaction products, and then only physical adsorption of MM takes place.

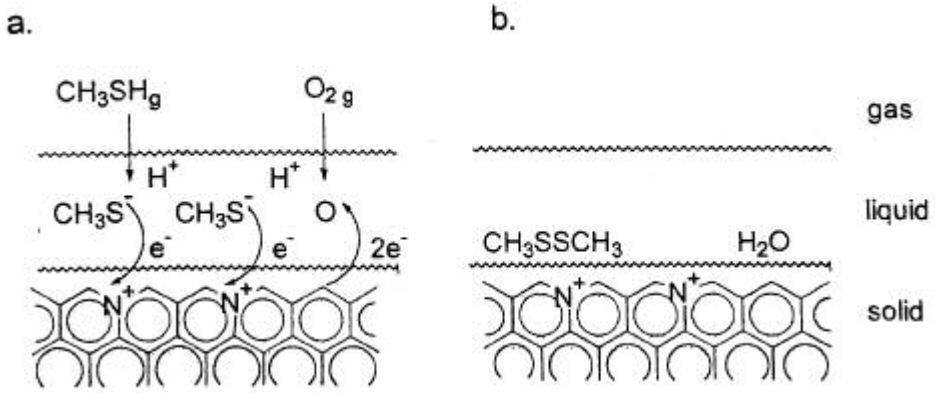

Figure 44. The mechanism of catalytic adsorption/oxidation of MM on nitrogen-containing carbons [192].

6. CONCLUSIONS

Results of the present work show the complexity of the MM adsorption/oxidation process on activated carbons. Each individual activated carbon is unique and has its own versatile nature that determines its ability to adsorb MM. The driving forces found responsible for the adsorption/oxidation of MM include: surface chemistry, composition of inorganic phase, presence of water, pH of the carbon surface, and structural characteristics.

The chemistry of the carbon surface is very complicated and was found to play a major role in the process of MM adsorption. Thus, both acidic and basic oxygen-containing groups are present on the carbon surface but only those of basic nature (pyrone-type) were found to increase the adsorption of MM. Such basic oxygen-containing groups affect the dissociation of MM and oxidation of thiolate ions to disulfides in wet conditions. They may also attract MM via weak acid-base interactions, which is likely the case in dry conditions.

Besides oxygen, nitrogen is another element present in the form of different functional groups on the carbon surface. Even though nitrogen is a natural component in bituminous coal-based carbons, for most of the carbons studied it was introduced by urea modification and heat treatment. As a result, it is incorporated into the carbon matrix in pyridine-like and “quaternary” configurations, which raises the basicity of the carbon surface and elevates its pH. Although this appears to be a very important factor in the process of MM adsorption/oxidation, the highest catalytic activity is noticed when N/C ratio for the carbons is equal to 0.02 and the minimum in the band gap occurs.

The complexity of surface chemistry is also determined by the presence of inorganic matter, which includes different metals that participate in the adsorption process. One of these metals, iron, is especially active and catalytically enhances the adsorption of MM. A good proof for this is a 3.3-fold increase in the MM removal capacity of the PCB carbon upon introduction of iron into its matrix.

This follows that both nitrogen and iron can play the role of a catalyst in the MM adsorption process. They will increase the adsorption of MM through the electron transfer mechanism and the formation of active thiolate radicals and superoxide species.

Another important feature of the carbon surface is the presence of water, which appears to have a dual role in the process of MM removal. It was found that DMDS, which is the main product of MM adsorption/oxidation, has to compete with water for the active adsorption sites on the surface. This phenomenon seems to be especially reasonable if taking into account the lack of disulfide solubility in water. However, in competition, DMDS is always the "winner" owing to its stronger adsorption forces. On the other hand, the formation of significant amount of DMDS is not possible without the presence of water in the system. Water facilitates dissociation of MM, leading to its oxidation by oxygen either from air, being chemisorbed on the carbon surface, or as a part of surface oxygen-containing groups. When water is not in the system, MM adsorption capacities for the carbons studied were at least twice smaller than those obtained in wet conditions. More so, the amounts of MM adsorbed are the same when the tests are run in dry air and dry nitrogen, indicating the lack of participation of oxygen from air, not chemisorbed or bonded to the surface.

Despite the importance of the surface chemistry, the process of adsorption cannot be effective without a developed pore structure where the products of adsorption/oxidation have to be stored. It was found that the pore volume and pore size are the critical parameters for the effective adsorption process. The pores of molecular size are most likely to enhance the amount adsorbed. In such pores the adsorption forces are stronger and energetic parameters of adsorption, such as characteristic energy of adsorption and heat of adsorption, are strongly enhanced due to overlapping of the adsorption potentials. Statistical-molecular calculations confirmed that in an activated carbon – water – DMDS system under equilibrium conditions, DMDS tends to substitute for water in the adsorbed state and the highest capacity for DMDS adsorption is found for microporous carbons.

Due to the presence of water, MM is expected to dissociate to thiolate ions and protons but this process will take place only if the pH of the carbon surface is higher than pK_a of MM. The latter value is reported to be 10.3 suggesting that the dissociative adsorption of MM may occur only on the very basic carbon surface. To explain the apparent dependence of MM adsorption capacity on the surface pH, two different mechanisms of adsorption/oxidation are proposed. In both cases it is assumed that adsorbed MM reacts with oxygen and is stored as DMDS in the carbon pore system. For the "dry" mechanism no pH dependence is found due to the lack of water on the surface. For the "island" mechanism, hyperbolic dependence is found due to coexistence of two scenarios, one on the dry part of the carbon surface, another inside the water islands. The pH threshold estimated from the set of equations describing adsorption/oxidation from wet air in dynamic conditions is found to be 7.6. Even though the surface pH of some of

the carbons studied is below 7.6, they still exhibit the significant MM capacity values. This could be explained by different pH values found on the surface and inside the carbon pores. Still for one carbon, BAX, the pH value is the lowest among the carbons studied and it might be just below the threshold value needed for the efficient MM removal.

It was also noticed that after adsorption of MM, the pH of carbon surface decreases and becomes more acidic. For some carbons the change in pH is 3-5 units, which could not have resulted just from the formation of DMDS. Even though the only other product of MM adsorption/oxidation detected by GC/MS is MMTS, the formation of sulfinic and methane sulfonic acid is also possible. The former one is not stable and is easily oxidized to sulfonic acid. The latter one is a very strong acid and its effect on the pH value could be a decrease of more than 3-5 units. However, if sulfonic acid is formed, it is likely to be adsorbed deep inside the carbon pores from where it is not easily extractable.

To conclude, it is clear that the adsorption process of MM on activated carbons is rather complicated and is governed by many carbon features. It is indeed the combination of surface basicity, oxygen, catalytically active metals, water, and developed microporosity that leads to the effective adsorption process.

8. APPLIED IMPACT

The description of the mechanism of MM adsorption/oxidation on activated carbons along with identifying the important features of carbon adsorbents will find the direct application in controlling natural and industrial processes where sulfur derivatives are present.

Some of the possible applications include:

- Pulp mills
- Food processing plants
- Livestock feedlots
- Municipal landfills
- Petroleum refineries
- Sewage treatment plants
- Plastics industry.

Nowadays much research is done in the area of fuel cells, which are expected to play a major role in the nation's energy future. One of the energy sources used in fuel cells for power generation is natural gas. It is clean, safe, and the most useful of all energy sources. However, it contains naturally occurring reduced sulfur compounds such as hydrogen sulfide, mercaptans and thiophenes, which due to their ability to poison the catalyst are detrimental to subsystems within the fuel processor and to the fuel cell stacks. Therefore, this research appears to be very useful in trying to remove these sulfur compounds prior to the fuel reforming operation.

REFERENCES

1. Donnet, J.B., Papier, E., Wang, W., Stoeckli, H.F. The Observation of Activated Carbons by Scanning Microscopy. *Carbon* **32**, 183 (1994).

2. Everett, D.H., Powl, J.C. *J.* Adsorption in Slit-like and Cylindrical Micropores in the Henry's Law Region. *Chem. Soc*., *Faraday Trans. 1*, **72**, 619 (1976).

3. Gregg, S.J.; Sing, K.S.W. "Adsorption, Surface Area and Porosity", Academic Press: London, 2nd Ed., 1982.

4. Bansal, R.C., Donnet, J.B., Stoeckli, F. "Active Carbon", Marcel Dekker: New York, 1988.

5. Marsh, H., Heintz, E.A., Rodriguez-Reinoso, F. Eds. "Introduction to Carbon Technologies", University of Alicante, Alicante, Spain, 1997.

6. Toles, C., Rimmer, S., Hower, J.C. Production of Activated Carbons from a Washington Lignite Using Phosphoric Acid Activation. *Carbon* **34**, 1419 (1996).

7. Caturla, F., Molina-Sabio, M., Rodriguez-Reinoso, F. Preparation of Activated Carbon by Chemical Activation with $ZnCl_2$. *Carbon* **29**, 999 (1991).

8. Jagtoyen, M., Thwaites, M., Stencel, J., McEnaney, B., Derbyshire, F. Adsorbent Carbon Synthesis from Coals by Phosphoric Acid Activation**.** *Carbon* **30**, 1089 (1992).

9. Teng, H., Yeh, T.-S., Hsu, L.-Y. Preparation of Activated Carbon from Bituminous Coal with Phosphoric Acid Activation. *Carbon* **36**, 1387 (1998).

10. Teng,H., Yeh, T.-S. Preparation of Activated Carbons from Bituminous Coals with Zinc Chloride Activation. *Ind. Eng. Chem. Res*. **37**, 58 (1998).

11. Lozano-Castello, D., Lillo-Rodenas, M.A., Cazorla-Amoros, D., Linares-Solano, A. Preparation of Activated Carbons from Spanish Anthracite: I. Activation by KOH. *Carbon* **39**, 741 (2001).

12. Lillo-Rodenas, M.A., Lozano-Castello, D., Cazorla-Amoros, D., Linares-Solano, A. Preparation of Activated Carbons from Spanish Anthracite: II. Activation by NaOH. *Carbon* **39**, 751 (2001).

13. Qiao, W., Ling, L., Zha, O., Liu, L. Preparation of a Pitch-based Activated Carbon with a High Specific Surface Area. *J. Mater. Sci.* **32**, 4447 (1997).

14. Hu, Z., Srinivasan, M.P. Mesoporous High-Surface-Area Activated Carbon. *Micropor. Mesopor. Mater.* **43**, 267 (2001).

15. Smisek, M., Cerny, S. "Active Carbon: Manufacture, Properties and Applications". *Elsevier*, Amsterdam, 1970.

16. Hayashi, J., Kazehaya, A., Muroyama, K., Watkinson, A.P. Preparation of Activated Carbon from Lignin by Chemical Activation. *Carbon* **38**, 1873 (2000).

17. Hayashi, J., Horikawa, T., Muroyama, K., Gomes, V.G. Activated Carbon from Chickpea Husk by Chemical Activation with K_2CO_3: Preparation and Characterization. *Micropor. Mesopor. Mater.* **55**, 63 (2002).

18. Puri, B.R, in "Chemistry and Physics of Carbon", Walker P.J., Ed.; Marcel Dekker: New York, 1970, Vol. **6**, pp. 191-282.

19. Thomas, J.M., in "Chemistry and Physics of Carbon", Walker P.L. Jr., Ed.; Marcel Dekker: New York, 1965, Vol. **1**, pp. 121-202.

20. Hennig, G.R., in "Chemistry and Physics of Carbon", Walker P.L. Jr., Ed.; Marcel Dekker: New York, 1966, Vol. **2**.

21. Yang, R.T., in "Chemistry and Physics of Carbon", Thrower, P.A., Ed.; Marcel Dekker: New York, 1984, Vol. **19**, pp. 163-210.

22. Boehm, H.P. Some Aspects of the Surface Chemistry of Carbon Blacks and Other Carbons. *Carbon* **32**, 759 (1994).

23. Boehm, H.P. Surface Oxides on Carbon and Their Analysis: A Critical Assessment. *Carbon* **40**, 145 (2002).

24. Radovic, L.R., Moreno-Castilla, C., Rivera-Utrilla, J., in "Chemistry and Physics of Carbon", Thrower, P.A., Ed.; Marcel Dekker: New York, 2001, Vol. **27**, pp. 227-405.

25. Leon y Leon, C.A., Solar, J.M., Calemma, V., Radovic, L.R. Evidence for the Protonation of Basal Plane Sites on Carbon. *Carbon* **30**, 797 (1992).

26. Boehm, H.P., In "Advances in Catalysis", Eley, D.D., Pines, H., and Weisz, P.B., Ed.; Academic press: New York, London, 1966, Vol. **16**, p.179.

27. Donnet, J.B. The Chemical Reactivity of Carbons**.** *Carbon* **6**, 161 (1968).

28. Contescu, A., Vass, M., Contescu, C., Putyera, K., Schwarz, J.A. Acid Buffering Capacity of Basic Carbons Revealed by Their Continuous pK Distribution. *Carbon* **36**, 247 (1998).

29. Voll, M., Boehm, H.P. Basische Oberflächenoxide auf Kohlenstoff—IV. Chemische Reaktionen zur Identifizierung der Oberflächengruppen. *Carbon* **9**, 481 (1971).

30. Lau, A.C., Furlong, D.N., Healy, T.W., Grieser, F. The Electrokinetic Properties of Carbon Black and Graphitized Carbon Black Aqueous Colloids. *Coll. Surf.* **18**, 93 (1986).

31. T. J. Fabish and D. E. Schleifer. Surface Chemistry and the Carbon Black Work Function**.** *Carbon* **22**, 19 (1984).

32. Montes-Moran, M.A., Menendez, J.A., Fuente, E., Suarez, D. Contribution of the Basal Planes to Carbon Basicity: An Ab Initio Study of the H_3O^+-π Interaction in Cluster Models. *J. Phys. Chem. B* **102**, 5595, (1998).

33. Suarez, D., Menendez, J.A., Fuente, E., Montes-Moran, M.A. Contribution of Pyrone-Type Structures to Carbon Basicity: An ab Initio Study. *Langmuir* **15**, 3897 (1999).

34. Fuente, E., Menendez, J.A., Suarez, D., Montes-Moran, M.A. Basic Surface Oxides on Carbon Materials: A Global View. *Langmuir* **19**, 3505 (2003).

35. Papirer, E., Sheng, L., Donnet, J.B. Contribution to the Study of Basic Surface Groups on Carbons. *Carbon* **25**, 243 (1987).

36. Boehm, H.P., Mair, G., Stöhr, T., de Rincon, A.R., Tereczki, B. The Effect of Demineralisation on Lignite Surface Properties. *Fuel* **63**, 1061 (1984).

37. Stöhr, T., Boehm, H.P., Schlögl, R. Enhancment of the Catalytic Activity of Activated Carbons in Oxidation Reactions by Thermal Treatment with Ammonia or Hydrogen Cyanide and Observation of a Superoxide Species as a Possible Intermediate. *Carbon* **29**, 707 (1992).

38. Mang, D., Boehm, H.P. Inhibiting Effect of Incorporated Nitrogen on the Oxidation of Microcrystalline Carbons. *Carbon* **30**, 391 (1992).

39. Jansen, R.J., Bekkum, H.V. XPS of Nitrogen-Containing Functional Groups on Activated Carbon**.** *Carbon* **33**, 1021 (1995).

40. Singoredjo, L., Kapteijn, F., Moulijn, J.A., Martin-Martinez, J.M., Boehm, H.P. Modified Activated Carbons for the Selective Catalytic Reduction of NO with NH_3. *Carbon* **31**, 213 (1993).

41. Abotsi, G.M.K., Scaroni, A.W. Reaction of Carbons with Ammonia: Effects of the Surface Charge and Molybdenum Adsorption. *Carbon* **28**, 79 (1990).

42. Bagreev, A., Bashkova, S., Bandosz, T.J. Adsorption of SO_2 on Activated Carbons: The Effect of Nitrogen Functionality and Pore Sizes. *Langmuir* **18**, 1257 (2002).

43. Adib, F., Bagreev, A., Bandosz, T.J. Adsorption/Oxidation of Hydrogen Sulfide on Nitrogen-Containing Activated Carbons. *Langmuir* **16**, 1980 (2000).

44. El-Sayed, Y., Bandosz, T.J. Acetaldehyde Adsorption on Nitrogen-Containing Activated Carbons. *Langmuir* **18**, 3213 (2002).

45. Bagreev, A., Menendez, A.J., Dukhno, I., Tarasenko, Y.A., Bandosz, T.J. Bituminous Coal-Based Activated Carbons Modified with Nitrogen as Adsorbents of Hydrogen Sulfide. *Carbon* **42**, 469 (2004).

46. Kapteijn, F., Moulijn, J.A., Matzner, S., Boehm, H.P. The Development of Nitrogen Functionality in Model Chars during Gasification in CO_2 and O_2. *Carbon* **37**, 1143 (1999).

47. Pels, J.R., Kapteijn, F., Moulijn, Zhu, Q., Thomas, K.M. Evolution of Nitrogen Functionalities in Carbonaceous Materials during Pyrolysis. *Carbon* **33**, 1641 (1995).

48. Lee, J.K., Shim, H.J., Lim, J.C., Choi, G.J., Kim, Y.D, Min, B.G., Park, D. Influence of Tension During Oxidative Stabilization on SO_2 Adsorption Characteristics of Polyacrylonitrile (PAN) Based Activated Carbon Fibers. *Carbon* **35**, 837 (1997).

49. Lahaye, J., Nanse, G., Bagreev, A., Strelko, V. Porous Structure and Surface Chemistry of Nitrogen Containing Carbons from Polymers. *Carbon* **37**, 585 (1999).

50. Lahaye, J., Nanse, G., Fioux, P., Bagreev, A., Broshnik, A., Strelko, V. Chemical Transformation During the Carbonisation in Air and the Pyrolysis under Argon of a Vinylpyridine–Divinylbenzene Copolymer by X-ray Photoelectron Spectroscopy. *Appl. Surf. Sci.* **147**, 153 (1999).

51. Kelemen, S.R., Gorbaty, M.L., Kwiatek, P.J. Quantification of Nitrogen Forms in Argonne Premium Coals. *Energy & Fuels* **8**, 896 (1994).

52. Mrozowski, S. Semiconductivity and Diamagnetism of Polycrystalline Graphite and Condensed Ring Systems. *Phys. Rev.* **85**, 609 (1952).

53. Strelko, V., Kuts, V.S., Thrower, P.A. On the Mechanism of Possible Influence of Heteroatoms of Nitrogen, Boron and Phosphorus in a Carbon Matrix on the Catalytic Activity of Carbons in Electron Transfer Reactions. *Carbon* **38**, 1499 (2000).

54. Dubinin, M.M. Water Vapor Adsorption and the Microporous Structures of Carbonaceous Adsorbents. *Carbon* **18**, 355 (1980).

55. Jankowska, H., Swiatowski, A., Oscik, J., Kusak, R. Adsorption from Benzene-Ethanol Binary Solutions on Activated Carbons with Different Contents of Oxygen Surface Complexes**.** *Carbon* **21**, 117 (1983).

56. Hagiwara, S., Tsutsumi, K., Takahashi, H. Interaction Between Active Hydrogen Sites on Carbon Black Surface and Alcohol Molecules**.** *Carbon* **19**, 107 (1981).

57. Davini, P. Adsorption of Sulphur Dioxide on Thermally Treated Active Carbon. *Fuel* **68**, 145 (1989).

58. Davini, P. Adsorption and Desorption of SO_2 on Active Carbon: The Effect of Surface Basic Groups**.** *Carbon* **28**, 565 (1990).

59. Anurov, S.A. Physicochemical Aspects of the Adsorption of Sulfur Dioxide by Carbon Adsorbents. *Russian Chemical Reviews* **65**, 663 (1996).

60. Matsumura, Y., Yamabe, K., Takahashi, H. The Effects of Hydrophilic Structures of Active Carbon on the Adsorption of Benzene and Methanol Vapors. *Carbon* **23**, 263 (1985).

61. Rodriguez-Reinoso, F., Milano-Sabio, M., Munecas, M.A. Effect of Microporosity and Oxygen Surface Groups of Activated Carbon in the Adsorption of Molecules of Different Polarity. *J. Phys. Chem.* **96**, 2707 (1992).

62. Kaneko, K., Inouye, K. Effect of Heat Treatment in Vacuo on the NO Adsorption Activity of α-FeOOH-Dispersed Activated Carbon Fibers. *Carbon* **24**, 772 (1986).

63. Carrasco-Marin, F., Mueden, A., Centeno, T.A., Stoeckli, F., Moreno-Castilla, C. Water Adsorption on Activated Carbons with Different Degrees of Oxidation. *J. Chem. Soc., Faraday Trans.* **93**, 2211 (1997).

64. Salame, I.I., Bandosz, T.J. Study of Water Adsorption on Activated Carbons with Different Degrees of Oxidation. *J. Colloid Interface Sci.* **210**, 367 (1999).

65. Bandosz, T.J., Jagiello, J., Schwarz, J.A., Krzyzanowski, A. Effect of Surface Chemistry on Sorption of Water and Methanol on Activated Carbon. *Langmuir* **12**, 6480 (1996).

66. Tressmer, C.H., Vidic, R.D., Uranowski, L.J. Impact of Oxygen-Containing Surface Functional Groups on Activated Carbon Adsorption of Phenol. *Environ. Sci. Technol.* **31**, 1872 (1997).

67. Rodriguez-Reinoso, F., Molina-Sabio, M., Gonzalez, M. Effect of Oxygen surface Groups on the Immersion Enthalpy of Activated Carbons in Liquids of Different Polarity. *Langmuir* **13**, 2354 (1997).

68. Lopez-Ramon, M.V., Stoeckli, F., Moreno-Castilla, C., Carrasco-Marin, F. Specific and Nonspecific Interactions between Methanol and Ethanol and Active Carbons. *Langmuir* **16**, 5967 (2000).

69. Molina-Sabio, M., Munecas, M.A., Rodriguez-Reinoso, F, McEnaney, B. Adsorption of CO_2 and SO_2 on Activated Carbons with a Wide Range of Micropore Size Distribution. *Carbon* **33**, 1777 (1995).

70. Westmoreland, P.R., Gibson, J.B., Harrison, D.P. Comparative Kinetics of High-Temperature Reaction between H_2S and Selected Metal Oxides. *Environ. Sci. Technol.* **11,** 488 (1977).

71. Yumura, M., Furimsky, E. Comparison of CaO, ZnO, and Fe_2O_3 as Adsorbents at High Temperatures. *Ind. Eng. Chem. Process Des. Dev.* **24**, 1165 (1985).

72. Stirling, D. The Sulfur Problem: Cleaning up Industrial Feedstocks. In "RSC Clean Technology Monographs", Clark, J.H., Ed.; Royal Society of Chemistry, Cambridge, 2000.

73. Davidson, J.M., Sohail, K. A DRIFTS Study of the Surface and Bulk Reactions of Hydrogen Sulfide with High Surface Area Zinc Oxide. *Ind. Eng. Chem. Res.* **34**, 3675 (1995).

74. Davidson, J.M., Lawrie, C.H., Sohail, K. Kinetics of the Adsorption of Hydrogen Sulfide by High Purity and Doped High Surface Area Zinc Oxide. *Ind. Eng. Chem. Res.* **34**, 2981 (1995).

75. Davidov, A., Chuang, K.T., Sanger, A.R. Mechanism of H_2S Oxidation by Ferric Oxide and Hydroxide Surfaces. *J. Phys. Chem. B* **102**, 4745 (1998).

76. Miura, K., Mae, K., Inoue, T., Yoshimi, T, Nakagawa, H., Hashimoto, K. Simultaneous Removal of COS and H_2S from Coke Oven Gas at Low Temperature by Use of an Iron Oxide. *Ind. Eng. Chem. Res.* **31**, 415 (1992).

77. Baird, T., Campbell, K.C., Holliman, P.J., Hoyle, R.W., Huxam, M., Stirling, D., Williams, B.P., Morris, M. Cobalt-Zinc Oxide Adsorbents for Low Temperature Gas Desulfurisation. *J. Mater. Chem*. **9**, 599 (1999).

78. Baird, T., Denny, P.J., Hoyle, R., McMonagle, F., Stirling, D., Tweedy, J. Modified Zinc Oxide Adsorbents for Low-temperature Gas Desulfurisation. *J. Chem. Soc., Faraday Trans*. **88**, 3375 (1992).

79. Ho, C.-S., Shih, S. - M. $Ca(OH)_2$/Fly Ash Sorbents for SO_2 Removal. *Ind. Eng. Chem. Res.* **31**, 1130 (1992).

80. Lastoskie, C., Gubbins, K.E., Quirke, N. Pore Size Distribution Analysis of Microporous Carbons: A Density Functional Theory Approach. *J. Phys. Chem.* **97**, 4786 (1993).

81. Lastoskie, C., Gubbins, K.E., Quirke, N. Pore Size Heterogeneity and the Carbon Slit Pore: A Density Functional Theory Model. *Langmuir* **9**, 2693 (1993).

82. Olivier, J. P., Conklin, W.B. Determination of Pore Size Distribution from Density Functional Theoretic Models of Adsorption and Condensation within Porous Solids. *Presented at the International Symposium on the Effects of Surface Heterogeneity in Adsorption and Catalysis on Solids,* Kazimierz Dolny*,* Poland (1992).

83. Olivier, J.P. Modeling Physical Adsorption on Porous and Nonporous Solids Using Density Functional Theory. *J. Porous Mater*. **2**, 217 (1995).

84. Olivier, J.P. Improving the Models Used for Calculating the Size Distribution of Micropore Volume of Activated Carbons from Adsorption Data. *Carbon* **36**, 1469 (1998).

85. Kaneko, K., Suzuki, T., Fujiwara, Y., Nishikawa, K. In *Characterisation of Porous Solids II*, Rodriquez- Reinoso et al., Eds.; Elsevier: Amsterdam, 1991.

86. Ravikovitch, P.I., Gusev, V.Y., Leon y Leon, C.A., Neimark, A.V. In *Proc. 23rd Biennial Conf. On Carbon*, Penn State University, 136 (1997), Vol.**1**.

87. Neimark, A.V., Ravikovitch, P.I. Calibration of Pore Volume in Adsorption Experiments and Theoretical Models. *Langmuir* **13**, 5148 (1997).

88. Ravikovitch, P.I., Vishnyakov, A., Russo, R., Neimark, A.V. Unified Approach to Pore Size Characterization of Microporous Carbonaceous Materials from N_2, Ar, and CO_2 Adsorption Isotherms. *Langmuir* **16**, 2311 (2000).

89. Davies, S., Packer, K.J. Pore-Size Distributions from Nuclear Magnetic Resonance Spin-Lattice Relaxation Measurements of Fluid-Saturated Porous Solids. I. Theory and Simulation. *J. Appl. Phys.* **67**, 3163 (1990). Davies, S., Kalam, M.Z., Packer, K.J., Zelaya, F.O. Pore-Size Distributions from Nuclear Magnetic Resonance Spin-Lattice Relaxation Measurements of Fluid-Saturated Porous Solids. II. Applications to Reservoir Core Samples. *J. Appl. Phys.* **67**, 3171 (1990).

90. Davis, M.E., Saldarriaga, C., Montes, C., Garces, J., Crowder, C. VPI-5: The First Molecular Sieve with Pores Larger Than 10 Ångstroms**.** *Zeolites* **8**, 362 (1988).

91. Johnson, J.W., Brody, J.F. Pillared Clays and Micas. *Solid State Ionics* **26**, 162 (1988).

92. Ramsay, J.D.F., Booth, B.O. Determination of Structure in Oxide Sols and Gels from Neutron Scattering and Nitrogen Adsorption Measurements. *J. Chem. Soc., Faraday Trans.* **79**, 173 (1983).

93. Ramsay, J.D.F., Swanton, S.W., Bunce, J. Swelling and Dispersion of Smectite Clay Colloids: Determination of Structure by Neutron Diffraction and Small-Angle Neutron Scattering. *J. Chem. Soc., Faraday Trans.* **86**, 3919 (1990).

94. Bandosz, T.J., Jagiello, J., Contescu, C., Schwarz, J.A. Characterization of the Surfaces of Activated Carbons in Terms of their Acidity Constant Distributions. *Carbon* **31**, 1193 (1993).

95. Jagiello, J., Bandosz, T.J., Putyera, K., Schwarz, J.A. Determination of Proton Affinity Distributions for Chemical Systems in Aqueous Environments Using a Stable Numerical Solution of the Adsorption Integral Equation. *J. Colloid Interface Sci.* **172**, 341 (1995).

96. Derbyshire, F.J., De Beer, V.H.J., Abotsi, G.M.K., Scaroni, A.W., Solar, J.M., Skrovanek, D.J. The Influence of Surface Functionality on the Activity of Carbon-Supported Catalysts**.** *Appl. Catal*. **27**, 117 (1986).

97. Venter, J.J., Vannice, M.A. Applicability of "Drifts" for the Characterization of Carbon-Supported Metal Catalysts and Carbon Surfaces**.** *Carbon* **26**, 889 (1988).

98. Meldrum, B.J., Rochester, C.H. *In situ* Infrared Study of the Surface Oxidation of Activated Carbon in Oxygen and Carbon Dioxide. *J. Chem. Soc., Faraday Trans.* **86**, 861 (1990).

99. Kelemen, S.R., George, G. N., Gorbaty, M.L. Direct Determination and Quantification of Sulphur Forms in Heavy Petroleum and Coals: 1. The X-ray Photoelectron Spectroscopy (XPS) Approach. *Fuel* **69**, 939 (1990).

100. Kelemen, S.R., Gorbaty, M.L., George, G.N., Kwiatek, P.J., Sansone, M. Thermal Reactivity of Sulphur Forms in Coal**.** *Fuel* **70**, 396 (1991).

101. Gorbaty, M.L., George, G.N., Kelemen, S.R. Direct Determination and Quantification of Sulphur Forms in Heavy Petroleum and Coals: 2. The Sulphur K edge X-ray Absorption Spectroscopy Approach. Fuel **69**, 945 (1990).

102. George, G.N., Gorbaty, M.L., Kelemen, S.R., Sansone, M. Direct Determination and Quantification of Sulfur Forms in Coals from the Argonne Premium**.** *Energy Fuels* **5**, 93 (1991).

103. Huffman, G.P., Mitra, S., Huggins, F.E., Shah, N., Vaidya, S., Lu, F. Quantitative Analysis of All Major Forms of Sulfur in Coal by X-ray Absorption Fine Structure Spectroscopy. *Energy Fuels* **5**, 574 (1991).

104. Brown, J.R., Kasrai, M., Bancroft, M.G., Tan, K.H., Ghen, J.M. Direct Identification of Organic Sulphur Species in Rasa Coal from Sulphur L-edge X-ray Absorption Near-Edge Spectra**.** *Fuel* **71**, 649 (1992).

105. Biniak, S., Szymanski, G., Siedlewski, J., Swiatkowski, A. The Characterization of Activated Carbons with Oxygen and Nitrogen Surface Groups. *Carbon* **35**, 1799 (1997).

106. Papier, E., Bantzer, J., Sheng, L., Donnet, J.B. Surface Groups on Nitric Acid Oxidized Carbon Black Samples Determined by Chemical Thermodesorption Analysis. *Carbon* **29**, 69 (1991).

107. Otake, Y., Jenkins, R.G. Characterization of Oxygen-Containing Surface Complexes Created on a Microporous Carbon by Air and Nitric Acid Treatment. *Carbon* **31**, 109 (1993).

108. Zhuang, Q-L., Kyotani, T., Tomita, A. DRIFT and TK/TPD Analyses of Surface Oxygen Complexes Formed during Carbon Gasification. *Energy Fuels* **8**, 714 (1994).

109. Jagiello, J., Bandosz, T.J., Schwarz, J.A. Application of Inverse Gas Chromatography at Infinite Dilution to Study the Effects of Oxidation of Activated Carbons. *Carbon* **30**, 63 (1992).

110. Jagiello, J., Bandosz, T.J., Schwarz, J.A. Inverse Gas Chromatographic Study of Activated Carbons: The Effect of Controlled Oxidation on Microstructure and Surface Chemical Functionality. *J Colloid Interface Sci.* **151**, 433 (1992).

111. Jagiello, J., Bandosz, T.J., Schwarz, J.A. Study of Carbon Microstructure by Using Inverse Gas Chromatography. *Carbon* **32**, 687 (1994).

112. Anurov, C.A., Keltsev, N.V., Smola, V.I., Torocheshnikov, N.S. Adsorbent from Natural Zeolite. In "Uspekhi Khimii", *Russian Chemical Reviews* **46**, 32 (1977).

113. Adib, F., Bagreev, A., Bandosz, T.J. Analysis of the Relationship between H_2S Removal Capacity and Surface Properties of Unimpregnated Activated Carbons. *Environ. Sci. Technol.* **34**, 686 (2000).

114. Shin, H-C., Park, J-W., Song, H-C. Removal Characteristics of Trace Compounds of Landfill Gas by Activated Carbon Adsorption. *Environ. Pollut.* **119**, 227 (2002).

115. Lee, Y-W., Choung, J-H., Park, J-W., Choi, D-K. Characteristics of NOx Adsorption and Surface Chemistry on Impregnated Activated Carbon. *Sep. Sci. Technol.* **37**, 937 (2002).

116. Lu, G.Q., Do, D.D. Retention of Sulfur Dioxide as Sulfuric Acid by Activated Reject Char. *Sep. Sci. Technol.* **3**, 106 (1993).

117. http://www.epa.gov/otaq/regs/ld-hwy/tier-2/frm/f99051.pdf

118. http://www.epa.gov/otaq/regs/fuels/diesel/frdslpre.pdf

119. Gardner, T.H., Berry, D.A., Lyons, K.D., Beer, S.K., Freed, A.D. Fuel Processor Integrated H_2S Catalytic Partial Oxidation Technology for Sulfur Removal in Fuel Cell Power Plants**.** *Fuel* **81***,* 2157 (2002).

120. Sano, Y., Choi, K-H., Korai, Y., Mochida, I. Adsorptive Removal of Sulfur and Nitrogen from a Straight Run Gas Oil over Activated Carbons for Its Deep Desulfurization. *Appl. Catal. B* **49**, 219 (2004).

121. Kopac, T. Non-Isobaric Adsorption Analysis of SO_2 on Molecular Sieve 13X and Activated Carbon by Dynamic Technique**.** *Chem. Eng. Process.* **38**, 45 (1999).

122. Hossain, M.M., Al-Saleh, M.A., Shalabi, M.A., Kimura, T., Inui, T. Thiophene Hydrodesulfurizaion over Noble Metal Modified Co-Clay Catalysts. *Appl. Catal. A* **274**, 42 (2004).

123. Mikhail, S., Zaki, T., Khalil, L. Desulfurization by an Economically Adsorption Technique. *Appl. Catal. A.* **227**, 265 (2002).

124. Iwasa, N., Kubota, T., Bando, K.K., Shirai, M. Hydrodesulfurization of Thiophenic Compounds over Synthetic Smectite-Type Clays. *J. Phys. Chem. Solids* **65**, 503 (2004).

125. Sychev, M., de Beer, V.H.J., van Santen, R.A. Chromia and Chromium Sulfide Pillared Clays Differing in Pillar Density**.** *Microporous Mater.* **8**, 255 (1997).

126. Shan, H.H., Li, C.Y., Yang, C.H., Zhao, H., Zhang, J.F. Mechanistic Studies on Thiophene Species Cracking over USY Zeolite. *Catal. Today* **77***,* 117 (2002).

127. Saintigny, X., van Santen, R.A., Clemendot, S., Hutschka, F. A Theoretical Study of the Solid Acid Catalyzed Desulfurization of Thiophene**.** *J. Catal.* **183***,* 107 (1999).

128. Lin, Y.S., Deng, S.G. Removal of Trace Sulfur Dioxide from Gas Stream by Regenerative Sorption Processes. *Sep. Purif. Technol.* **13**, 65 (1998).

129. Sarbak, Z. Desulfurization of Ethanethiol over Cadmium and Mercury Modified Zeolite NaX. *Appl. Catal. A* **147**, 47 (1996).

130. Severino, F., Laine, J., Lopez-Agudo, A. Compensation Effect and Dual Promotion Effect in Activated Carbon-Supported CoNiMo Hydrodesulfurization Catalysts. *J. Catal.* **189**, 244 (2000).

131. Calafat, A., Laine, J., Lopez-Agudo, A., Palacios, J.M. Effect of Surface Oxidation of the Support on the Thiophene Hydrodesulfurization Activity of Mo, Ni, and NiMo Catalysts Supported on Activated Carbons. . *J. Catal.* **162**, 20 (1996).

132. Koranyi, T.I., Rozanov, V., Kremo, R., Paal Z. Activation of Carbon-Supported Cobalt-Molybdenum Catalysts in Thiophene Hydrodesulfurization. *J. Mol. Catal.* **63**, 31 (1990).

133. Vissers, J.P.R., Scheffer, B., de Beer, V.H.J., Moulijn, J.A., Prins, R. Effect of the Support on the Structure of Mo-Based Hydrodesulfurization Catalysts: Activated Carbon versus Alumina. *J. Catal*. **105**, 277 (1987).

134. Yin, C., Liu, C. Hydrodesulfurization of Cracked Naphtha over Zeolite-Supported Ni-Mo-S Catalysts. *Appl. Catal. A* **273**, 177 (2004).

135. Breysse, M., Djega-Mariadassou, G., Pessayre, S., Geantet, C., Vrinat, M., Pérot, G., Lemaire, M. Deep Desulfurization: Reactions, Catalysts and Technological Challenges**.** *Catal. Today* **84**, 129 (2003).

136. F. Bataille, F., Lemberton, J.L, Pérot, G., Leyrit, P., Cseri, T., Marchal, N., Kasztelan, S. Sulfided Mo and CoMo Supported on Zeolite as Hydrodesulfurization Catalysts: Transformation of Dibenzothiophene and 4,6-Dimethyldibenzothiophene. *Appl. Catal. A* **220**, 191 (2001).

137. Brooks, C.S. Thiophene Hydrodesulfurization over Nickel Mordenite II. Kinetics. *Surf. Technol.* **9**, 135 (1979).

138. Egorova, M., Prins, R. Hydrodesulfurization of Dibenzothiophene and 4,6-Dimethyldibenzothiophene over Sulfided NiMo/γ-Al_2O_3, CoMo/γ-Al_2O_3, and Mo/γ-Al_2O_3 Catalysts. *J. Catal.* **225**, 417 (2204).

139. Saih, Y., Segawa, K. Tailoring of Alumina Surfaces as Supports for NiMo Sulfide Catalysts in the Ultra Deep Hydrodesulfurization of Gas Oil: Case Study of TiO_2-Coated Alumina Prepared by Chemical Vapor Deposition Technique. *Catalysis Today* **86***,* 61 (2003).

140. Kabe, T., Aoyama, Y., Wang, D., Ishihara, A., Qian, W., Hosoya, M., Zhang, Q. Effects of H_2S on Hydrodesulfurization of Dibenzothiophene and 4,6-Dimethyldibenzothiophene on Alumina-Supported NiMo and NiW. *Appl. Catal. A* **209**, 237 (2001).

141. Olguin, E., Vrinat, M., Cedeno, L., Ramirez, J., Borque, M., Lopez-Agudo, A. The Use of TiO_2---Al_2O_3 Binary Oxides as Supports for Mo-Based Catalysts in Hydrodesulfurization of Thiophene and Dibenzothiophene. *Appl. Catal. A* **165**, 1 (1997).

142. Aegerter, P.A., Quigley, W.W.C., Simpson, G.J., Ziegler, D.D., Logan, J.W., McCrea, K.R., Glazier, S., Bussell, M.E. Thiophene Hydrodesulfurization over Alumina-Supported Molybdenum Carbide and Nitride Catalysts: Adsorption Sites, Catalytic Activities, and Nature of the Active Surface. *J. Catal.* **164**, 109 (1996).

143. Turaga, U.T., Song, C. MCM-41-Supported Co-Mo Catalysts for Deep Hydrodesulfurization of Light Cycle Oil**.** *Catal. Today* **86***,*129 (2003).

144. Song, C., Reddy, K.M. Mesoporous Molecular Sieve MCM-41 Supported Co–Mo Catalyst for Hydrodesulfurization of Dibenzothiophene in Distillate Fuels. *Appl. Catal. A* **176**, 1 (1999).

145. Lin, R-B., Shih, S-M., Liu, C-F. Characteristics and Reactivities of $Ca(OH)_2$/Silica Fume Sorbents for Low-Temperature Flue Gas Desulfurization**.** *Chem. Eng. Sci.* **58***,* 3659 (2003).

146. Van Der Grift, C.J., De Boer, M., Geus, J.W**.** The Reactivity of a Copper-Based Flue Gas Desulfurization Absorbent**.** *Solid State Ionics* **32-33***,* 974 (1989).

147. Karchmer, J.H. "The Analytical Chemistry of Sulfur and its Compounds", Wiley: New York, 1960, Vol.1, 466.

148. International Chemical Safety Cards: 0299, CEC, IPCS, 1993.

149. Allinger, N.L., Cava, M.P., de Jongh, D.C., Johnson, C.R., Lebel, N.A., Stevens, C.L. "Organic Chemistry", Worth Publishers Inc.: New York, 2nd Ed.,1976, 790.

150. Kortum, G., Vogel, W., Andrussow, K. Dissociation Constants of Organic Acids in Aqueous Solutions", Butterworth: London, 1961.

151. Lide, D.R. *CRC Handbook of Chemistry and Physics*, 82nd Ed.; CRC Press: Boca Raton, Fl, 2001-2002.

152. Katoh, H., Kuniyoshi, I., Hirai, M., Shoda, M. Studies of the Oxidation Mechanism of Sulphur-Containing Gases on Wet Activated Carbon Fibre. *Appl. Catal*. *B* **6**, 255 (1995).

153. Castro, M.E., White, J.M. Decomposition of Methanethiol on Ni (III): A TPD and SSIMS Study. *Surf. Sci*. **257**, 22 (1991).

154. Huntley, D.R. Adsorption and Reactions of Methanethiol on Clean and Modified Nickel (110). *J. Phys. Chem*. **93**, 6156 (1989).

155. Bao, S., McConville C.F., Woodruff, D.P. An Angle-Resolved Photoemission Study of the Reaction of CH_3SH and $(CH_3S)_2$ with Cu(111) and Ni(100). *Surf. Sci. Lett*. **187**, A319 (1987).

156. Albert, M.R., Lu, J.P., Bernasek, S.L., Cameron, S.D., Gland, J.L. The Mechanism of the Decomposition of Methanethiol on Fe (100). *Surf. Sci*. **206**, 348 (1988).

157. Batteas, J.D., Rufael, T.S., Friend, C.M. Influence of Surface Modifiers on the Thermal Decomposition of Methanethiol on Fe (110). *Langmuir* **15**, 2391 (1999).

158. Sexton, B.A., Nyberg, G.L. A Vibrational and TDS Study of Sulfur Adsorbates on Cu (100): Evidence for CH_3S Species. *Surf. Sci*. **165**, 251 (1986).

159. Mullins, D.R., Lyman, P.F. Adsorption and Reaction of Methanethiol on Tungsten (001). *J. Phys. Chem*. **97**, 9226 (1993).

160. Benziger, J.B., Preston, R.E. Organosulfur Chemistry on Tungsten (211) Surfaces. 1. A Comparison of Methanethiol and Methanol. *J. Phys.Chem*. **89**, 5002 (1985).

161. Rufael, T.S., Prasad, J., Fischer, D.A., Gland, J.L. Hydrogenolysis of Adsorbed Methylthiolate on the Pt (111) Surface**.** *Surf. Sci*. **278**, 41 (1992).

162. Mullins, D.R., Overburry, S., Huntley, D., Castro, M.E. In *Proc. American Vacuum Society Meeting* (1990).

163. Wiegand, B.C., Uvdal, P., Friend, C.M. The Local Structure of Adsorbed Methyl Thiolate: The Reactions of Methanethiol on Mo (110). *Surf. Sci*. **279**, 105 (1992).

164. Lai, Y.-H., Yeh, C.-T., Yeh, C.-C., Hung, W.-H. Thermal Reactions of Methanethiol and Ethanethiol on Si (100). *J. Phys. Chem. B* **107**, 9351 (2003).

165. Shen, W., Nyberg, G.L. The Adsorption and Bonding of Methanethiol on Aluminum. *Surf. Sci*. **296**, 49 (1993).

166. Friend, C.M., Chen, D.A. Fundamental Studies of Hydrodesulfurization by Metal Surfaces. *Polyhedron* **16**, 3165 (1997).

167. Pecoraro, T.A., Chianelli, R.R. Hydrodesulfurization Catalysis by Transition Metal Sulfides. *J. Catal.* **67**, 430 (1981).

168. Koestner, R.J., Stohr, J., Gland, J.L., Kollin, E.B., Sette, F. Observation of Novel Intermediates from CH_3SH Decomposition on Pt (111) with HREELS and NEXAFS**.** *Chem. Phys. Lett*. **120**, 285 (1985).

169. Peterson, S., Schulz, K.H. Ethanethiol Decomposition Pathways on MoS_2 (0001). *Langmuir* **12**, 941 (1996).

170. Voorhoeve, R.J.H., Stuiver, J.C.M. The Mechanism of the Hydrogenation of Cyclohexene and Benzene on Nickel-Tungsten Sulfide Catalysts**.** *J. Catal*. **23**, 243 (1971).

171. Roberts, J.T., Friend, C.M. Reactions of Ethanethiol on Mo (110): Formation and Decomposition of a Surface Alkyl Thiolate. *J. Phys. Chem*. **92,** 5205 (1988).

172. Dvorak, J., Jirsak, T., Rodriguez, J.A. Fundamental Studies of Disulfurization Processes: Reaction of Methanethiol on ZnO and Cs/ZnO. *Surf. Sci*. **479**, 155 (2001).

173. Travert, A., Manoilova, O.V., Tsyganenko, A.A., Mauge, F., Lavallev, J.C. Effect of Hydrogen Sulfide and Methanethiol Adsorption on Acidic Properties of Metal Oxides: An Infrared Study. *J. Phys. Chem. B* **106**, 1350 (2002).

174. Ziolek, M., Decyk, P. Relation Between Chemisorption and Catalytic Transformation of R_2S Compounds on Fujasite-Type Zeolites. *Langmuir* **15**, 5781 (1999).

175. Mortier, W.J. Zeolite Electronegativity Related to Physicochemical Properties. *J. Catal*. **55**, 138 (1978).

176. Garcia, C.L., Lercher, J.A. Hydrogen Bonding of Sulfur Containing Compounds Adsorbed on Zeolite HZSM5**.** *J. Mol. Struct*. **293**, 235 (1993).

177. Dalai, A.K., Tollefson, E.L., Yang, A, Sasaoka, E. Oxidation of Methyl Mercaptan over an Activated Carbon in a Fixed-Bed Reactor. *Ind. Eng. Chem. Res*. **36**, 4726 (1997).

178. Shin, C.S., Kim, K.H., Choi, B.K., Ryu, S.K. Removal of Methyl Mercaptan by Impregnated ACF. In *Proc. Biennial Conference on Carbon*, Charleston (USA): American Carbon Society, 356 (1999).

179. Shin, C.S., Kim, K.H., Yu, S.H., Ryu, S.K. Adsorption of Methyl Mercaptan and Hydrogen Sulfide on the Impreganted Activated Carbon Fiber and Activated Carbon. Presented at *7th International Conference on Fundamentals of Adsorption*, Nagasaki, Japan (2001).

180. Turk, A., Sakalis, E., Lessuck, J., Karamitsos, H., Rago, O. Ammonia Injection Enhances Capacity of Activated Carbon for Hydrogen Sulfide and Methyl Mercaptan. *Environ. Sci. Technol*. **23**, 1242 (1989).

181. Nitta, T., Suzuki, T., Katayama, T. Gas-Phase Adsorption Equilibria for Aceton, Diethylether, Methanol, and Water on Activated Carbon Fiber. *J. Chem. Eng. Japan* **24**, 160 (1991).

182. Timmermans, J. *Physico-Chemical Constants of Pure Organic Compounds*, Elsevier: Amsterdam, Vol.2, 1965.

183. Puziy, A.M.; Poddubnaja, O.I.; Ritter, J.A.; Ebner, A.D.; Holland, C.E. Elucidation of the Ion Binding Mechanism in Heterogeneous Carbon-Composite Adsorbents. *Carbon* **39**, *2313* (2001).

184. Jagiello, J. Stable Numerical Solution of the Adsorption Integral Equation Using Splines. *Langmuir* **10**, 2778 (1994).

185. Kiselev, V.A., Yashin, Y.I. Gas Adsorption Chromatography. Plenum Press: New York, 1969.

186. Dubinin, M.M. in *Chemistry and Physics of Carbon*; P. L. Walker, Ed.; M. Dekker: New York, 1966; Vol. 2.

187. Jagiello, J., Schwarz, J.A. Energetic and Structural Heterogeneity of Activated Carbons Determined Using Dubinin Isotherms and an Adsorption Potential in Model Micropores. *J. Colloid Interface Sci*. **154**, 225 (1992).

188. Bandosz, T.J., Jagiello, J, Schwarz, J.A. Comparison of Methods to Assess Surface Acidic Groups on Activate Carbons. *Anal. Chem*. **64**, 891 (1992).

189. Bashkova, S., Bagreev, A., Bandosz, T.J. Effect of Surface Characteristics on Adsorption of Methyl Mercaptan on Activated Carbons. *Ind. Eng. Chem. Res*. **41**, 4346 (2002).

190. Adib, F., Bagreev, A., Bandosz, T.J. Effect of Surface Characteristics of Wood-Based Activated carbons on Adsorption of Hydrogen Sulfide. *J. Colloid Interface Sci*. **214**, 407 (1999).

191. Adib, F., Bagreev, A., Bandosz, T.J. Effect of pH and Surface Chemistry on the Mechanism of H_2S Removal by Activated Carbons. *J. Colloid Interface Sci*. **216**, 360 (1999).

192. Bashkova, S., Bagreev, A., Bandosz, T.J. Adsorption/Oxidation of CH_3SH on Activated Carbons Containing Nitrogen. *Langmuir* **19**, 6115 (2003).

193. http://www.cchem.berkeley.edu/trngrp/traunerweb/Miscellaneous/pKatable.pdf

194. Bashkova, S., Bagreev, A., Bandosz, T.J. Catalytic Properties of Activated Carbon Surface in the Process of Adsorption/Oxidation of Methyl Mercaptan. *Catalysis Today* **99**, 323 (2005).

195. Bagreev, A., Bashkova, S., Bandosz, T.J. Dual Role of Water in the Process of Methyl Mercaptan Adsorption on Activated Carbons. *Langmuir* **18**, 8553 (2002).

196. Bashkova, S., Bagreev, A., Bandosz, T.J. Adsorption of Methyl Mercptan on Activated Carbons. *Environ. Sci. & Technol.* **36**, 2777 (2002).

197. Salame, I.I., Bandosz, T.J. Experimental Study of Water Adsorption on Activated Carbons. *Langmuir* **15**, 587 (1999).

198. Nuzzo, R.G., Zegarski, B.R., Dubois, L.H. Fundamental Studies of the Chemisorption of Organosulfur Compounds on Gold (111). Implications for Molecular Self-Assembly on Gold Surfaces. *J. Am. Chem. Soc*. **109**, 733 (1987).

199. Bagreev, A., Rahman, H., Bandosz, T.J. Initial Heats of H_2S Adsorption on Activated Carbons: Effect of Surface Features**.** *Carbon* **39**, 1319 (2001).

200. Lodewyckx, P., Vansant, E.F. The Dynamic Adsorption of Water Vapour on Activated Carbon**.** *Carbon* **36**, 304 (1998).

201. Avgul, N.N., Kiselev, A.V., in "Chemistry and Physics of Carbon", Walker P.J., Ed.; Marcel Dekker: New York, 1970, Vol. **6**.

202. Kiselev, A.V. Intermolecular Interactions in Adsorption and Chromatography. Visshaja Shkola: Moscow, 1986.

203. Steele, W.A. The Physical Interaction of Gases with Crystalline Solids: I. Gas-Solid Energies and Properties of Isolated Adsorbed Atoms**.** *Surf. Sci*. **36**, 317 (1973).

204. Viktorov, M.M. Methods of Simulation of Physicochemical Parameters and Applied Calculation. Khimija: Moscow, 1977.

205. Bagreev, A., Adib, F., Bandosz, T. Initial Heats of H_2S Adsorption on Activated Carbons: Effect of Surface Features. *J. Colloid Interface Sci.* **219**, 327 (1999).

206. Bagreev, A., Bandosz, T.J. A Role of Sodium Hydroxide in the Process of Hydrogen Sulfide Adsorption/Oxidation on Caustic-Impregnated Activated Carbons. *Ind. Eng. Chem. Res*. **41**, 672 (2002).

207. McCallum, C.L., Bandosz, T.J., McGrother, S.C., Muller, E.A., Gubbins, K.E. A Molecular Model for Adsorption of Water on Activated Carbon: Comparison of Simulation and Experiment. *Langmuir* **15**, 533 (1999).

208. Bagreev, A., Adib, F., Bandosz, T.J. pH of Activated Carbon Surface as an Indication of Its Suitability for H_2S Removal from Moist Air Streams. *Carbon* **39,** 1897 (2001).

209. Przyjazny, A., Janicki, W., Chrazanowski, W., Staszewski, R. Headspace Gas Chromatographic Determination of Distribution Coefficients of Selected Organosulfur Compounds and their Dependence on Some Parameters. *J. Chromatogr*. **280**, 249 (1983).